이학박사학위논문

간에서의 RORα에 의한 지방 항상성 유지 조절 기작에 관한 연구

Studies on the Regulatory Mechanism of Hepatic Lipid Homeostasis by RORα

2017년 8월

서울대학교 대학원

생명과학부

김 경 규

Studies on the Regulatory Mechanism of Hepatic Lipid Homeostasis by RORα

by

Kyeongkyu Kim

Advisor

Professor Sung Hee Baek, Ph.D.

A Thesis for the Degree of Doctor of Philosophy

August, 2017

School of Biological Sciences
Seoul National University

ABSTRACT

Kyeongkyu KIM
School of Biological Sciences
The Graduate School
Seoul National University

Hepatic metabolic dysregulation has been shown to induce fatty liver, insulin resistance and obesity. The retinoic acid receptor-related orphan receptor α (RORα) is an important regulator of various biological processes, including cerebellum development, circadian rhythm, and cancer. Here, I find that hepatic RORα regulates lipid homeostasis by negatively regulating transcriptional activity of peroxisome proliferators-activated receptor γ (PPARγ), a nuclear receptor that mediates hepatic lipid metabolism. Liver-specific *Rorα* deficient mice develop hepatic steatosis, obesity, and insulin resistance, when challenged with a high fat diet (HFD). Global transcriptome analysis reveals that liver-specific deletion of *Rorα* leads to the dysregulation of PPARγ signaling to increase hepatic glucose and lipid metabolism. RORα specifically binds and recruits HDAC3 to the PPARγ target promoters for the transcriptional repression of PPARγ activity. Finally, PPARγ antagonism remarkably restores metabolic homeostasis in HFD-fed liver-specific

Rorα deficient mice. Taken together, my data indicate that RORα plays a pivotal role in the regulation of hepatic lipid homeostasis. Therefore, therapeutic strategies designed to modulate RORα activity may be beneficial for the treatment of metabolic disorders, including hepatic steatosis and obesity.

Key words

Retinoic acid receptor-related orphan receptor α (RORα), Liver-specific *Rorα* deficient mice, High fat diet, Obesity, Liver, Lipid metabolism, Peroxisome proliferators-activated receptor γ (PPARγ), Histone deacetylase 3 (HDAC3), GW9662

Student Number: 2011-30106

CONTENTS

	Page
ABSTRACT	**i**
CONTENTS	**iii**
LIST OF FIGURES AND TABLES	**vi**
CHAPTER I. Introduction	**1**
I-1. Orphan Nuclear Receptors and RORα	**2**
1.1. General information of orphan nuclear receptors	2
1.2. Structure of orphan nuclear receptors	2
1.3. General information of RORα	5
1.4. RORα in metabolism	7
I-2. Peroxisome proliferator-activated receptor γ (PPARγ)	**9**
2.1. General information of PPARγ	9
2.2. PPARγ activators, Thiazolidinediones	9

2.3 PPARγ in metabolism 11

I-3. Histone deacetylase 3 (HDAC3) **14**

3.1. General information of Histone deacetylases 14

3.2. Physiological functions of HDAC3 16

I-4. Metabolic disorder **18**

4.1. Obesity 18

4.2. Hepatic steatosis 19

CHAPTER II. Liver-specific *Rorα* deficient mice are susceptible to diet-induced obesity **22**

II-1. Summary 23

II-2. Introduction 24

II-3. Results 27

II-4. Discussion 47

II-5. Materials and Methods 49

CHAPTER III. RORα requires HDAC3 to regulate PPARγ signaling to maintain hepatic lipid homeostasis in response to over-nutrient cue **56**

III-1. Summary 57

III-2. Introduction 58

III-3. Results 61

III-4. Discussion 106

III-5. Materials and Methods 109

CHAPTER IV. Conclusion **115**

REFERENCES **123**

국문초록 / ABSTRACT IN KOREAN **135**

LIST OF FIGURES AND TABLES

Figure I-1. Illustration of orphan nuclear receptor structure

Figure I-2. Illustration of PPARγ activation effect on metabolism related organ

Figure I-3. Illustration of the process of hepatic steatosis progression

Figure II-1. Generation of conditional *Rorα* deficient mouse

Figure II-2. Identification of RORα deficiency and the liver developmental process in RORα^{LKO} mice

Figure II-3. Metabolic characterization of RORα$^{f/f}$ and RORα^{LKO}mice fed CD

Figure II-4. Liver-specific *Rorα* dificient mice are susceptible to diet-induced obesity

Figure II-5. Expression of inflammatory cytokine genes in eWAT and thermogenesis genes in BAT is impaired in HFD-fed RORα^{LKO} mice

Figure II-6. Expression of inflammatory cytokine genes in eWAT and thermogenesis genes in BAT is impaired in HFD-fed RORα^{LKO} mice

Figure II-7. Illustration of increased energy expenditure of BAT by bile acid

Figure II-8. Expression of hepatic bile acid related genes and serum bile acid pool size are decreased in RORα^{LKO} mice fed HFD

Figure II-9. Liver-specific *Rorα* deleted mice are susceptible to diet-induced hepatic steatosis

Figure II-10. Expression of hepatic lipid metabolism related genes is increased in the liver of RORα^{LKO} mice fed HFD but is no obvious change in the liver of RORα^{LKO} mice fed CD

Figure II-11. Insulin sensitivity is impaired in liver-specific *Rorα* deficient mice

Figure III-1. Transcriptome analysis of hepatic gene expression profile in RORα^{LKO} mice

Table III-1. Summary of the alignment results for mRNA-sequencing data

Table III-2. GOBPs and KEGG pathways represented by the genes in Groups 1-4

Table III-3. List of genes affected by depletion of RORα

Table III-4. Key transcription factors significantly regulating the genes in Group 1

Figure III-2. PPARα and RORα do not affect their roles in the mice liver with each other

Figure III-3. RORα inhibits the transcriptional activity of PPARγ

Figure III-4. RORα recruits to PPRE and inhibits transcription activity of PPARγ, but does not interact with PPARγ

Figure III-5. RORα interacts with HDAC3 to repress PPARγ transcriptional activity

Figure II-6 RORα recruits to the PPARγ target gene promoters with HDAC3 in liver of mice fed HFD

Figure III-7. The recruitment of PPARγ to the PPARγ target gene promoters is similar between RORα$^{f/f}$ and RORα^{LKO} mice fed CD unlike mice fed HFD

Figure III-8. PPARα recruitment is almost absent in the target gene promoter of PPARγ

Figure III-9. Expression of PPARγ target genes changes in response to Rosi.+washout

experimental conditions

Figure III-10. ChIP assay in response to Rosi.+washout experimental conditions

Figure III-11. The recruitment of RORα to PPARγ target genes promoter increases when PPARγ signal is reduced and it is opposite to PPARγ recruitment

Figure III-12. RORα is required to recruit HDAC3 to PPARγ target genes promoter

Figure III-13. PPARα fails to influence on PPARγ transcriptional network but HDAC3 affects PPARγ transcriptional network

Figure III-14. Recruitment of RORα and PPARγ to the PPARγ target gene promoters are mutually exclusive

Figure III-15. RORα and HDAC3 compete with PPARγ for the binding to the target gene promoter

Figure III-16. The presence of HDAC3 affected the recruitment of RNA polymerase II to the PPARγ target gene promoters

Figure III-17. PPARγ antagonism restores metabolic homeostasis in RORα^{LKO} mice

Figure IV-1. Graphical summary of the newly identified role of RORα that negatively regulated PPARγ signaling via HDAC3 recruitment to the PPARγ target promoters

CHAPTER I

Introduction

I-1. Orphan Nuclear Receptors and RORα

1.1 General information of orphan nuclear receptors

The nuclear receptor superfamily plays many important roles in development, differentiation, reproduction and metabolic homeostasis (Bain et al., 2007; Ribeiro et al., 1995). Nuclear receptors are composed of independent functional domains that include the amino-terminal domain (NTD), the DNA-binding domain (DBD) and Ligand-binding domain (LBD) (Giguere, 1999). Nuclear receptors are receptors for physiological ligands, including steroid hormones, lipids and fatty acids (Kojetin and Burris, 2014) (Fig. I-1). However, the orphan nuclear receptor family comprises a set of proteins sharing significant sequence homology to known nuclear receptors, but for which the ligands have not yet been identified (Giguere, 1999). Similar to the other members of nuclear receptors, orphan nuclear receptors are composed of functional domains that include the DBD and the LBD (Aranda and Pascual, 2001).

1.2 Structure of orphan nuclear receptors

The amino-terminal domain (NTD), also referred to as the modulator domain, shows the most flexibility domain both in terms of sequence length and primary sequence (Wang and Sadar, 2006). The NTD shows promoter- and cell-specific activity, suggesting that it is likely to contribute to the specificity of function (Shao and Lazar, 1999). The DNA-binding domain (DBD) confers the ability to recognize specific target sequences and activate genes.

This is the most highly conserved region of the orphan nuclear receptor, and its interactions with DNA have been well characterized (Zilliacus et al., 1995). The DBD contains nine cysteines, as well as other residues that are conserved across the nuclear receptor superfamily and are required for high-affinity DNA binding (Weatherman et al., 1999). The Ligand-binding domain (LBD) is a multifunctional domain that mediates binding of ligand, homo- and hetero- dimerization, interaction with co-regulator proteins, transactivation functions (Dubbink et al., 2006). The LBD is folded into a three-layered, antiparallel helical sandwich. A central core layer of three helices is packed between two additional layers to create a cavity, the ligand-binding pocket, which accommodates the ligand. This domain is mainly hydrophobic and is buried within the bottom half of the LBD. Contacts with the ligand can be extensive and include different structural elements through the LBD (Moras and Gronemeyer, 1998). However, the orphan nuclear receptor family has no defined ligands for the LBD.

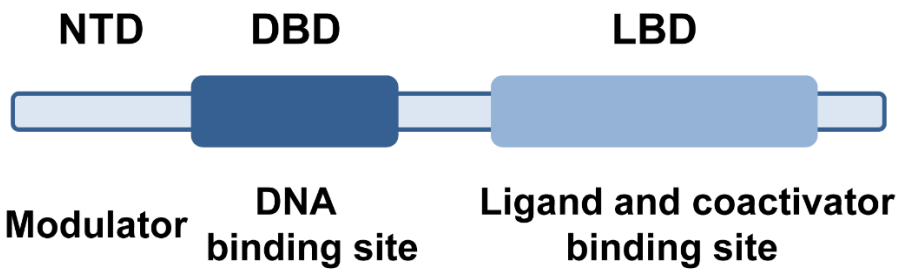

Figure I-1. Illustration of orphan nuclear receptor structure
Orphan nuclear receptors are composed of independent functional domains that include the NTD, DBD and LBD. The NTD that located at the amino termini has transcription activation function. The DBD has the functions of which are to recognize specific DNA sequences and the LBD is the domain where specific ligands and cofactors bind.

1.3 General information of RORα

The retinoic acid receptor (RAR)-related orphan receptor α (RORα) is a member of the ROR subfamily that composed of RORα, RORβ and RORγ (Carlberg et al., 1994; Giguere et al., 1994). The RORα gene is located in human chromosome 15q22.2 and covers a relatively large 730 kb genomic region comprised of 15 exons (Zhu et al., 2006). By the alternative splicing mechanism, RORα has four isoforms referring to RORα1 to RORα4 in human, with different promoters and the NTD region but identical DBD and LBD regions, whereas in mice only two isoforms, RORα1 and RORα4 (Becker-Andre et al., 1993; Giguere et al., 1994).

RORα regulates transcription by binding as monomers to ROR response elements (RORE), which consist of the core sequence "(A/G)GGTCA" preceded by a 6-bp A/T-rich sequence, in the regulatory region of target genes (Giguere et al., 1995). The activation function-2 (AF-2) domain that localized at the C-terminus in the LBD is involved in the recruitment of co-activators that mediate the transcriptional activation by RORα. PGC1α, p300, SRC1, SRC2, GRIP1, Tip60, β-catenin and CBP have been reported as co-activator of RORα by interacting with LBD of RORα (Atkins et al., 1999; Chopra et al., 2008; Gold et al., 2003; Harris et al., 2002; Jetten and Joo, 2006). In addition, RORα is widely expressed in many tissues, including cerebellar Purkinje cells, the liver, thymus, skeletal muscle, skin, lung, adipose tissue and kidney (Hamilton et al., 1996). DNA damage-induced expression of RORα leads to stabilize p53 and activates p53 transcription in HAUSP/Usp7-dependent manner. Interestingly, microarray analysis revealed that RORα-mediated p53

stabilization leads to the activation of a subset of p53 target genes that are specifically involved in apoptosis (Kim et al., 2011). Therefore, RORα has many regulatory functions of various cellular signaling through different combinations with co-activators.

Post translational modification is important mechanism to regulate transcriptional activity of RORα. Phosphorylation by Wnt5a/PKCα to serine residue 35 of RORα plays a role to link RORα to Wnt/β-catenin signaling, and leads to repress expression of Wnt/β-catenin target genes. Interestingly, phosphorylation of RORα is reduced in colorectal tumor compared to normal counterpart. RORα has an important role to link the canonical and the noncanonical Wnt signaling pathways by attenuating expression of Wnt/β-catenin target genes (Lee et al., 2010). In addition, methylation by polycomb group Ezh2 to lysine residue 38 of RORα triggers ubiquitination of RORα permitting to degradation. Methylation of lysine residue 38 of RORα is recognized by Cul4/DDB1 E3 ligase complex and caused to ubiquitination. Furthermore, upregulation of Ezh2 and downregulation of RORα are correlated with each other in breast tumor (Lee et al., 2012). In conclusion, RORα functions as tumor suppressor through regulating by post translational modification.

Staggerer mice that reported in 1962 have a severe cerebellar ataxia because of cell-autonomous defect in the development of Purkinje cells (Herrup and Mullen, 1979; Sidman et al., 1962). In 1996, *Staggerer* mice were found to have spontaneous RORα deficiency (Hamilton et al., 1996). Given that *Staggerer* mice have huge cerebellar defects, it is still possible that physiological changes observed in *Staggerer* mice are indirect effects. Thus, the physiological roles of RORα to control transcriptional networks to modulate other

physiological pathway still remain unclear.

1.4 RORα in metabolism

Staggerer mice are protected against age- and diet- induced obesity and the development of several obesity-linked pathologies, including adipose tissue-associated inflammation, hepatic steatosis and insulin resistance (Kang et al., 2011; Lau et al., 2011; Lau et al., 2008). Despite their higher food consumption, aging *Staggerer* mice exhibit a reduced body fat index. Adipocytes are smaller in brown and white adipose tissue of *Staggerer* mice than WT mice and the level of triglycerides is lower in liver of *Staggerer* mice than WT mice (Lau et al., 2008). Besides, the expression of sterol regulatory element-binding protein 1, isoform c (Srebp1c), which is an important regulator of lipogenesis and several lipogenic genes like fatty acid synthase (Fas), are significantly reduced in liver and skeletal muscle of *Staggerer* mice (Jetten, 2009; Lau et al., 2008). In addition, the expression of several genes involved in the main and alternative pathway of triglyceride synthesis, including glycerol-3-phosphate acyltransferase (Gpam), acyl-glycerol-3-phosphate acyltransferase 9 (Agpat9) and Mono-acyl-glycerol O-Acyl-transferase 1 (Mogat1) were significantly diminished in *Staggerer* mice liver (Kang et al., 2011). However, *Staggerer* mice has huge disadvantage to study metabolism because of cerebellar defect. *Staggerer* mice show a staggering gait and mild tremor, therefore *Staggerer* mice have eating and drinking difficulties. In other words, the reason why obesity does not occur in *Staggerer* mice is not because RORα play a role in promoting obesity, but is simply due to a disturbance of

feeding and drinking. In addition, overexpression of RORα in mouse liver by infection with adenovirus encoding RORα suppresses the lipid accumulation and protects high fat diet-induced hepatic steatosis (Kim et al., 2012). Accordingly, studies using specifically conditional knockout mice of RORα is useful for elucidating the role of RORα in metabolism.

I-2. Peroxisome proliferator-activated receptor γ (PPARγ)

2.1 General information of PPARγ

The peroxisome proliferator-activated receptors (PPARs) are members of the nuclear receptor superfamily of ligand-inducible transcription factors. In mammals, there are three PPARs: PPARα, PPARβ/δ and PPARγ (Evans et al., 2004). PPARα, the first identified PPAR, is mainly expressed in liver, heart and brown adipose tissue (BAT) and is the main activator of the fatty acid oxidation pathway (Poulsen et al., 2012). PPARβ/δ functions like PPARα but is expressed in ubiquitous and plays an important role in fatty acid oxidation in major metabolic tissues such as skeletal muscle, liver and heart (Barish et al., 2006).

PPARγ is abundantly expressed in white adipose tissue (WAT) and BAT, where it is a major regulation organ of adipogenesis, as well as a potent regulator of systemic lipid metabolism and insulin sensitivity. Because of alternative splicing and differential promoter usage, PPARγ is present as two isoforms, PPARγ1 and PPARγ2, with the latter containing an additional 30 amino acids at its N terminus (Tontonoz and Spiegelman, 2008). While PPARγ1 is expressed in many tissues, the expression of PPARγ2 is restricted to adipose tissue under physiological conditions but can be induced in other tissues by a high-fat diet (Medina-Gomez et al., 2007).

2.2 PPARγ activators, Thiazolidinediones

Although fatty acids and their derivatives can activate PPARγ, the identification of defined endogenous PPARγ ligands has been difficult. In contrast, synthetic ligands,

Thiazolidinediones (TZDs), are potent activators of PPARγ with robust insulin-sensitizing activities (Forman et al., 1996). Consequences of highly effective oral medications used in the treatment of difficult-to-manage type 2 diabetes that chronically activate PPARγ include side effect like weight gain, fluid retention and osteoporosis (Nissen and Wolski, 2007). Meta-analyses of clinical trials have shown the TZD, especially rosiglitazone, increases the risk of congestive heart failure, myocardial infarction, cardiovascular disease and all-cause mortality, severely limited accession in the United States and a recommendation for market withdrawal in Europe and several other jurisdictions (Wilcox et al., 2008). Thus, a deeper understanding of how different TZDs cause an alternative pathway for PPARγ activation, will potentially lead to new and improved treatments for type 2 diabetes. Recently, in part because of powerful new technologies, much progress has been made in understanding the signaling, regulation and tissue-specific roles of PPARγ (Choi et al., 2011; Dutchak et al., 2012). Many of these advances provide new insights into the mechanisms of PPARγ-mediated insulin sensitization and related side effects by providing opportunities to develop new types of molecules that reduce or eliminate the side effects associated with TZD. TZDs, potent lipogenic and antidiabetic ligands that acts by binding and activating PPARγ, has reinforced the importance of PPARγ in insulin sensitization and has facilitated numerous studies on this nuclear receptor, PPARγ (Agarwal and Garg, 2002; Savage et al., 2003). Thus, direct targeting of PPARγ remains a 'golden standard' for the treatment of metabolic diseases, despite a lot of caveats (Lehmann et al., 1995).

2.3 PPARγ in metabolism

PPARγ is originally described as a factor induced during adipocyte differentiation and is best known for the regulation of adipogenic and lipogenesis pathways (Tontonoz et al., 1994). Generation of the PPARγ-null mouse, which is completely devoid of adipose tissue, firmly established PPARγ as a master regulator of adipocyte differentiation (Barak et al., 1999). PPARγ is also essential for mature adipocyte function, and it has been found that adipocytes survive only for a few days after selectively depletion of PPARγ from mature adipocytes (Imai et al., 2004). In addition to its role in adipocyte differentiation and lipid metabolism, PPARγ is also crucial for controlling gene networks involved in glucose homeostasis, including increasing the expression of glucose transporter type 4 (Glut4) and c-Cbl–associated protein (CAP). Moreover, PPARγ modulates the expression of numerous factors secreted from adipose tissue, such as adiponectin, resistin, leptin and tumor necrosis factor-α (TNF-α), which also affects insulin sensitivity (Tomaru et al., 2009; Tontonoz and Spiegelman, 2008).

However, the functions of PPARγ in the liver and the effects of PPARγ agonism on the liver remain under debate. Some studies show that PPARγ agonists in the liver promote hepatic steatosis through upregulation of genes involved in lipid uptake and storage (Way et al., 2001). Other studies show that PPARγ agonists in the liver prevent hepatic steatosis and fibrosis, possibility by sequestering fatty acids in adipose tissue and preventing hepatic stellate cell activation (Mayerson et al., 2002; Musso et al., 2012) (Fig. I-2).

Studies in liver PPARγ knockout mice with adipose tissue, showed that they developed relative fat intolerance, increased adiposity, hyperlipidemia, and insulin resistance. PPARγ

exhibits an impaired plasma uptake of triglycerides (TGs) and TG deposition in muscle and adipose tissue, which contributes to insulin resistance. Thus hepatic PPARγ contributes to TG homeostasis, regulating both TG clearance and lipogenesis (Gavrilova et al., 2003) (Fig. I-2).

PPARγ is also expressed in pancreatic beta cells, where it induces the expression of major genes involved in glucose-stimulated insulin secretion (GSIS), and TZDs improves GSIS in insulin-resistant rodents and humans (Higa et al., 1999; Kim et al., 2002). However, results from *in vivo* studies have been conflicting, with one study showing alterations in beta-cell mass but no change in glucose homeostasis in beta-cells of PPARγ deficient mice and recent study showing that knockout of PPARγ in the whole pancreas results in hyperglycemia with impaired GSIS (Rosen et al., 2003) (Fig. I-2). Taken together, PPARγ plays an important role in various metabolic organ, but exact metabolic role of PPARγ is still on debate.

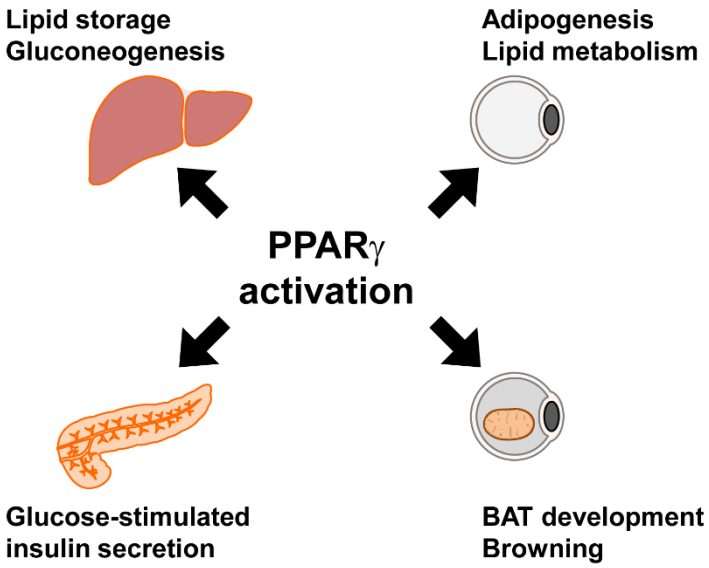

Figure I-2. Illustration of PPARγ activation effect on metabolism related organ
Metabolic responses that occur when PPARγ is activated in organs involved in metabolism such as liver, pancreas, WAT, BAT.

I-3. Histone deacetylases and HDAC3

3.1 General information of Histone deacetylases

Histone, as major components of chromatin, wraps DNA and regulates expression of DNA by its acetylation and deacetylation (Kruhlak et al., 2001). Levels of histone acetylation depend on the activities of histone acetylases (HATs) and Histone deacetylases (HDACs), which add or remove acetyl groups from protein substrates, respectively (Sun et al., 2003). HDACs are a class of enzymes that remove acetyl groups from amino acid on a histones (Sun et al., 2003). Generally, an increase in histone acetylation leads to remodeling of chromatin from condensed form to decondensed form, which subsequently causes transcriptional activation (Kazantsev and Thompson, 2008; Strahl and Allis, 2000). In other words, a decrease in histone acetylation causes chromatin structure to condense and result in transcriptional silencing. Therefore, HDACs play a role in suppressing gene expression in principle.

The superfamily of HDACs is classified five main subtypes depending on sequence homology; class I, IIa and IIb, and IV, and the structurally distinct class III (Gregoretti et al., 2004). Class I, II and IV are considered "classical" HDACs whose have a zinc ion dependent active site, while Class III is a family of NAD+-dependent enzymes known as sirtuins (Thiagalingam et al., 2003).

Class I HDACs consist of the ubiquitously expressed HDAC1, HDAC2 and HDAC3, and the muscle-specific expressed HDAC8. HDAC1 and HDAC2 are predominantly localized

in the nucleus, whereas HDAC3 shuttles between the nucleus and cytoplasm. HDAC1 and HDAC2 are almost identical and are components of stable transcriptional repressive complexes termed SIN3A, NuRD, CoReST and PRC2 complexes (Yang and Seto, 2003). These complexes are recruited to gene promoters by DNA binding proteins, which suggests gene specific rather than global transcriptional regulation (Wen et al., 2000). HDAC3 is found in distinct complexes such as the NCoR, SMRT complex (Yang et al., 2002), whereas no complex has been described for HDAC8 (Yang and Seto, 2008).

Class IIa HDACs consist of HDAC4, HDAC5, HDAC7 and HDAC9 with distinct tissue specific patterns of expression, predominantly in muscle and heart (Martin et al., 2007). These HDACs have conserved binding sites for the transcription factor myocyte enhancer factor 2 (MEF2) and the chaperone protein 14-3-3, which fine-tune HDACs signal responsive (Butler and Bates, 2006). Following phosphorylation by kinases, such as calcium/calmodulin-dependent protein kinase (CaMK) and protein kinase D (PKD), these HDACs bind 14-3-3 and shuttle from the nucleus to the cytoplasm (McKinsey et al., 2000). Modulated phosphorylation of lass IIa HDACs provide a mechanism for connecting extracellular signals with transcription and play an important role in many tissues during development and disease.

Class IIb HDACs consist of HDAC6 and HDAC10. HDAC6 is the main cytoplasmic deacetylase in mammalian cells and functions as deacetylation of a-tubulin and alters microtubule stability (Zhang et al., 2008). HDAC10 has been found in a complex with HDAC3, although the exact function of HDAC10 is not known (Fischer et al., 2002).

Class IV HDAC consist only of HDAC11. Expression of HDAC11 is enriched in the brain, heart, muscle, kidney and testis, but little is known about its function (Gao et al., 2002).

3.2 Physiological functions of HDAC3

HDAC3 is one of the Class I HDACs family. HDAC3 is present in a distinct complex that contains either NCOR or its homolog SMRT (Perissi et al., 2010). However, HDAC3 not only forms a complex with NCoR/SMRT but also requires interaction with the deacetylase activating domain (DAD) of NCOR/SMRT for its enzyme activity (Guenther et al., 2001). Inositol tetraphosphate molecule Ins(1,4,5,6)P4 (IP4) which embedded at the interface between HDAC3 and DAD stabilizes the interaction between HDAC3 and DAD (Watson et al., 2012). Interestingly, knockin mice with mutations in NCOR and SMRT DADs live to adulthood despite the undetectable deacetylase activity in the embryos. On the other hand, the global deletion of HDAC3 is embryonic lethal (You et al., 2013). This suggests HDAC3 deacetylase function is not essential for survival.

Deletion of HDAC3 in cardiomyocytes induced to an increase in ligand-induced lipid storage in the heart. In the heart, these genes that control fatty acid uptake and metabolism are under the control of the nuclear receptor PPARα, and the inhibition by loss of HDAC3 leads to metabolic disorder observed in diabetic cardiomyopathy. Furthermore, loss of HDAC3 in the heart results in robust interstitial fibrosis, which is phenotypically independent of PPARα activity. Overexpresion of HDAC3 in the heart leads to increased thickness of the myocardium, which is due to increased cardiomyocyte hyperplasia without

hypertrophy. In conclusion, Hdac3 is a novel regulator of cardiac myocyte proliferation during cardiac development (Trivedi et al., 2008).

Loss of HDAC3 in the liver impairs lipid and cholesterol homeostasis, leading to an accumulation of lipids and a decrease in glycogen storage. These changes are usually caused by inhibition of the gene program under the control of thyroid hormone receptors and nuclear hormone receptors such as PPARγ, which control the major steps of lipid and cholesterol biosynthesis in the early postnatal liver (Knutson et al., 2008). Liver specific Hdac3 deficient mice have higher insulin sensitivity without any changes in insulin signaling or body weight compared to wild-type mice. Perilipin 2, which coats lipid droplets, is induced upon Hdac3 depletion and contributes to both hepatic steatosis and improved glucose tolerance. Hdac3 depletion reroutes metabolic precursors towards lipid synthesis and storage within lipid droplets and away from hepatic glucose production (Sun et al., 2012).

I-4. Metabolic disorders

4.1 Obesity

Obesity is a medical condition that is caused by accumulating of excess body fat and negatively affect people's health. The World Health Organization has listed obesity as one of the top ten global health problems in Western cultures; some consider it the most dangerous disease in the world today (Heymsfield and Wadden, 2017). There are various factors that induce obesity; increasing per capita food supplies and consumption, decreasing time spent in physical activities; increasing usage of medicines that have weight gain as a side effect; insufficient sleep. These factors cause the energy balance to collapse and cause chronic weight gain (Heymsfield and Wadden, 2017).

Almost ten years ago, the cloning of the ob gene (encoding leptin) opened a new era of obesity research. Leptin is a fat-derived cytokine that is directly associated with body fat mass and transfers the energy state of the organism to the brain (Zhang et al., 1994). An abnormally leptin signaling is recognized as starvation by brain, leading to starvation and energy conservation even in the state of extreme obesity. The existence of this neuroendocrine system implies that excessive eating behavior is not just the will of the individual, but regulates by genes (Seeley and Woods, 2003). Another factor which relates with obesity, PPARγ is a master regulator of the differentiation of adipocytes and their ability to function normally. PPARγ is induced during adipocyte differentiation and forced expression of PPARγ in non-adipogenic cells effectively converts to mature adipocytes

(Tontonoz et al., 1994). In conclusion, recent research indicates that the genetic changes are also important, although the living environmental factors are important factor to cause obesity.

4.2 Hepatic steatosis

Hepatic steatosis is one of the most prevalent metabolic disorders in the world, defining the clinical characteristics of non-alcoholic fatty liver disease (NAFLD) (Cohen et al., 2011). Hepatic steatosis is an abnormal accumulation of TGs in the cytoplasm of hepatocytes (Fig. I-3). Hepatic steatosis is a premorbid condition, which increases the vulnerability of liver to progress to steatohepatitis and to more advanced stages of liver disease (Brunt and Tiniakos, 2010). In contrast to healthy livers, up-regulation of PPARγ expression is a common property of steatotic livers (Memon et al., 2000).

Consistent with these findings, hepatic PPARγ overexpression has been linked to exacerbated steatosis by activation of de novo lipogenesis and increased hepatic TG concentrations. Similarly, liver-specific knockout of PPARγ in obese *ob/ob* mice reduces hepatic lipid accumulation and reduces the expression of many genes important for lipid metabolism (Gavrilova et al., 2003; Matsusue et al., 2003). Moreover, the administration of TZD shows increased lipid storage and improves hepatic steatosis in NAFLD patients by the primary insulin sensitizing effect on adipose tissue (Ratziu et al., 2008). In contrast, prolonged treatment of TZD in obese KKA^{y} mice, which show elevated levels of PPARγ in the liver, results that severe hepatic steatosis may be present and adversely affect

intrahepatic lipid metabolism in people with altered liver expression of PPARγ (Bedoucha et al., 2001).

Overall, these results indicate that the precise role of PPARγ in hepatocytes and whether the expression level of PPARγ is a causative element or a consequence of hepatic steatosis, are still controversial.

.

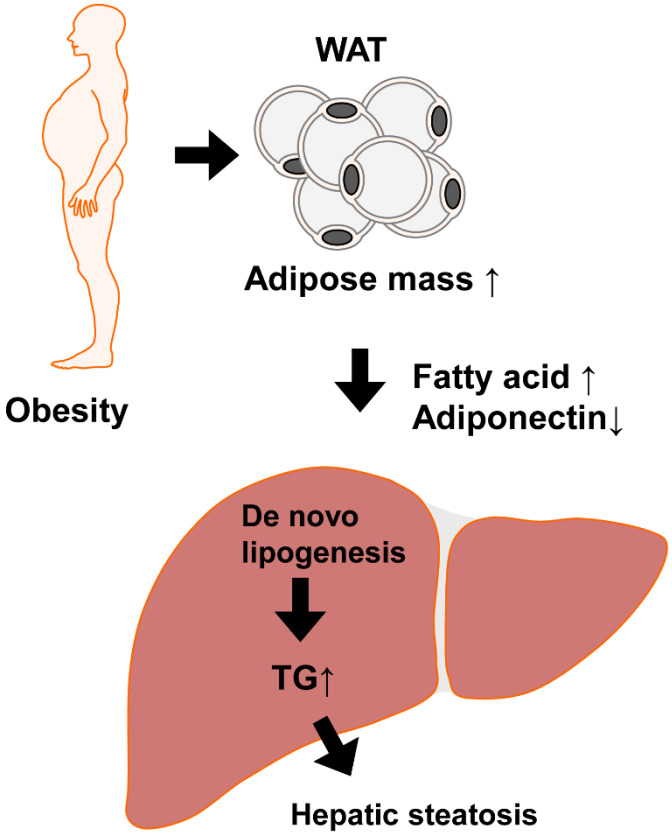

Figure I-3. Illustration of the process of hepatic steatosis progression
When obesity is induced by overeating or decline of physical activity, adipose mass is increased in WAT. Increased adipose mass leads to the production of fatty acids and inhibits the secretion of adiponectin. As a result, the de novo lipogenesis process in the liver becomes active, so that the production and accumulation of triglyceride are increased, resulting in hepatic steatosis.

CHAPTER II

Liver-specific *Rorα* deficient mice are susceptible to diet-induced obesity

II-1. Summary

RORα is known to be involved in various biological processes as an ONR whose ligand is yet defined. In the meantime, the in vivo function of RORα was studied using natural spontaneous RORα mutant mice, *Staggerer* mice. However, use of *Staggerer* mice has provided a limitation to the study on the in vivo function of RORα due to the side effect from ataxia.

To solve this problem, I generated RORα conditional knockout mice. Using these mice, I generated liver-specific *Rorα* deficient mice, which could be used to study function of RORα in the liver. When liver-specific *Rorα* deficient mice were given over-nutrient stress by feeding HFD, severe obesity and hepatic steatosis were induced in liver-specific *Rorα* deficient mice compared to WT mice. Thus, I observed that the weight and adipocyte size of WAT were also increased. By demonstrating the increased expression of inflammatory genes in WAT and the decreased expression of thermogenesis gene in BAT, I confirmed that genetic changes were also induced in adipose tissue due to obesity. Histological analysis showed that accumulation of lipid droplets in the liver of liver-specific *Rorα* deficient mice resulted in severe hepatic steatosis. Similar to adipose tissues, expression of genes involved in lipid synthesis and lipid sequestration was increased in the liver. Finally, the GTT and ITT experiments have confirmed that glucose tolerance and insulin sensitivity were also impaired. Together, I generated liver-specific *Rorα* deficient mice and found that the deficiency of RORα in liver leads to severe obesity and hepatic steatosis.

II-2. Introduction

Obesity is a medical condition in which the accumulation of fat is excessive. Thus, obesity is a high risk metabolic disorder, leading to various complications, including cardiovascular disease, hyperlipidemia, and type II diabetes (Despres and Lemieux, 2006; Heymsfield and Wadden, 2017). Ectopic accumulation of fat in various tissues activates numerous cellular stress and inflammatory signaling pathways, resulting in insulin resistance, pancreatic β cell dysfunction, and hepatic steatosis (Rutkowski et al., 2015). Hepatic steatosis is a typical NAFLD disease caused by the accumulation of liver fat. It is known that when hepatic steatosis exacerbates, it progresses to hepatitis, liver cirrhosis and liver cancer (Cohen et al., 2011). The liver is the central metabolic organ to regulate key aspects of glucose and lipid metabolism including gluconeogenesis, fatty acid β-oxidation, lipoprotein uptake and secretion, and lipogenesis (van den Berghe, 1991). Given that portal vein is a critical path to convey insulin signaling from pancreas during fed state, the hepatic glucose and lipid metabolism are directly under control of nutrient signaling.

Dysregulation of hepatic lipid metabolism results in the development of hepatic steatosis, contributing to the chronic insulin resistance and steatotic hepatitis (Browning and Horton, 2004). The hepatic metabolic pathways are governed by highly dynamic transcriptional networks of orphan nuclear receptors (ONRs), including PPARs, farnesoid X receptor (FXR), and liver X receptor (LXR) (Chawla et al., 2001a). Many ONRs are expressed in tissues involved in metabolism, such as skeletal muscle, adipose tissue, and liver (Bookout et al., 2006), and play critical roles in the regulation of metabolism (Pearen

and Muscat, 2012). Genetic studies have shown that many ONRs regulate nutrient metabolism and physiology of obesity and type II diabetes (Li et al., 2009). Given that numerous synthesized ligands for ONRs are used for developing putative drugs for human metabolic diseases (Katz et al., 2009), ONRs are emerging as therapeutic targets for the treatment of metabolic diseases.

Previously, RORα, a member of ONRs, possesses tumor suppressive function by transrepressing canonical Wnt/β-catenin signaling leading to inhibition of colon cancer growth and by increasing p53 stability upon DNA damage response (Kim et al., 2011; Lee et al., 2010). However above all, RORα is known to regulate cerebellum development (Vogel et al., 2000). The *Staggerer* mice, natural *Rorα* spontaneous mutant mice, display ataxia and severe cerebellar atrophy (Doulazmi et al., 1999). Moreover, RORα functions to regulate circadian rhythm as a key regulator of the cyclic expression of BMAL1 together with REV-ERBα (Guillaumond et al., 2005). The RORα/REV-ERBα feedback loop controls the circadian expression pattern of BMAL1, indicating that RORα plays a key role in the core circadian clock (Sato et al., 2004). In addition, *Staggerer* mice show lower expression levels of genes involved in lipid metabolism, including apolipoprotein A-1 (*apoA1*) and apolipoprotein C-III (*apoCIII*) (Mamontova et al., 1998; Vu-Dac et al., 1997). Besides, the expression of several genes involved in the main and alternative pathway of triglyceride synthesis, including Gpam, Agpat9 and Mogat1 were significantly diminished in *Staggerer* mice liver. Thus, *Staggerer* mice exhibit less body weight gain compared with wild-type (WT) mice despite their higher food consumption (Lau et al., 2008). When

Staggerer mice get old, exhibit a reduced body fat index. Adipocytes are smaller in brown and white adipose tissue of *Staggerer* mice than WT mice and the level of triglycerides is lower in liver of *Staggerer* mice than WT mice (Kang et al., 2011). However, when RORα is overexpressed in liver by adenovirus infection system, lipid accumulation, hepatic steatosis, and expression of genes involved in lipogenesis are reduced (Kim et al., 2012). The reason for this contradiction is that *Staggerer* mice have huge cerebellar defects, it is still possible that physiological changes observed in *Staggerer* mice are indirect effects. Thus, the physiological roles of RORα to control transcriptional networks to modulate lipogenesis and gluconeogenesis still remain unclear.

In this study, I report that RORα plays a key role to control hepatic lipid metabolism to protect against diet-induced obesity and hepatic steatosis, using liver-specific *Rorα* deficient mouse model. HFD-fed liver-specific *Rorα* deficient mice ($ROR\alpha^{LKO}$ mice) show severe metabolic defects, including hepatic steatosis, obesity, and insulin resistance, although no physiological changes have been observed with control diet (CD).

II-3. Results

Generation of conditional *Rorα* deficient mice

To determine the physiological roles of RORα in the liver, I generated Rorα floxed mice (hereafter named RORα$^{f/f}$) by gene targeting in ES cells (Fig. II-1A). To generate mice with a floxed RORα allele, FRT-flanked puromycin cassette containing a loxP sequence was inserted at the front of RORα exon 4 and the single loxP site was inserted at the back of RORα exon 5. Then, this targeted vector was electroporated to E14Tg2A ES cells. Surviving clones of ES cells after puromycin selection were expanded and analyzed by Southern blot to confirm for recombinant ES clones. After BamHI digestion, the bands representing WT and mutant alleles are 9.0 and 6.8 kb, respectively (Fig. II-1B). ES cells were injected into the C57BL/6 blastocyst to produce chimeras, then male chimeras were mated with C57BL/6 female mice to select for germline transmission. After that, I crossed Rorα floxed mice with Albumin-Cre (Alb-Cre) mice to selectively create liver-specific *Rorα* conditional knockout (KO) mice (hereafter named RORα^{LKO}) (Fig. II-1C).

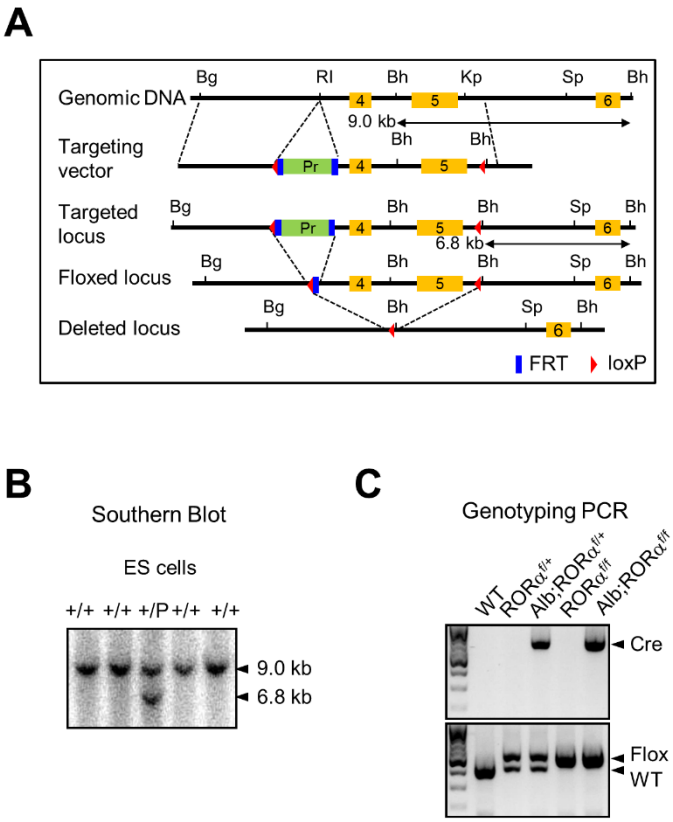

Figure II-1. Generation of conditional *Rorα* deficient mouse

(**A**) Schematic representation of the *Rorα* gene-targeting strategy to generate a hepatic-specific *Rorα* deficient mouse, including a map of the RORα exon 4 and 5 allele (yellow box) and the targeting vector with loxP sites (red arrowhead), FRT sites (blue box), and puromycin selection gene (Pr, green box). Bg: BglII, RI: EcoRI, Bh: BamHI, Kp: KpnI, Sp: SpeI. (**B**) Southern blot analysis to screen correctly targeted Rorα +/puro ES cell clones. For BamHI digestion, the bands representing WT and mutant alleles were 9.0 kb and 6.8 kb, respectively. (**C**) PCR analyses with genomic DNA extracted from tail of WT, RORα$^{f/+}$, Alb; RORα$^{f/+}$, RORα$^{f/f,}$ and Alb; RORα$^{f/f}$ mice are shown. PCR were performed to amplify the cre (top), floxed and deleted allele (bottom) with indicated primers.

RORα has no effect the development of the liver

To ensure that the liver-specific RORα knockout mice were made correctly, I checked the mRNA and protein levels of hepatic RORα. The mRNA and protein levels of endogenous hepatic RORα were remarkably depleted in RORα^{LKO} mice compared with littermate controls, RORα$^{f/f}$ in both liver and primary hepatocyte (Fig. II-2A-D). Above all, it is well known that RORα is involved in the development of the cerebellar. Therefore, I examined whether there is any defect in the liver developmental process of RORα^{LKO} mice as RORα can affect the liver development process. H&E staining of 12 weeks old RORα$^{f/f}$ and RORα^{LKO} mice liver showed no significant defect in the liver developmental process (Fig. II-2E). Through this, further research is proceeded based on the fact that the liver development process is normal.

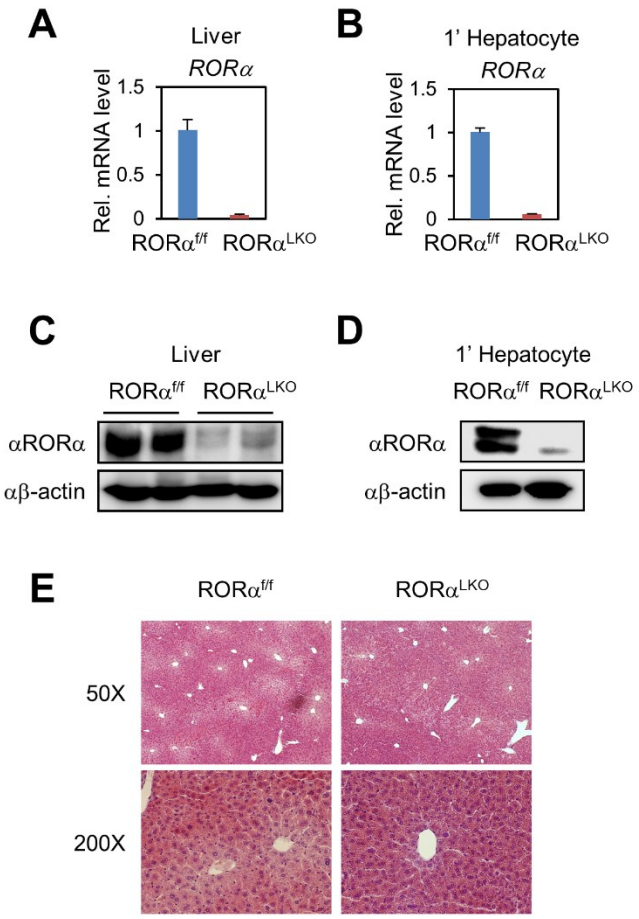

Figure II-2. Identification of RORα deficiency and the liver developmental process in RORα^{LKO} mice

(**A** and **B**) mRNA expression level of *RORα* in liver extract (**A**) and primary hepatocyte (**B**) from RORα$^{f/f}$ and RORα^{LKO} mice. Expression was normalized to 18s rRNA expression. Data expressed as mean ± S.E.M. (**C** and **D**) Protein expression level of RORα in liver extract (**C**) and primary hepatocyte (**D**). (**E**) Representative image of liver from 12 weeks old RORα$^{f/f}$ and RORα^{LKO} mice stained with hematoxylin and eosin. Magnification is shown in the figure.

Metabolic changes are not observed in liver specific RORα knockout mice at normal conditions

In previous experiments, I observed that RORα did not have a significant effect in the liver developmental process; after that I examined whether metabolic changes occurred in RORα^{LKO} mice. Body composition analysis revealed that RORα^{LKO} mice exhibited similar fat/lean mass, free body fluid and adipocytes size with those of RORα$^{f/f}$ when RORα$^{f/f}$ and RORα^{LKO} mice fed CD during 10 weeks from 8 weeks old (Fig. II-3A, B). Then, I examined metabolic changes in RORα$^{f/f}$ and RORα^{LKO} mice fed CD using the metabolic cage system. As a result, no obvious changes were observed between CD-fed RORα$^{f/f}$ and RORα^{LKO} mice. O2 consumption, CO2 production, respiratory exchange ratio, energy expenditure and food consumption were very similar in CD-fed RORα$^{f/f}$ and RORα^{LKO} mice (Fig. II-3C-G). These results suggest that RORα^{LKO} mice do not show metabolic changes under normal conditions of feeding CD.

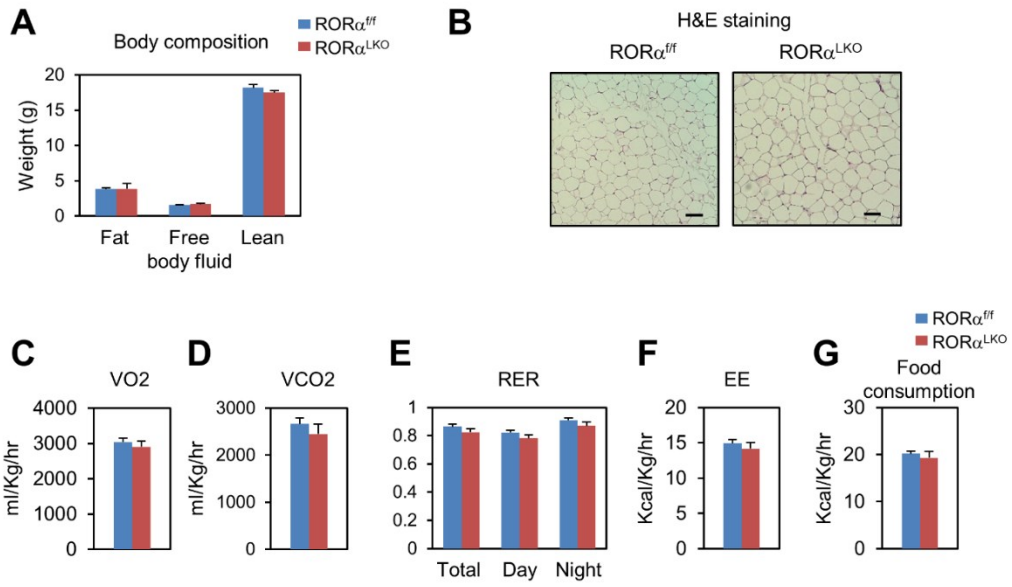

Figure II-3. Metabolic characterization of RORα$^{f/f}$ and RORα^{LKO} mice fed CD

(**A**) Body composition analysis of RORα$^{f/f}$ and RORα^{LKO} mice fed CD for 10 weeks (n=6/group). (**B**) Representative image of eWAT from RORα$^{f/f}$ and RORα^{LKO} mice fed CD for 10 weeks stained with hematoxylin and eosin. Scale bar, 100 μm. (**C-G**) Metabolic cage studies were performed in RORα$^{f/f}$ and RORα^{LKO} mice fed CD for 10 weeks (n=6 mice/group). O_2 consumption (VO2) (**C**), CO_2 production (VCO2) (**D**), respiratory exchange ratio (RER) (**E**), energy expenditure (EE) (**F**) and food consumption (**G**) were represented. Data expressed as mean ± S.E.M.

High fat diet induces extraordinary obesity in liver-specific *Rorα* deficient mice

To determine RORα affects metabolism in the liver, I decided to observe metabolic changes in RORα$^{f/f}$ and RORα^{LKO} mice under metabolic stress conditions like feeding HFD. First, I measured the growth rate of RORα^{LKO} mice and observed that they attained body weights similar to RORα$^{f/f}$ mice fed CD during 10 weeks from 8weeks old (Fig. II-4A). However, when placed on a HFD, RORα^{LKO} mice exhibited a significant increase of the weight gain (20 vs. 25 gram) compared with their RORα$^{f/f}$ littermates, resulting in extraordinary obesity (Fig. II-4A). Body composition analysis and macroscopic view revealed that RORα^{LKO} mice had more fat mass (Fig. II-4B, C). All white and brown fat depots from RORα^{LKO} mice were significantly increased in mass relative to RORα$^{f/f}$ (Fig. II-4D). During obesity, adipose tissue expands by hyperplastic and/or hypertrophic growth. The cross-sectional area of adipocytes in visceral fat tissue was markedly increased in RORα^{LKO} mice compared with RORα$^{f/f}$ mice (Fig. II-4E).

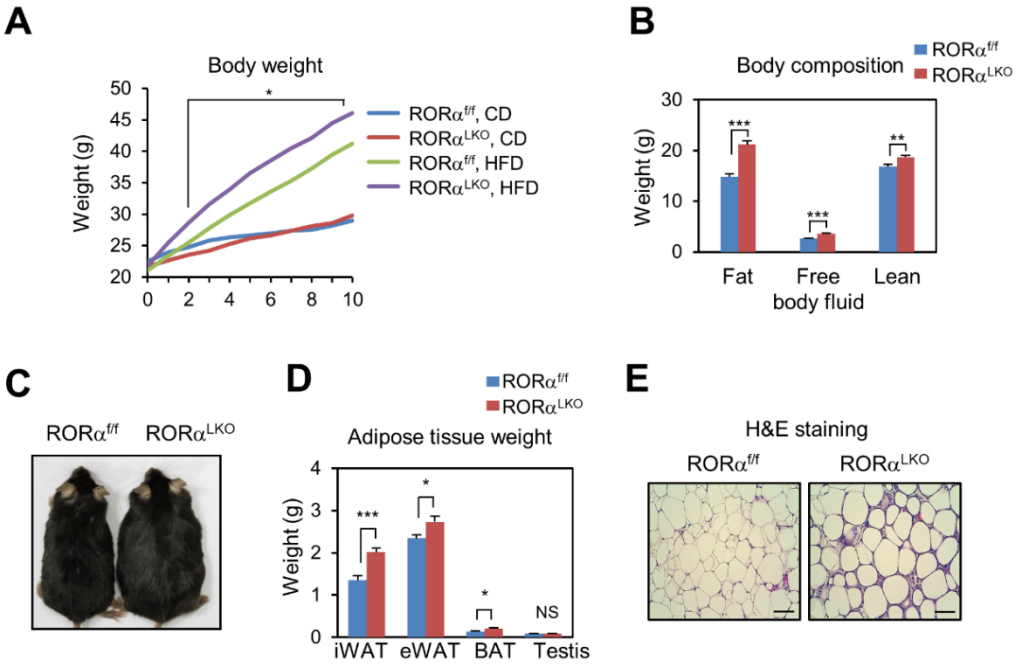

Figure II-4. Liver-specific *Rorα* deficient mice are susceptible to diet-induced obesity
(**A**) Body weight change in RORα$^{f/f}$ and RORα^{LKO} mice fed CD or HFD for 10 weeks (n=9-12/group). Data expressed as mean ± S.E.M. Statistical analysis was performed using Student's unpaired t-test. *p<0.05, RORα$^{f/f}$ vs. RORα^{LKO}, HFD. (**B**) Body composition analysis of RORα$^{f/f}$ and RORα^{LKO} mice fed HFD for 10 weeks (n=6/group). Data expressed as mean ± S.E.M. Statistical analysis was performed using Student's unpaired t-test. **p<0.01, ***p<0.001. (**C**) Macroscopic views of body size in RORα$^{f/f}$ and RORα^{LKO} mice. (**D**) Adipose tissue weight of RORα$^{f/f}$ and RORα^{LKO} mice fed HFD for 10 weeks (n=6-7/group). Data expressed as mean ± S.E.M. Statistical analysis was performed using Student's unpaired t-test. *p<0.05, ***p<0.001, NS=Non-Significant. (**E**) Representative image of eWAT from RORα$^{f/f}$ and RORα^{LKO} mice fed HFD for 10 weeks stained with hematoxylin and eosin. Scale bar, 100 μm.

Expression of pro-inflammatory genes in white adipose tissue and thermogenesis genes in brown adipose tissue is abnormal in HFD-fed liver-specific *Rorα* deficient mice

Through H&E staining of eWAT, I confirmed that macrophage infiltrated into eWAT of RORα^{LKO} mice and eWAT of RORα^{LKO} mice formed crown-like shape. This is a histological evidence that inflammation is increased in adipocytes by obesity. In addition, through previous studies, several proinflammatory factors are produced in adipose tissue with increasing obesity. Compared with that of lean mice, adipose tissue in obese mice shows higher expression of pro-inflammatory genes (Samad et al., 1998). Therefore, I examined expression level of pro-inflammatory genes in eWAT. Consequentially, induction of pro-inflammatory genes, including *Mcp1, Ifnγ*, and *F4/80* in visceral fat depot were potentiated in RORα^{LKO} mice (Fig. II-5A).

The activities of brown adipose tissue reduce metabolic disorder, including obesity. Expression of genes that induce thermogenesis in brown adipose tissue is reduced when mice are obese (Harms and Seale, 2013). Consistent with a significant weight gain in HFD-fed RORα^{LKO} mice, gene expression analysis revealed reduction of *Pgc1α*, as well as a number of genes involved in thermogenesis, mitochondrial biogenesis, and fatty acid oxidation in brown adipose tissue of RORα^{LKO} mice compared with that of RORα$^{f/f}$ littermates (Fig. II-5B).

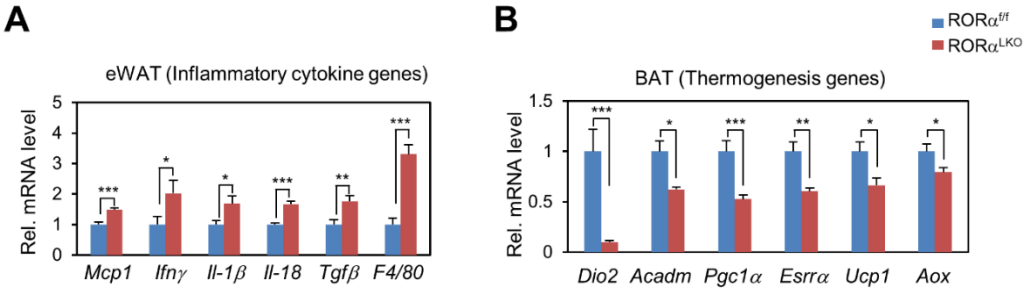

Figure II-5. Expression of inflammatory cytokine genes in eWAT and thermogenesis genes in BAT is impaired in HFD-fed RORα^{LKO} mice

(**A**) Expression levels of inflammatory cytokine genes in eWAT extract from RORα$^{f/f}$ and RORα^{LKO} mice fed HFD for 10 weeks (n=4-5/group) as determined by qRT-PCR. Expression was normalized to L32 expression. (**B**) Expression levels of thermogenesis genes in BAT extract from RORα$^{f/f}$ and RORα^{LKO} mice fed HFD for 10 weeks (n=4-5/group) as determined by qRT-PCR. Expression was normalized to L32 expression. Data expressed as mean ± S.E.M. Statistical analysis was performed using Student's unpaired t-test. *p<0.05, **p<0.01, ***p<0.001.

Whole-body metabolic rate and production of bile acid reduce in HFD-fed RORα^{LKO} mice

The observation that energy expenditure in brown fat has been impaired in HFD-fed RORα^{LKO} mice led us to examine whether they have global metabolic defects. Although no obvious defects were observed in CD-fed mice (Fig. II-3C-G), HFD-fed RORα^{LKO} mice were found to produce far less CO_2, consume less O_2 and expend less energy than RORα$^{f/f}$ littermates, indicating that oxidative phosphorylation is impaired by the hepatic deletion of RORα (Fig. II-6A-C). However, RER and food consumption were no difference between RORα$^{f/f}$ and RORα^{LKO} mice (Fig. II-6D, E).

Previously, bile acids have been reported to increase energy expenditure by promoting intracellular thyroid hormone activation in brown adipose tissue (Watanabe et al., 2006) (Fig. II-7). I observed that expression of key genes involved in hepatic bile acid synthesis was remarkably reduced in HFD-fed RORα^{LKO} mice (Fig. II-8A). Consistently, serum bile acid pool sizes in HFD-fed RORα^{LKO} mice were markedly less than RORα$^{f/f}$ littermates (Fig. II-8B), implicating that reduction of bile acid synthesis and bile acid pool size led to reduced energy expenditure in brown adipose tissue of HFD-fed RORα^{LKO} mice.

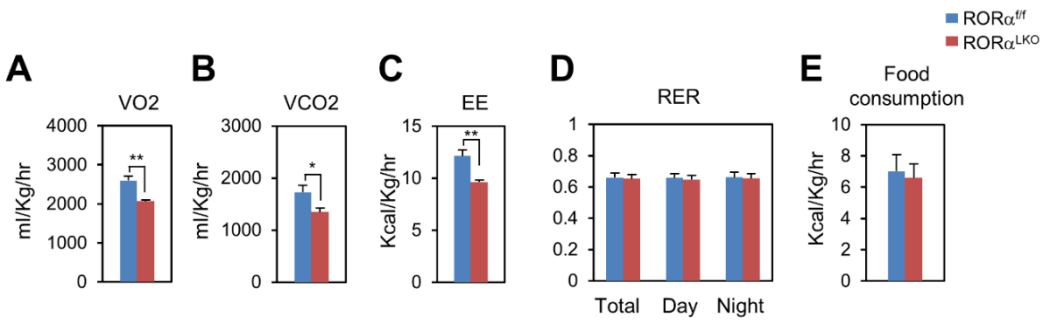

Figure II-6. Whole-body metabolic rate is depressed in HFD-fed RORα^{LKO} mice
(**A-E**) Metabolic cage studies were performed in RORα$^{f/f}$ and RORα^{LKO} mice fed HFD for 10 weeks (n=5-6 mice/group). O2 consumption (VO2) (**A**), CO2 production (VCO2) (**B**), respiratory exchange ratio (RER) (**C**), energy expenditure (EE) (**D**) and food consumption (**E**) were represented. Data expressed as mean ± S.E.M. Statistical analysis was performed using Student's unpaired t-test. *p<0.05, **p<0.01, ***p<0.001.

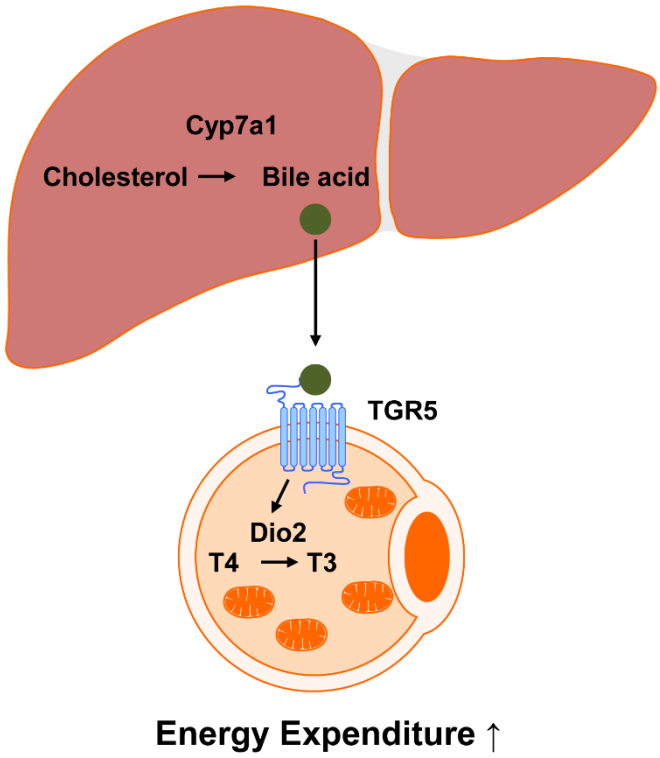

Figure II-7. Illustration of increased energy expenditure of BAT by bile acid
The synthesis of bile acid from cholesterol is increased by the Cyp genes in the liver. The bile acid is secreted from the liver and binds to TGR5 of BAT. Activated TGR5 increases the expression of Dio2 that converts inactive thyroxine (T4) into active 3,5,3′-triiodothyronine (T3), then stimulates energy expenditure in BAT.

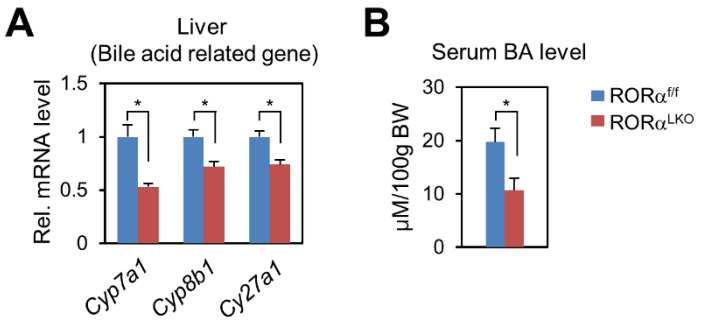

Figure II-8. Expression of hepatic bile acid related genes and serum bile acid pool size are decreased in RORα^{LKO} mice fed HFD

(**A**) Expression levels of bile acid related genes in liver extract from RORα$^{f/f}$ and RORα^{LKO} mice fed HFD for 10 weeks (n=7/group) as determined by qRT-PCR. Expression was normalized to 36B4 expression. (**B**) Bile acid level of serums that were collected from RORα$^{f/f}$ and RORα^{LKO} mice fed HFD for 10 weeks (n=6/group). BW, body weight. Data expressed as mean ± S.E.M. Statistical analysis was performed using Student's unpaired t-test. *p<0.05.

RORα protects against HFD-induced hepatic steatosis

Obesity is largely associated with hepatic steatosis in humans as well as in rodents. Consistent with obese phenotype in RORα^{LKO} mice, large lipid vesicles with increased amounts were observed in the hepatocytes of HFD-fed RORα^{LKO} mice (Fig. II-9A), whereas no difference was observed in CD-fed RORα$^{f/f}$ and RORα^{LKO} mice because CD-fed RORα$^{f/f}$ and RORα^{LKO} mice had no significant phenotypically difference (Fig. II-9B). Macroscopically, liver from HFD-fed RORα^{LKO} mice was markedly enlarged and paler compared with HFD-fed RORα$^{f/f}$ liver (Fig. II-9C). Consistently, HFD-fed RORα^{LKO} mice exhibited a remarkable increase of liver weight compared with HFD-fed RORα$^{f/f}$ mice (Fig. II-9D). In accordance with hematoxylin and eosin staining, oil red O staining, and hepatic triglyceride (TG) analysis showed a dramatic increase in lipid level in the HFD-fed RORα^{LKO} liver compared with the HFD-fed RORα$^{f/f}$ liver, whereas no difference was observed in CD-fed RORα$^{f/f}$ and RORα^{LKO} mice (Fig. II-9E-G). While hepatic gene expression profiles were similar among CD-fed genotypes (Fig. II-10A), hepatic gene expression profiles of lipogenesis, gluconeogenesis, and lipid sequestration in the HFD-fed RORα^{LKO} were largely increased, indicating that RORα protects against HFD-induced hepatic steatosis (Fig. II-10B).

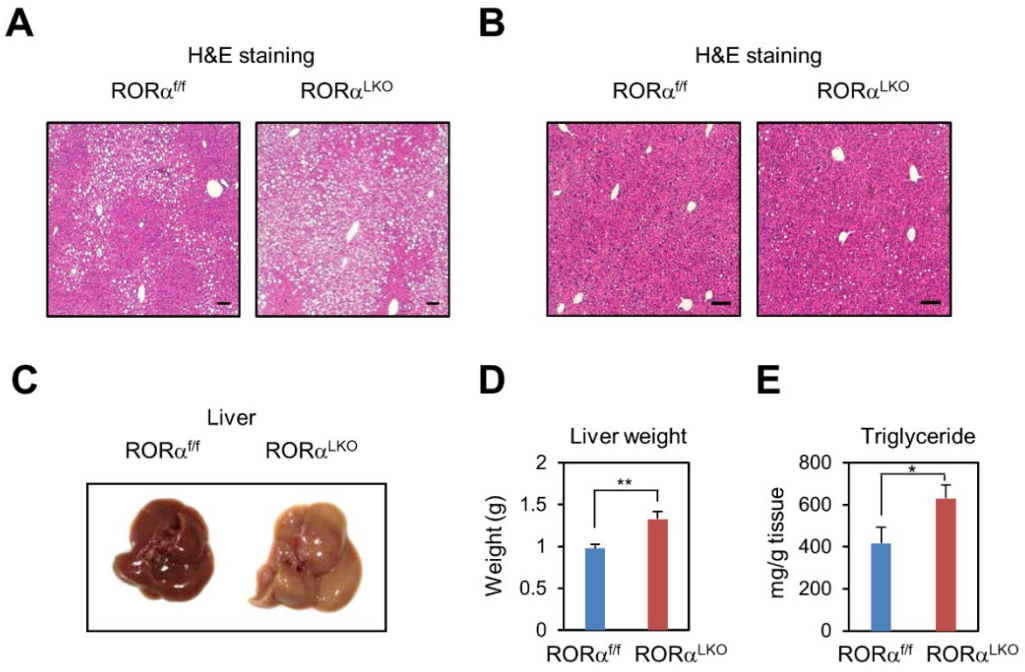
A
H&E staining
RORα f/f
RORα LKO
B
H&E staining
RORα f/f
RORα LKO
C
Liver
RORα f/f
RORα LKO
D
Liver weight
Weight (g)
2
1.5
1
0.5
0
**
RORα f/f
RORα LKO
E
Triglyceride
mg/g tissue
800
600
400
200
0
*
RORα f/f
RORα LKO

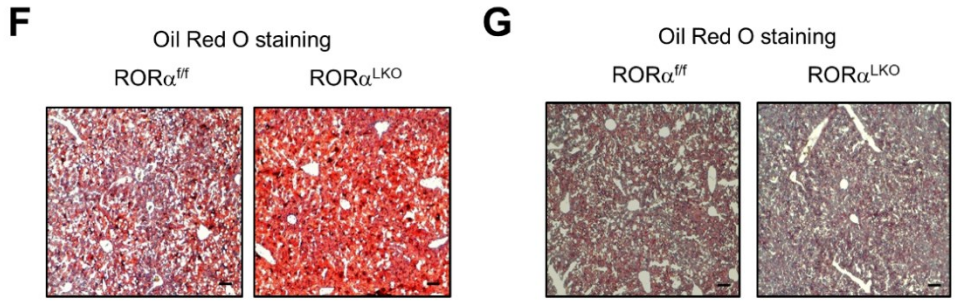
F
Oil Red O staining
RORα f/f
RORα LKO
G
Oil Red O staining
RORα f/f
RORα LKO

Figure II-9. Liver-specific *Rorα* deficient mice are susceptible to diet-induced hepatic steatosis

(**A-G**) RORα$^{f/f}$ and RORα^{LKO} mice were fed with HFD or CD for 10 weeks. (**A** and **B**) Representative liver histological section images of HFD-fed RORα$^{f/f}$ and RORα^{LKO} mice (**A**) or CD-fed RORα$^{f/f}$ and RORα^{LKO} mice (**B**) stained with hematoxylin and eosin. Scale bar, 100 μm. (**C**) Macroscopic view of livers from HFD-fed RORα$^{f/f}$ and RORα^{LKO} mice. (**D**) Liver weights of HFD-fed RORα$^{f/f}$ and RORα^{LKO} mice (n=10-11/group). Data expressed as mean ± S.E.M. Statistical analysis was performed using Student's unpaired t-test. **p<0.01. (**E**) Triglyceride content of livers from HFD-fed RORα$^{f/f}$ and RORα^{LKO} mice (n=8/group). Data expressed as mean ± S.E.M. Statistical analysis was performed using Student's unpaired t-test. *p<0.05. (**F** and **G**) Representative liver histological section images of HFD-fed RORα$^{f/f}$ and RORα^{LKO} mice (**F**) or CD-fed RORα$^{f/f}$ and RORα^{LKO} mice (**G**) stained with Oil Red O. Scale bar, 100 μm.

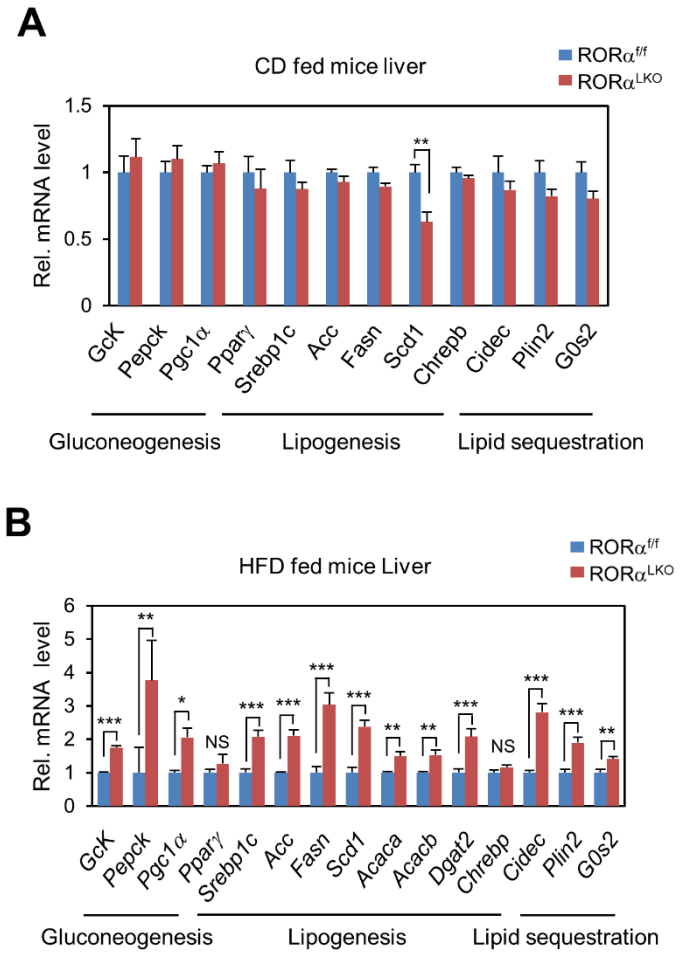

Figure II-10. Expression of hepatic lipid metabolism related genes is increased in the liver of RORα^{LKO} mice fed HFD but is no obvious change in the liver of RORα^{LKO} mice fed CD

(**A** and **B**) RORα$^{f/f}$ and RORα^{LKO} mice were fed with HFD or CD for 10 weeks. Hepatic gene expression profile involved in metabolism from the livers of CD-fed RORα$^{f/f}$ and RORα^{LKO} mice (n=5/group) (**A**) or HFD-fed RORα$^{f/f}$ and RORα^{LKO} mice (n=4/group) (**B**) as determined by qRT-PCR. Expression was normalized to 36B4 expression. Data expressed as mean ± S.E.M. Statistical analysis was performed using Student's unpaired t-test. *p<0.05, **p<0.01, ***p<0.001, NS=Non-Significant.

Hepatic steatosis impairs insulin sensitivity in liver-specific *Rorα* deficient mice

Obesity and hepatic steatosis often predispose rodents and humans to impaired glucose homeostasis and insulin resistance (Kahn and Flier, 2000; Moller and Kaufman, 2005). Hepatic deficiency of RORα resulted in elevated fasting insulin levels in RORα^{LKO} mice (Fig. II-11A). As elevated fasting insulin level is an indication of insulin resistance, RORα^{LKO} mice predisposed to severe insulin resistance than RORα$^{f/f}$ mice. Consistent with elevated fasting insulin level, an investigation of insulin signaling pathways confirmed reduction of phosphorylated AKT, indicating that insulin signaling was impaired in HFD-fed RORα^{LKO} mice (Fig. II-11B). As insulin signaling was impaired in the liver, I performed glucose tolerance tests (GTTs) and insulin tolerance tests (ITTs) to determine if glucose homeostasis was impaired in HFD-fed RORα^{LKO} mice. Glucose intolerance and insulin resistance were observed in HFD-fed RORα^{LKO} mice, although CD-fed RORα^{LKO} mice exhibited little or no difference in glucose homeostasis compared with CD-fed RORα$^{f/f}$ mice (Fig. II-11C, D). Altogether, my data strongly demonstrate that hepatic RORα is required for prevention against insulin resistance.

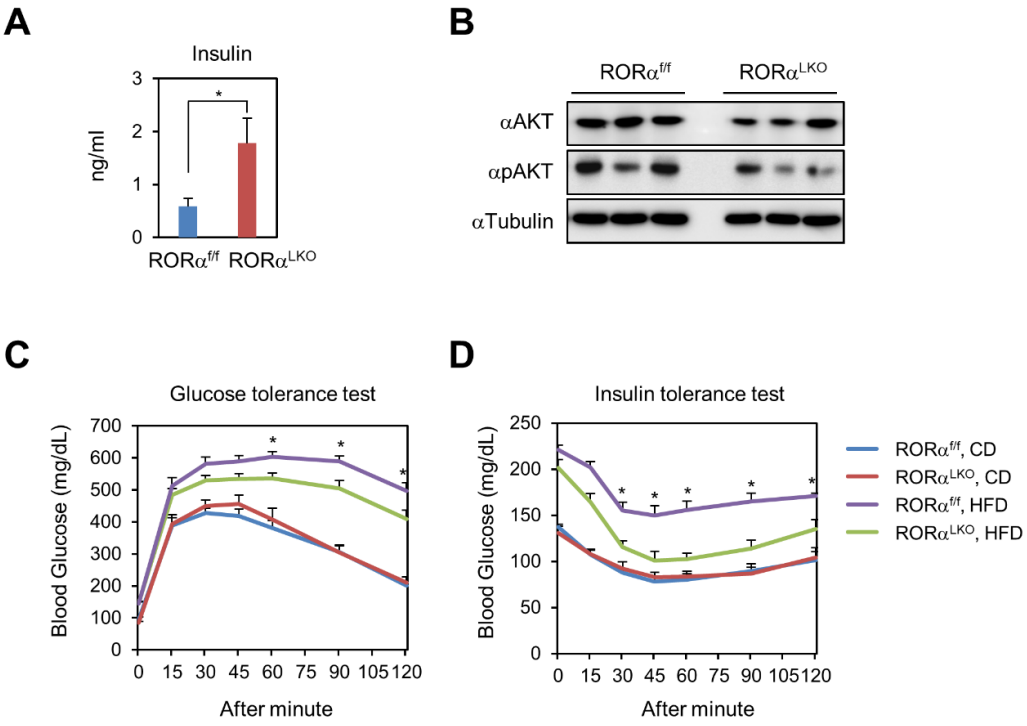

Figure II-11. Insulin sensitivity is impaired in liver-specific *Rorα* deficient mice
(**A**) Fasting insulin levels in HFD-fed RORα$^{f/f}$ and RORα^{LKO} mice (n=6-7/group). Data expressed as mean ± SEM. Statistical analysis was performed using Student's unpaired t-test. *p<0.05. (**B**) Immunoblot analysis was performed from liver extracts of HFD-fed RORα$^{f/f}$ and RORα^{LKO} mice. (**C** and **D**) Glucose tolerance test (GTT) (**C**) and insulin tolerance test (ITT) (**D**) on RORα$^{f/f}$ and RORα^{LKO} mice fed on CD or HFD for 10 weeks. (n=4-9/group). Data expressed as mean ± S.E.M. Statistical analysis was performed using Student's unpaired t-test. *p<0.05, RORα$^{f/f}$ vs RORα^{LKO}, HFD.

II-4. Discussion

In this study, I generated and used RORα conditional knockout mice instead of natural RORα spontaneous mutant mice, *Staggerer* mice. Until this time, *Staggerer* mouse was inevitable for in vivo study of RORα. In *Staggerer* mice, physical behavior is restricted by its ataxia and cerebellar atrophy, so the physiological side-effect was very great that it was difficult to study about in vivo function of RORα (Doulazmi et al., 1999). However, this study allowed to study in vivo function of RORα in various organs using RORα conditional knockout mice.

RORα is known to participate in the regulation of various metabolic processes including lipid metabolism. In particular, studies using *Staggerer* mice confirmed that the expression of genes involved in TG production and lipogenesis is decreased (Kang et al., 2011; Lau et al., 2008). As a result, *Staggerer* mice are less obese and progression of hepatic steatosis is slower, and the size of adipocyte is also smaller than that of wild type mice. However, when RORα was overexpressed in the liver, it was found that the progress of hepatic steatosis was rather slow. Thus, the role of RORα in the regulation of metabolic processes in the liver was controversial due to limitations of studies using *Staggerer* mice.

In this study, liver-specific *Rorα* deficient mice were generated and available for research. When liver-specific *Rorα* deficient mice were fed the HFD, it was surprisingly found that size of adipocytes and weight gain were increased unlike *Staggerer* mice. Various metabolic rates of liver-specific *Rorα* deficient mice also decreased due to obesity. The expression of inflammatory genes in WAT and thermogenesis genes in BAT were decreased in liver-

specific *Rorα* deficient mice. In addition, hepatic steatosis was more severe than wild type mice and TG accumulation in the liver was also increased. The expression of genes involved in lipogenesis and lipid sequestration in the liver was increased. Finally, I confirmed that glucose tolerance and insulin sensitivity in liver-specific *Rorα* deficient mice were impaired by GTT and ITT experiments. All of these phenomena did not occur when mice fed CD, but only when mice fed HFD. Previous studies have shown that RORα plays a role in mitigating stress under environmental stress. In other words, in the liver, RORα plays a protective role under the stress condition such as feeding HFD.

II-5. Materials and Methods

Generation of conditional *Rorα* deficient mice and animal care

To generate mice with a floxed RORα allele, a 16.5-kb region used to construct the targeting vector was first subcloned from a BAC clone (bMQ-293I20, Source BioScience) into a pBluescript phagemid system. The FRT-flanked puromycin cassette containing a loxP sequence was inserted at the front of exon 4 and the single loxP site was inserted at the back of exon 5. The target region was ~15.2 kb which included exon 4 and 5. Twenty micrograms of the targeting vector was linearized by SalI and then electroporated to E14Tg2A ES cells. Surviving clones after puromycin selection were expanded and analyzed by Southern blot to confirm recombinant ES clones. After BamHI digestion, the bands representing WT and mutant alleles are 9.0 and 6.8 kb, respectively. Targeted ES cells were selected for microinjection into C57BL/6 blastocysts to generate chimeras. The male chimeras were bred with C57BL/6 female mice to select for germline transmission. To remove the puromycin selection cassette, targeted heterozygous F1 was crossed with Flp deleter strain (FLPeR mice, The Jackson Laboratory strain 003946). The mice were backcrossed to C57BL/6 then crossed with Alb-Cre mice (The Jackson Laboratory strain 003574) to generate liver-specific *Rorα* deficient mice. Male RORα$^{f/f}$ and RORα^{LKO} mice at 8 weeks of age were fed a CD or a 60% kcal fat HFD (Research diet, D12492) during 10 weeks. The sample sizes for all animal studies were announced in each figure legend. Mice were housed in a specific pathogen-free AAALAC-accredited facility under controlled conditions of

temperature (25°C) and light (12 hr light:12 hr dark, lights switched on at 7:00 AM). Food and water were available ad libitum. All mice used in these experiments were backcrossed to C57BL/6 at least seven generations. The primers used in PCR analysis for genotyping floxed alleles are: forward 5′-GCTTGTGGGTTTCTCCTACA-3′ and reverse 5′-GCAGCAAGTGTTGTGTCCCA-3′. This study was reviewed and approved by the Institutional Animal Care and Use Committee (IACUC) of National Cancer Center Research Institute.

Body composition

Fat and lean body masses were assessed by ^{1}H magnetic resonance spectroscopy (Bruker BioSpin).

Indirect calorimetry

Oxygen consumption (VO2), carbon dioxide production (VCO2), respiratory exchange ratios (RER), energy expenditure (EE) and food consumption were measured using an indirect calorimetry system PHENOMASTER (TSE System). Mice in each chamber were maintained at a constant environmental temperature of 22 °C.

Isolation and culture of primary mouse hepatocytes

Mouse primary hepatocytes were isolated from the liver of 8 weeks old male ROR$\alpha^{f/f}$ and RORα^{LKO} mice or WT and PPARα null mice. The hepatocyte isolation method used was

described previously (Kang et al., 2016). Dissociation into individual hepatocytes was performed in Dulbecco's modified Eagles' medium (DMEM) (Welgene) containing 10% heat-inactivated FBS, 1% antibiotics, 20mM HEPES, 100 nM insulin, 1 nM dexamethasone. For each hepatocyte preparation, cell viability was estimated by the exclusion of trypan blue.

Total bile acid (TBA) measurement

The quantitative determination of TBA of mice serum that was collected after centrifugation of mice blood was measured using the total bile acids assay kit (DZ042A-K, Diazyme Laboratories), according to the manufacturer's instructions.

Histology

When mice were sacrificed by CO_2 exposure, livers and WATs were rapidly fixed in 10% formalin (Sigma) at 4°C overnight. After fixation, tissues were sequentially dehydrated in ethanol with increasing concentrations ranging from 50 % to 100 %. Dehydrated specimens were subsequently infiltrated with 100 % xylene and embedded in paraffin wax. For hematoxylin and eosin (H&E) staining, tissues were sectioned at 5 μm thickness, deparaffinized, rehydrated and stained with hematoxylin for 3 min followed by counterstaining with eosin for 1 min. For Oil red O staining, fresh samples of liver embedded in OCT tissue freezing medium (Sakura Finetek). 0.5 % Oil red O solution was prepared by dissolving 0.5 g Oil red O powder (Sigma) in 100 ml propylene glycol (sigma).

Fresh frozen specimens were cryosectioned at 8 μm thickness and air dried. Then fix in ice cold 10 % formalin for 10 min, air dried again, and rinsed with distilled water. Sections were placed in 100 % propylene glycol for 5 min and stained with pre-warmed 0.5 % Oil red O solution in propylene glycol for 15 min in 60 °C oven. Then sections were rinsed with distilled water and followed by counterstaining with hematoxylin. Images were acquired using digital microscopes (Leica DMD108, Leica microsystems) equipped with 10 x and 20 x objective lenses.

Quantitative real-time RT-PCR

Total RNAs were extracted using Trizol (Invitrogen) and reverse transcription was performed from 2.5 μg of total RNAs using the M-MLV cDNA Synthesis kit (Enzynomics). The abundance of mRNA was detected by a CFX384 Touch™ Real-Time PCR Detection System (Bio-Rad) with SYBR Green (Enzynomics). The quantity of mRNA was calculated using ΔΔCt method and normalized by using primers indicated in each figure legend. All reactions were performed as triplicates. Primers used for analysis are as follows:

mRorα Forward(Fwd) :5′-CAATGCCACCTACTCCTGTCC-3′ and Reverse (Rev): 5′-GCCAGGCATTTCTGCAGC-3′; *m18s rRNA* Fwd: 5′-CCGCAGCTAGGAATAATGGA-AT-3′ and Rev: 5′-GCCAGGCATTTCTGCAGC-3′; *mMcp1* Fwd: 5′-GGCTCAGCCAGA-TGCAGTTAAC-3′ and Rev: 5′-AGCCTACTCATTGGGATCATCTTG-3′; *mIfnγ* Fwd: 5′-ATGAACGCTACACACTGCATC-3′ and Rev: 5′-CCATCCTTTTGCCAGTTCCTC-3′; *mIl-1β* Fwd: 5′-CGGCACACCCACCCTG-3′ and Rev: 5′-AAACCGCTTTTCCATCTTC-

TTCT-3′; *mIl-18* Fwd: 5′-CAGGCCTGACATCTTCTGCAA-3’ and Rev: 5′-TCTGACAT-GGCAGCCATTGT-3′; *mTgfβ* Fwd: 5′-CTTCAATACGTCAGACATTCGGG-3′ and Rev: 5′-GTAACGCCAGGAATTGTTGCTA-3′; *mF4/80* Fwd: 5′-TGACAACCAGACGGCTT-GTG-3′ and Rev: 5′-GCAGGCGAGGAAAAGATAGTGT-3′; *mDio2* Fwd; 5′-AATTATG-CCTCGGAGAAGACCG-3′ and Rev: 5′-GGCAGTTGCCTAGTGAAAGGT-3′; *mAcadm* Fwd: 5′-AGGGTTTAGTTTTGAGTTGACGG-3′ and Rev: 5′-CCCCGCTTTTGTCATAT-TCCG-3′; *mPgc1α* Fwd: 5′-TATGGAGTGACATAGAGTGTGCT-3′ and Rev: 5′-CCACT-TCAATCCACCCAGAAAG-3′; *mEsrrα* Fwd: 5′-AGGTGGACCCTTTGCCTTTC-3′ and Rev: 5′-GGCATGGCGTACAGCTTCT-3′; *mUcp1* Fwd: 5′-AGGCTTCCAGTACCATTA-GGT-3′ and Rev: 5′-CTGAGTGAGGCAAAGCTGATTT-3′; *mAox* Fwd: 5′-TAACTTCCT-CACTCGAAGCCA-3′ and Rev: 5′-AGTTCCATGACCCATCTCTGTC-3′; *mL32* Fwd:5′-GAAACTGGCGGAAACCCA-3′ and Rev: 5′-GGATCTGGCCCTTGAACCTT-3′; *mCyp7a1* Fwd: 5′-TCATTGCTTCAGGGCTCCTG-3′ and Rev: 5′-TGGGCATCT-CAAGCAAACAC-3′; *mCyp8b1* Fwd: 5′-CCTCTGGACAAGGGTTTTGTG-3′ and Rev: 5′-GCACCGTGAAGACATCCCC-3′; *mCyp27a1* Fwd: 5′-CCAGGCACAGGAGAGTAC-G-3′ and Rev: 5′-GGGCAAGTGCAGCACATAG-3′; *mGcK* Fwd: 5′-CTGGATGACAGA-GCCAGGATG-3′ and Rev: 5′-AGTTGGTTCCTCCCAGGTCT-3′; *mPepck* Fwd: 5′-AAAAGCCTTTGGTCAACAAC-3′ and Rev: 5′-AAACTTCATCCAGGCAATGT-3′; *mPparγ* Fwd: 5′-TCGCTGATGCACTGCCTATG-3′ and Rev: 5′-GAGAGGTCCACAGA-GCTGATT-3'; *mSrebp1c* Fwd: 5′-GAAGCTGTCGGGGTAGCGTCT-3′ and Rev: 5′-CTCTCAGGAGAGTTGGCACCTG-3′; *mAcc* Fwd: 5′-GGACAGACTGATCGCAGAG-AAAG-3′ and Rev: 5′-TGGAGAGCCCCACACACA-3′; *mFasn* Fwd: 5′-GCTGCGGAA-

ACTTCAGGAAAT-3′ and Rev: 5′-AGAGACGTGTCACTCCTGGACTT-3′; *mScd1* Fwd: 5′-TTCTTGCGATACACTCTGGTGC-3′ and Rev: 5′-CGGGATTGAATGTTCTTGTCG-T-3′; *mAcaca* Fwd: 5′-ATGGGCGGAATGGTCTCTTTC-3′ and Rev: 5′-TGGGGACCTT-GTCTTCATCAT-3′; *mAcacb* Fwd: 5′-CGCTCACCAACAGTAAGGTGG-3′ and Rev: 5′-GCTTGGCAGGGAGTTCCTC-3′; *mDgat2* Fwd: 5′-GCGCTACTTCCGAGACTACTT-3′ and Rev: 5′-GGGCCTTATGCCAGGAAACT-3′; *mChrebp* Fwd: 5′-CATTGCCAACATA-AGCATCTTC-3′ and Rev: 5′-GTCCGATATCTCCGACACACTC-3′; *mCidec* Fwd: 5′-ATGGACTACGCCATGAAGTCT-3′ and Rev: 5′-CGGTGCTAACACGACAGGG-3′; *mPlin2* Fwd: 5′-GACCTTGTGTCCTCCGCTTAT-3′ and Rev: 5′-CAACCGCAATTTGT-GGCTC-3′; *mG0S2* Fwd: 5′-TAGTGAAGCTATACGTTCTGGGC-3′ and Rev: 5′-GTCTC-AACTAGGCCGAGCA-3′.

Intraperitoneal glucose or insulin tolerance tests

For GTTs, 2 g of glucose per kg of mice body weight was injected i.p. to overnight fasted mice. For ITTs, 0.75 U of insulin (Humulin R, Eli Lilly) per kg of mice body weight was injected i.p. to 6 hr fasted mice. Mice blood was drawn at indicated time intervals from the tail tip puncture, and blood glucose level was measured by accu-check perfoma glucometer (Roche).

Antibodies

Commercially available antibodies were used: anti-RORα (sc-28612; 1:1,000 dilution for

IB analysis) and anti-AKT (sc-8312; 1:1,000 dilution for IB analysis) from Santa Cruz Biotechnology; anti-β-actin (A5441; 1:5,000 dilution for IB analysis) from Sigma; anti-phospho-AKT(Ser473) (#4051S, 1:1,000 dilution for IB analysis) from Cell Signaling.

Statistical analysis

The statistical analysis of different groups is realized using the Student's unpaired t-test or one-way ANOVA followed by Tukey post hoc test or two-way ANOVA. SPSS software (IBM) was used for all analyses.

CHAPTER III

RORα requires HDAC3 to regulate PPARγ signaling to maintain hepatic lipid homeostasis in response to over-nutrient cue

III-1. Summary

To determine how RORα inhibits diet-induced obesity through molecular mechanisms, I analyzed total transcriptome of the liver through mRNA sequencing data of the liver. As a result, RORα inhibited the PPARγ signaling. I have demonstrated that RORα suppresses PPARγ signal by observing the increase of expression of several PPARγ target genes involved in various lipid metabolism including lipid synthesis in liver-specific RORα deficient mice.

RORα binds to DNA without binding to PPARγ and inhibits the transcriptional activity of PPARγ. I found that RORα competes with PPARγ on PPRE through that the AGGTCA sequence of the DR1 motif of PPRE is the same as the core motif sequence of RORE, which inhibits the transcriptional activity of PPARγ. At this time, it was shown that RORα binds to HDAC3 rather than to PPARγ to inhibit the transcriptional activity of PPARγ.

Since RORα is involved in the metabolism process via the inhibition of PPARγ signaling, inhibition of the PPARγ signaling, independent of RORα, will restore the phenotype of liver-specific RORα deficient mice. Therefore, I administrated GW9662, a synthetic antagonist of PPARγ, to liver-specific *Rorα* deficient mice. As a result, liver-specific *Rorα* deficient mice were found to be inhibited in the progression of obesity and hepatic steatosis. Together, I confirmed RORα inhibits PPARγ signaling and regulates diet-induced obesity.

III-2. Introduction

PPARγ is mainly expressed in WAT and BAT, where it is a major regulation organ of adipogenesis. Therefore PPARγ is known for a regulator of lipid metabolism and insulin sensitivity (Tontonoz and Spiegelman, 2008). PPARγ is activated by various ligands. After ligand binding to PPARγ, PPARγ heterodimerizes with retinoid X receptor α (RXRα) and activates genes involved in lipid metabolism and insulin sensitivity (Chawla et al., 2001b). Whereas PPARγ is mainly expressed in WAT and BAT, PPARγ is expressed in liver by a high-fat diet (Medina-Gomez et al., 2007). In addition, liver-specific deletion of PPARγ in mice established its role as a pro-steatotic factor in the development of NAFLD (Way et al., 2001). Contrary, the activation of PPARγ by TZD promotes the release of free fatty acids in the liver, while increasing fat mass and consequently improving insulin sensitivity (Mayerson et al., 2002; Musso et al., 2012). Therefore, it is unclear what precise function of PPARγ is in hepatic lipid metabolism.

The mode of action of PPARγ in liver was suggested to promote insulin sensitivity but with concomitant development of fatty liver. PPARγ1 is overexpressed in PPARα knockout mice using adenovirus. These PPARγ1 overexpressed PPARα knockout mice showed PPARγ1 induced adipocyte specific gene expression patterns in the liver (Yu et al., 2003). Therefore, elevated PPARγ activity can lead to the development of hepatic steatosis. In addition, hepatic adenoviral overexpression of PPARγ2 in lean mice increased liver triglyceride content and induced hypertension (Uno et al., 2006). Then, in studies using A-ZIP/F-1 (AZIP) mice models in which PPARγ was reduced in the liver, showed severe

lipoatrophic diabetes, attenuation of hepatic steatosis but compromised triglyceride clearance (Gavrilova et al., 2003). Moreover, when PPARγ agonist, rosiglitazone, was administrated to AZIP mice, an improvement of glucose metabolism was observed. Hepatocyte specific PPARγ deficient mice protected mice due to lipid accumulation in a high fat diet feeding, thus further suggesting its role in the development of hepatic steatosis. They also showed that the PPARγ in Kupffer cells might not be involved in the development of hepatic steatosis (Moran-Salvador et al., 2011). In addition, a mouse model of dyslipidemia showed that hepatic PPARγ2 upregulation induced hepatic de novo lipogenesis. These mice are obese, insulin resistant and have hepatic steatosis (Zhang et al., 2006). Taken together, these studies strongly implicate PPARγ in the development of hepatic steatosis.

HDAC3 is the Class I HDACs, it is a member of corepressor complex NCOR and SMRT (Perissi et al., 2010). Depletion of HDAC3 in liver impairs lipid and cholesterol homeostasis, so lipid accumulation is increased and glycogen storage is decreased. Moreover, liver specific Hdac3 deficient mice have improved insulin sensitivity, but insulin signaling pathway or body weight have no changes compared with wild-type mice (Knutson et al., 2008). HDAC3 depletion reroutes metabolic precursors towards lipid synthesis and storage within lipid droplets and away from hepatic glucose production (Sun et al., 2012).

Here, genome-wide transcriptome analysis reveals that PPARγ signaling is remarkably elevated in RORα^{LKO} mice. RORα specifically recruits HDAC3 to the PPARγ target promoters to suppress PPARγ transcriptional activity. Finally, PPARγ antagonism by using

PPARγ antagonist GW9662, largely ameliorates body weight gain and hepatic steatosis in HFD-fed RORα^{LKO} mice, indicating that dysregulated PPARγ signaling is a critical metabolic cue, leading to metabolic defects in HFD-fed RORα^{LKO} mice. Together, my data demonstrate that RORα controls PPARγ signaling to protect against hepatic metabolic homeostasis and obesity in response to HFD.

III-3. Results

HFD-fed RORα^{LKO} mice exhibit enhanced PPARγ transcriptional activity

To explore molecular mechanism by which hepatic deletion of RORα induces obesity and insulin resistance, I performed mRNA-sequencing analysis of liver tissues obtained from HFD-fed RORα$^{f/f}$, HFD-fed RORα^{LKO}, CD-fed RORα$^{f/f}$, and CD-fed RORα^{LKO} mice (Table III-1). Using the resulting mRNA expression profiles, I first identified 343 differentially expressed genes (DEGs; $P< 0.05$) between HFD-fed RORα^{LKO} and HFD-fed RORα$^{f/f}$ mice (RORα^{LKO}/RORα$^{f/f}_{HFD}$ in Fig. III-1A) and also 395 DEGs between CD-fed RORα^{LKO} and CD-fed RORα$^{f/f}$ mice (RORα^{LKO}/RORα$^{f/f}_{CD}$ in Fig. III-1A). Moreover, I further compared log_2-fold-changes of the DEGs in the two comparisons above ((RORα^{LKO}/RORα$^{f/f}_{HFD}$)/(RORα^{LKO}/RORα$^{f/f}_{CD}$) in Fig. III-1A) and identified the genes specifically affected by RORα under HFD condition as the DEGs showing significant ($P< 0.05$) differences in the log_2-fold-changes. I categorized these DEGs into 8 groups (Groups 1-8) based on differential expression patterns in the three comparisons above. My data above showed that I only found significant weight gain of RORα^{LKO} mice under HFD condition. Of Groups 1-8, thus, I first focused on Groups 1-4 showing significant changes under HFD condition (Fig. III-1A).

To understand cellular processes represented by Groups 1-4, I performed enrichment analysis of gene ontology biological processes (GOBPs) and Kyoto Encyclopedia of Genes and Genomes (KEGG) pathways for the genes in Groups 1-4 using DAVID software (Huang da et al., 2009a, b) (Table III-2). Group 1 is mainly involved in the processes related

to PPAR and adipocytokine signaling pathways and fatty acid/retinol metabolism (Fig. III-1B and Table III-2, 3). Group 4 is mainly involved in the processes related to circadian rhythm (Table III-2, 3). Since Group 1 is highly associated with the weight gain of HFD-fed RORα^{LKO}, I next examined which transcription factors (TFs) account for up-regulation of the genes in Group 1 under HFD condition. By performing TF enrichment analysis of the genes in Group 1 using ChEA2 software (Kou et al., 2013), PPARγ turned out to be the most enriched TF in Group 1 (Fig. III-1C and Table III-4). Quantitative RT-PCR analysis confirmed that the genes in Group 1 including PPARγ target genes are largely elevated in HFD-fed RORα^{LKO} mice (Fig. III-1D), indicating that PPARγ transcriptional activity is enhanced in the absence of RORα.

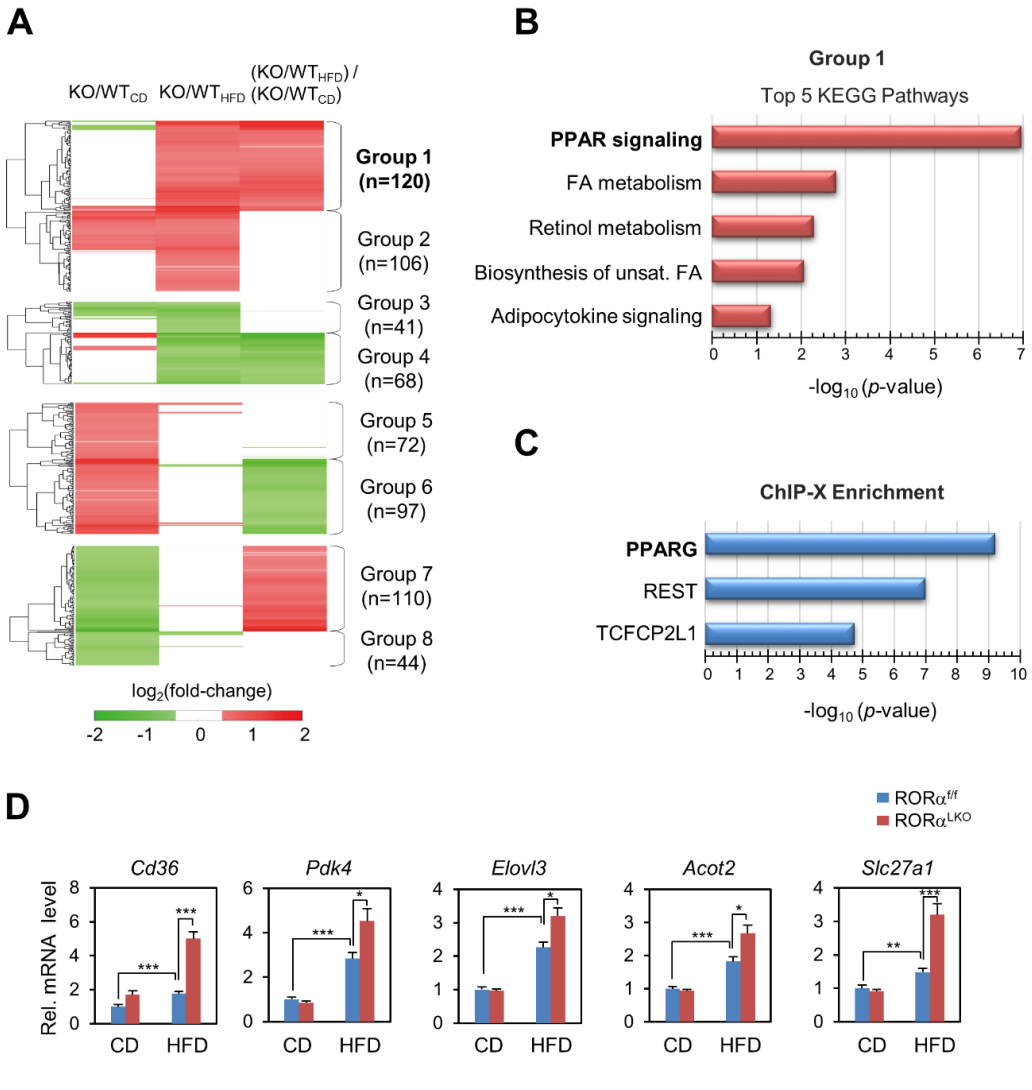
A
KO/WT_CD
KO/WT_HFD
(KO/WT_HFD) / (KO/WT_CD)
Group 1 (n=120)
Group 2 (n=106)
Group 3 (n=41)
Group 4 (n=68)
Group 5 (n=72)
Group 6 (n=97)
Group 7 (n=110)
Group 8 (n=44)
log2(fold-change)
-2 -1 0 1 2
B
Group 1
Top 5 KEGG Pathways
PPAR signaling
FA metabolism
Retinol metabolism
Biosynthesis of unsat. FA
Adipocytokine signaling
0 1 2 3 4 5 6 7
-log10 (p-value)
C
ChIP-X Enrichment
PPARG
REST
TCFCP2L1
0 1 2 3 4 5 6 7 8 9 10
-log10 (p-value)
D
RORα^f/f
RORα^LKO
Rel. mRNA level
Cd36
Pdk4
Elovl3
Acot2
Slc27a1
CD HFD

Figure III-1. Transcriptome analysis of hepatic gene expression profile in RORα^{LKO} mice

(**A**) Up- and down-regulated genes in RORα^{LKO} compared to RORα$^{f/f}$ mice. These genes were categorized into 4 groups of the up- (Groups 1, 2) and down-regulated genes (Groups 3, 4) in HFD-fed RORα^{LKO}. Besides Groups 1-4, remain genes were also categorized into 4 groups of the up- (Groups 5, 6) and down-regulated genes (Groups 7, 8) in CD-fed RORα^{LKO}. Groups 1, 2 (or Groups 3, 4) were further divided by the specificity of the RORα effect under HFD condition. Log_2-fold changes in the following comparisons were displayed: RORα^{LKO}/RORα$^{f/f}{}_{HFD}$, RORα^{LKO}/RORα$^{f/f}{}_{CD}$, and (RORα^{LKO}/RORα$^{f/f}{}_{HFD}$)/(RORα^{LKO}/RORα$^{f/f}{}_{CD}$). Hierarchical clustering of the DEGs in Groups 1-8 (Euclidian distance as a dissimilarity measure and average linkage) were used to display the log_2-fold changes. (**B**) KEGG pathways enrichment analysis for the genes in Group 1. The bars represent the enrichment scores, $-log_{10}$ (*P* value). (**C**) TF enrichment analysis for the genes in Group 1 using ChEA2 software. Top 3 TFs are shown. The bars represent the enrichment scores, $-log_{10}$ (*P* value). (**D**) Expression levels of group 1 genes (up-regulated genes in RORα^{LKO} mice fed HFD compared with RORα$^{f/f}$ mice) in liver extract from RORα$^{f/f}$ and RORα^{LKO} mice fed CD or HFD for 10 weeks (n=5-9/group) as determined by qRT-PCR. Expression was normalized to 36B4 expression. Data expressed as mean ± S.E.M. Statistical analysis was performed using two-way ANOVA. *p<0.05, **p<0.01, ***p<0.001.

Sample	Raw reads	Mapped reads	Mapping rate	Uniquely mapped reads	Unique mapping rate	Exom Coverage(X)
KO_CD_1	38,672,532	38,120,866	98.6%	35,033,080	91.9%	32.8
KO_CD_2	33,939,426	33,446,553	98.5%	30,602,631	91.5%	29.6
KO_HFD_1	39,760,880	39,207,039	98.6%	37,153,527	94.8%	33.4
KO_HFD_2	40,499,390	39,917,339	98.6%	37,403,886	93.7%	34.5
WT_CD_1	40,241,230	39,666,441	98.6%	35,625,037	89.8%	34.7
WT_CD_2	34,516,784	33,918,521	98.3%	30,177,765	89.0%	29.3
WT_HFD_1	33,456,648	32,989,512	98.6%	30,283,398	91.8%	28.4
WT_HFD_2	38,211,808	37,632,914	98.5%	35,435,387	94.2%	32.4

Table III-1. Summary of the alignment results for mRNA-sequencing data

Among the raw reads generated from Illumina Hiseq-2500, the reads after trimming low quality and adapter sequences were used for the alignment. On average, each 98.5 % of the reads (Mapped reads and Mapping rate) were aligned to a reference mouse genome (GRCm38). Of the mapped reads, 92.1 % (Unique mapping rate) of the mapped reads were aligned to unique location (Uniquely mapped reads) in the genome. Exom Coverage denotes the fold of coverage of the mapped reads for the annotated exon region.

Gene ontology and KEGG enrichment analysis of the Group 1

Category	Term	Count	P-Value
GOTERM	fatty acid metabolic process	9	4.00E-06
GOTERM	lipid biosynthetic process	7	3.20E-03
GOTERM	organic acid biosynthetic process	5	5.70E-03
GOTERM	carboxylic acid biosynthetic process	5	5.70E-03
GOTERM	oxidation reduction	10	6.70E-03
GOTERM	fatty acid biosynthetic process	4	8.10E-03
GOTERM	positive regulation of foam cell differentiation	2	1.50E-02
GOTERM	regulation of foam cell differentiation	2	2.00E-02
GOTERM	positive regulation of immune system process	5	2.10E-02
GOTERM	positive regulation of immune response	4	3.20E-02
GOTERM	immune response	7	3.20E-02
GOTERM	long-chain fatty acid transport	2	3.50E-02
GOTERM	fat cell differentiation	3	3.80E-02
KEGG_PATHWAY	PPAR signaling pathway	8	1.10E-07
KEGG_PATHWAY	Fatty acid metabolism	4	1.60E-03
KEGG_PATHWAY	Retinol metabolism	4	5.10E-03
KEGG_PATHWAY	Biosynthesis of unsaturated fatty acids	3	8.60E-03
KEGG_PATHWAY	Adipocytokine signaling pathway	3	4.70E-02

Gene ontology and KEGG enrichment analysis of the Group 2

Category	Term	Count	P-Value
GOTERM	fatty acid metabolic process	6	1.40E-03
GOTERM	lipid transport	5	2.00E-03
GOTERM	lipid localization	5	2.60E-03
GOTERM	monocarboxylic acid transport	3	3.20E-03
GOTERM	brown fat cell differentiation	3	7.40E-03
GOTERM	fat cell differentiation	3	3.10E-02
KEGG_PATHWAY	PPAR signaling pathway	7	6.60E-06
KEGG_PATHWAY	Fatty acid metabolism	5	1.40E-04
KEGG_PATHWAY	Biosynthesis of unsaturated fatty acids	3	1.20E-02
KEGG_PATHWAY	ABC transporters	3	3.00E-02

Gene ontology and KEGG enrichment analysis of the Group 3

Category	Term	Count	P-Value
GOTERM	oxidation reduction	6	1.90E-03
KEGG_PATHWAY	Primary bile acid biosynthesis	2	2.10E-02

Gene ontology and KEGG enrichment analysis of the Group 4

Category	Term	Count	P-Value
GOTERM	cellular cation homeostasis	4	8.70E-03
GOTERM	negative regulation of JAK-STAT cascade	2	1.40E-02
GOTERM	cation homeostasis	4	1.50E-02
GOTERM	regulation of transcription, DNA-dependent	10	1.70E-02
GOTERM	chemical homeostasis	5	1.80E-02
GOTERM	regulation of RNA metabolic process	10	1.90E-02
GOTERM	homeostatic process	6	2.20E-02
GOTERM	carbohydrate biosynthetic process	3	2.20E-02
GOTERM	rhythmic process	3	3.10E-02
GOTERM	vasoconstriction	2	3.60E-02
GOTERM	cellular ion homeostasis	4	3.60E-02
GOTERM	cellular chemical homeostasis	4	3.90E-02
GOTERM	ion homeostasis	4	4.80E-02
KEGG_PATHWAY	Circadian rhythm	3	1.50E-03
KEGG_PATHWAY	Complement and coagulation cascades	4	4.50E-03

Table III-2. GOBPs and KEGG pathways represented by the genes in Groups 1-4
The GOBPs and KEGG pathways represented by the genes in Groups 1-8 are shown. For each GOBP or KEGG pathway term, the count of the genes involved in the term and the enrichment P-values for the term are shown. The GOBPs and KEGG pathways with P-value<0.05 and Count >2 were selected as representative ones.

Group 1 (n=120)				
Unc119	Npr1	9130409I23Rik	mt-Rnr2	Gm13710
Plin4	Trim2	Agbl3	Cyp4a10	Gm16174
Cd36	Bcl10	Mtg1	Slc22a27	snoU89
Ndrg1	Trp53inp1	Abhd2	Lgals1	Gm15758
Spc25	Tpm2	Rcan2	Gpr98	Gm16541
Krt23	Cyp4a31	Cpeb2	Rdh16	Efna5
Mogat1	Lzic	Cd53	Slfn2	Gm8893
Lpl	Fam126a	Tspyl2	Bhlhb9	Gm17023
Lnx2	Mthfr	Rassf4	Efcab7	Gm20419
Abi3	Mad2l1	D930007J09Rik	Fign	RNaseP_nuc
Cd68	Rab30	Serpinb1a	Ept1	Hmgcs1
Acsl1	Ctbp2	Olig1	Gm12854	RP23-58L22.2
Pdk4	Sh3bgrl	Ermp1	Cpt1b	
Rfx4	Slc27a1	Arl4a	Gm7609	
Lgr5	Anxa2	8430408G22Rik	H2-Q1	
Bcap29	Elovl5	Themis	B230307C23Rik	
Ten1	Cyp2c38	9030619P08Rik	Mup-ps14	
Acot2	Rasgrp2	Smagp	Gm15064	
Arhgef3	Rnf125	Gbp10	2810453I06Rik	
Tsc22d1	Ly6d	Cyp3a11	Gm14202	
Chrna2	Art3	Gm12396	Gm14584	
Ehhadh	Cxcl10	Hamp2	Gm15146	
Gpd1	Acss3	Zfp53	Gm14734	
Cdkn1a	Scd1	Cfd	Gm15817	
Slc15a3	Fbxw17	Ces2c	Gm15952	
Arhgef9	Egr1	Hist1h4k	1110028F11Rik	
Car3	Elovl3	mt-Rnr1	Gm15690	

Group 4 (n=68)		
Cyp17a1	Pde4a	Gm14308
Cav1	Cln6	Cd47
E2f3	Deb1	Mup-ps19
Ubb	B3galt1	Gm12941
Socs2	Thrsp	SNORA48
Egfr	Acta2	Gm15962
Adarb1	Hsd3b5	2010001M06Rik
Lrrc16a	Rtel1	Marcksl1-ps4
Scara5	Fmo2	Gm11707
C6	D0H4S114	Gm15756
Tgm1	Onecut1	Eif4ebp3
Tef	Gimap5	Gm17041
Keg1	Rassf8	Serpina4-ps1
Cyp26a1	Bmyc	GAPDH
Got1	B3gnt2	
Ngef	Mup5	
Upp2	Dbp	
Gar1	Gstp1	
Enho	Ces3b	
Per3	Tnnt1	
Sds	4930522L14Rik	
C8b	Serpina1e	
Bhlhe40	Mup7	
Bhlhe41	2810410L24Rik	
Timm17b	AU041133	
F11	Gm4070	
Mt2	Mup16	

Table III-3. List of genes affected by depletion of RORα

List of up- (Group 1) and down- (Group 4) regulation of the genes affected by RORα depletion in the following three comparisons are shown: 1) CD-fed $ROR\alpha^{LKO}$ versus CD-fed $ROR\alpha^{f/f}$(KO/WT_{CD}), 2) HFD-fed $ROR\alpha^{LKO}$ versus HFD-fed $ROR\alpha^{f/f}$(KO/WT_{HFD}), and 3) their log_2-fold-change differences ((KO/WT_{HFD})/(KO/WT_{CD})).

Term	P-value	-LOG10 (p-value)	Overlap	Genes
PPARG	6.202E-10	9.21	28	RDH16;SH3BGRL;2810453I06RIK; CDKN1A;FAM126A;PDK4;LPL; ELOVL5;ART3;GM7609;MOGAT; RNF125;FIGN;ACSL1;EHHADH; EGR1;CAR3;EPT1;EFNA5; EFCAB7;CD36;CD68;GPD1; ACOT2;MTHFR;TRIM2;ANXA2; SCD1
REST	1.037E-07	6.98	22	RDH16;LGR5;ARL4A;EGR1; CAR3;OLIG1;CDKN1A; TRP53INP1;CYP3A11;CPT1B; 9130409I23RIK;LZIC;RFX4; CXCL10;ART3;CD53; RNF125;ACOT2;CPEB2;FIGN; H2-Q1;SCD1
TCFCP2L1	1.847E-05	4.73	15	SLC27A1;ARL4A;ARHGEF9; CAR3;FBXW17;CDKN1A;CPT1B; SERPINB1A;GPR98;MAD2L1; NDRG1;LNX2;RNF125;UNC119; KRT23

Table III-4. Key transcription factors significantly regulating the genes in Group 1
TFs significantly enriched by the genes in Group 1 (P-value < 0.01) are shown. For each TF, the number of genes and the list of genes targeted by the TF are also provided.

RORα regulates PPARγ transcriptional network but does not affect PPARα transcriptional network in the mice liver

PPARα is a transcriptional factor that conducts a key role in hepatic lipid metabolism and shares similar response elements with PPARγ on the target promoters (Dreyer et al., 1992; Lee et al., 2014). To determine whether RORα also mediates PPARα transcriptional network in the liver, I examined the expression of well-known hepatic PPARα target genes, including *Acox1* and *Fgf21*. The hepatic gene expressions of *Acox1* and *Fgf21* in HFD-fed RORα^{LKO} mice were similar to those of HFD-fed RORα$^{f/f}$ mice, suggesting that RORα deficiency would not further enhance hepatic PPARα transcriptional network (Fig. III-2A) under HFD condition. I next examined the expression of PPARα target genes in the physiological setting of PPARα activation. It has been widely accepted that PPARα is activated under conditions of energy deprivation (Kersten et al., 1999). The induction of PPARα target genes in RORα^{LKO} mice was quite similar to that of RORα$^{f/f}$ mice (Fig. III-2B). Chromatin immunoprecipitation (ChIP) assay clearly revealed little or no difference of PPARα recruitment to PPAR-response element (PPRE) on the promoters of PPARα target genes (Fig. III-2C). Recently, PPARα has been reported to bind autophagic gene promoters to coordinate autophagy in response to nutrient deprivation (Lee et al., 2014). I observed that the induction of autophagic genes including *LC3a* and *Sesn2* of RORα^{LKO} mice were similar to those of RORα$^{f/f}$ mice (Fig. III-2D). Taken together, these data indicate that RORα mainly controls PPARγ transcriptional network rather than PPARα in the liver in response to environmental stress such as HFD.

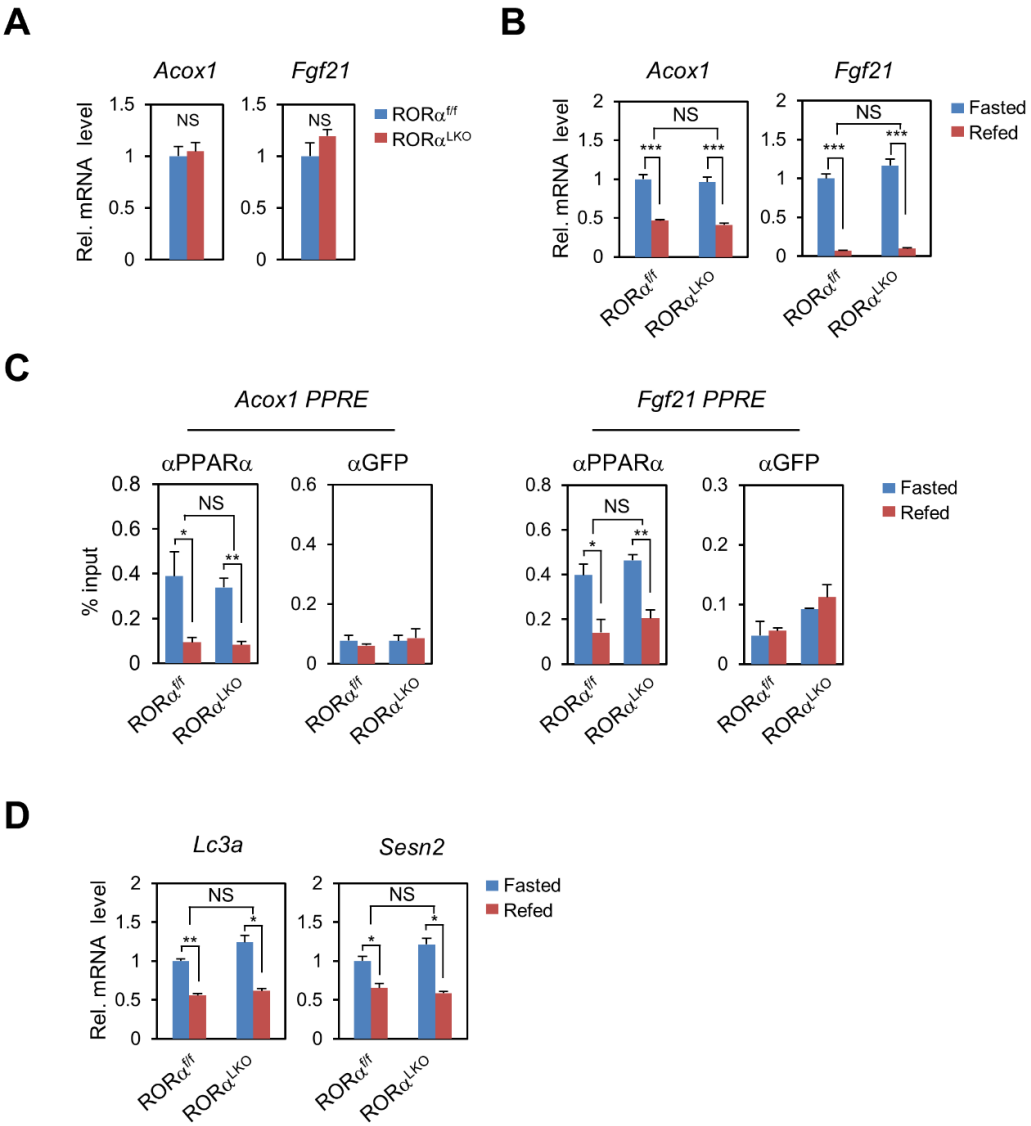
A
Acox1
Fgf21
Rel. mRNA level
NS
RORα f/f
RORα LKO
B
Acox1
Fgf21
Rel. mRNA level
NS
***
Fasted
Refed
RORα f/f
RORα LKO
C
Acox1 PPRE
Fgf21 PPRE
αPPARα
αGFP
% input
NS
*
**
Fasted
Refed
RORα f/f
RORα LKO
D
Lc3a
Sesn2
Rel. mRNA level
NS
*
**
Fasted
Refed
RORα f/f
RORα LKO

Figure III-2. PPARα and RORα do not affect their roles in the mice liver with each other

(**A**) Expression levels of PPARα target genes in liver from RORα$^{f/f}$ and RORα^{LKO} mice fed CD or HFD for 10 weeks (n=7-9/group) as determined by qRT-PCR. Expression was normalized to 36B4 expression. Data expressed as mean ± S.E.M. Statistical analysis was performed using Student's unpaired t-test. NS=Non-Significant. (**B-D**) 24 h fasted and 24 h refed after 24 h fasting RORα$^{f/f}$ and RORα^{LKO} mice were euthanized to collect livers. (**B**) Expression levels of PPARα target genes in liver from RORα$^{f/f}$ and RORα^{LKO} mice fasted or refed (n=3/group) as determined by qRT-PCR. Expression was normalized to 36B4 expression. (**C**) ChIP assays were performed on the *Acox1* and *Fgf21* promoters in liver extract form RORα$^{f/f}$ and RORα^{LKO} mice fasted or refed (n=3/group). Promoter occupancy by PPARα and GFP was analyzed. (**D**) Expression levels of autophagy-related PPARα target genes in liver from RORα$^{f/f}$ and RORα^{LKO} mice fasted or refed (n=3/group) as determined by qRT-PCR. Expression was normalized to 36B4 expression. Data expressed as mean ± S.E.M. Statistical analysis was performed using two-way ANOVA. *$p<0.05$, **$p<0.01$, ***$p<0.001$, NS=Non-Significant.

RORα inhibits the transcriptional activity of PPARγ regardless of the various co-activator of PPARγ

Since PGC1α is a well-known coactivator for PPARγ (Puigserver and Spiegelman, 2003), I examined whether introduction of RORα inhibits PPARγ/PGC1α-dependent transcriptional activation using PPRE-containing luciferase reporter. Expression of PGC1α dramatically increased PPARγ transcriptional activity, and increased expression of RORα progressively attenuated the PPARγ/PGC1α-dependent transcriptional activation (Fig. III-3A). In addition, I examined whether RORα inhibits NCOA1 and NCOA2-mediated PPARγ transcriptional activation. NCOA1 and NCOA2, as p160 family members, are also coactivators for PPARγ (Hong et al., 1996). Consistently, RORα significantly reduced NCOA1 and NCOA2-mediated transcriptional activation (Fig. III-3B, C).

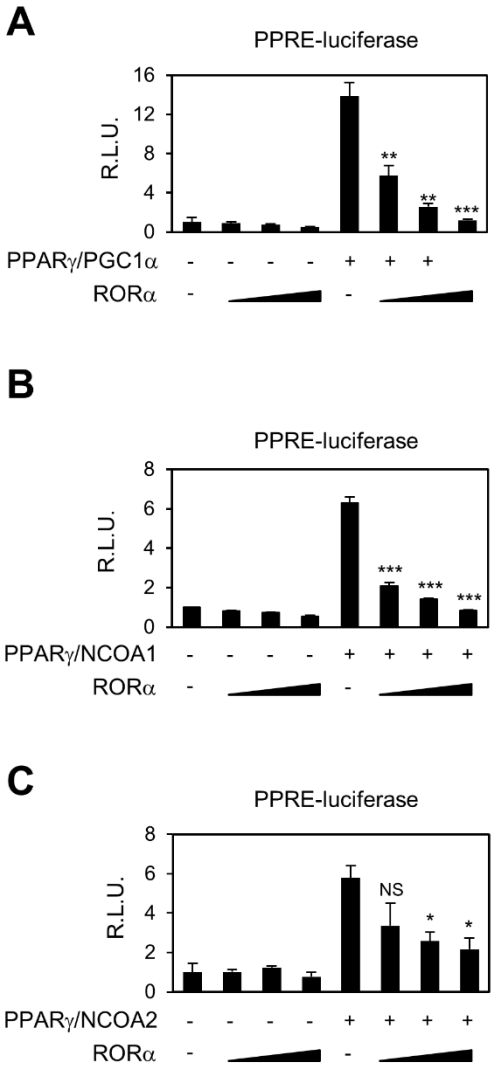

Figure III-3. RORα inhibits the transcriptional activity of PPARγ

(**A-C**) Effect of overexpression of RORα on PPRE-luciferase reporter activity with coactivator PGC1α (**A**) or NCOA1 (**B**) or NCOA2 (**C**). Data expressed as mean ± S.E.M. Statistical analysis was performed using one-way ANOVA followed by Tukey's post hoc analysis. *p<0.05, **p<0.01, ***p<0.001, NS=Non-Significant, compared to PPARγ/coactivator group.

RORα does not bind to PPARγ, but directly binds to DNA and to inhibit transcriptional activity of PPARγ

To evaluate the role of RORα in attenuation of the PPARγ-dependent transcriptional activation, I treated Hep3B cells with rosiglitazone, a PPARγ synthetic agonist, and then measured PPRE-luciferase activity. Knockdown of RORα markedly enhanced PPRE-luciferase activity, indicating that RORα functions to repress PPARγ transcriptional activity (Fig. III-4A). To determine if DNA binding domain (DBD) of RORα is required for inhibiting PPARγ transcriptional activation, I introduced DBD-deleted RORα mutant (RORα ΔDBD). I observed that RORα WT markedly suppressed PPARγ transcriptional activation, whereas the RORα-mediated repression was remarkably relieved by introduction of RORα ΔDBD (Fig. III-4B). As RORα failed to interact with PPARγ (Fig. III-4C), my data proposed that RORα suppresses PPARγ transcriptional activation through DBD and possibly competes with PPARγ for the binding to PPRE. Consistently, the recruitment of RORα was markedly reduced in PPRE-deleted synthetic promoter region (Fig. III-4D).

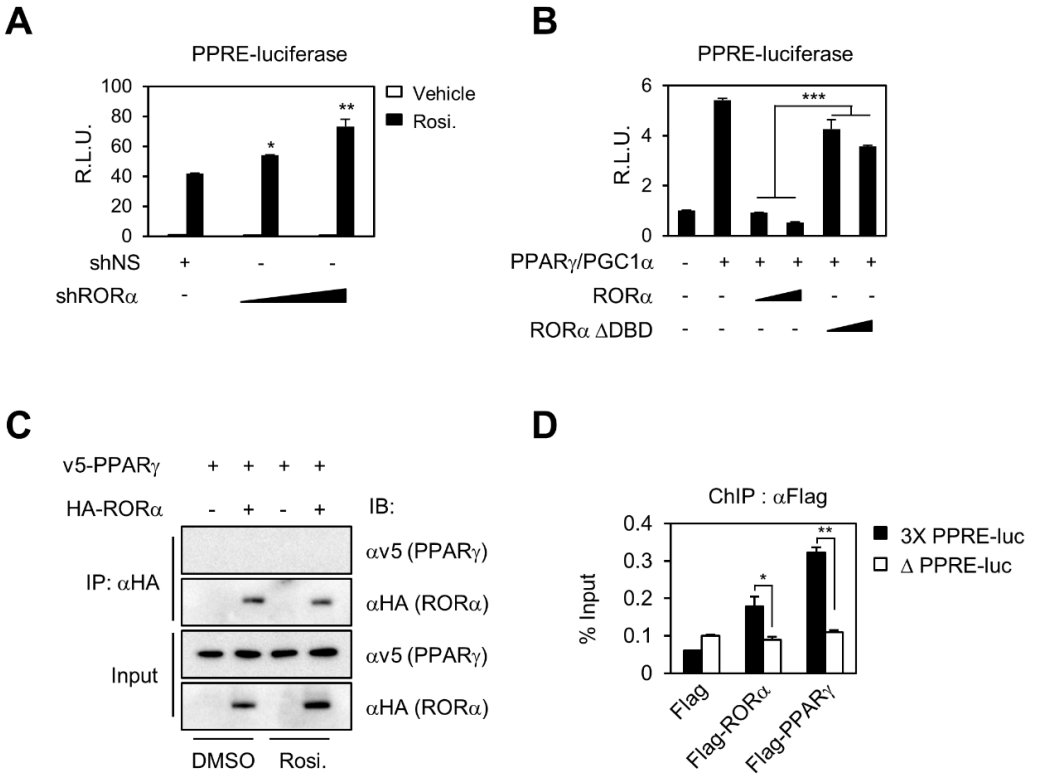

Figure III-4. RORα recruits to PPRE and inhibits transcription activity of PPARγ, but does not interact with PPARγ

(**A**) Effect of knockdown of RORα on PPRE-luciferase reporter activity. Cells were treated with DMSO (vehicle), rosiglitazone (20 μM) for 24 hr. Data expressed as mean ± SEM. Statistical analysis was performed using one-way ANOVA followed by Tukey's post hoc analysis. *p<0.05, **p<0.01, compared to shNS group. (**B**) Effect of RORα ΔDBD mutant on PPRE-luciferase reporter activity. Data expressed as mean ± S.E.M. Statistical analysis was performed using one-way ANOVA followed by Tukey's post hoc analysis. ***p<0.001. (**C**) Co-immunoprecipitation assay was performed to detect the interaction between RORα and PPARγ of HEK293T cells. (**D**) WT PPRE promoter and PPRE deleted mutant promoter containing luciferase reporter plasmid and Flag/Flag-RORα/Flag-PPARγ plasmid were transfected into Hep3B cells. ChIP assays were performed on promoter region of reporter plasmid in Hep3B cells. Promoter occupancy by Flag was analyzed. Data expressed as mean ± S.E.M. Statistical analysis was performed using Student's unpaired t-test. *p<0.05, **p<0.01.

RORα represses PPARγ transcriptional activity via interacting with HDAC3

Since histone acetylation promotes transcriptional activation, I next examined whether RORα interacts with specific histone deacetylases for the repression of PPARγ transcriptional activity. Co-immunoprecipitation assay revealed that RORα specifically interacts with HDAC3 (Fig. III-5A, B). To determine if HDAC3 is required for RORα-mediated repression of PPARγ transcriptional activity, I further examined repressive function of HDAC3 for PPRE-luciferase activity in the presence or absence of RORα. Intriguingly, knockdown of RORα relieved the HDAC3-dependent repressive function indicating that HDAC3 exerted repressive function on PPARγ transcriptional activity in the presence of RORα (Fig. III-5C). Consistently, knockdown of HDAC3 largely reversed RORα-mediated repression of PPARγ transcriptional activity (Fig. III-5D-F). These results indicate that RORα recruits HDAC3 to potentiate repression of PPARγ transcriptional activity.

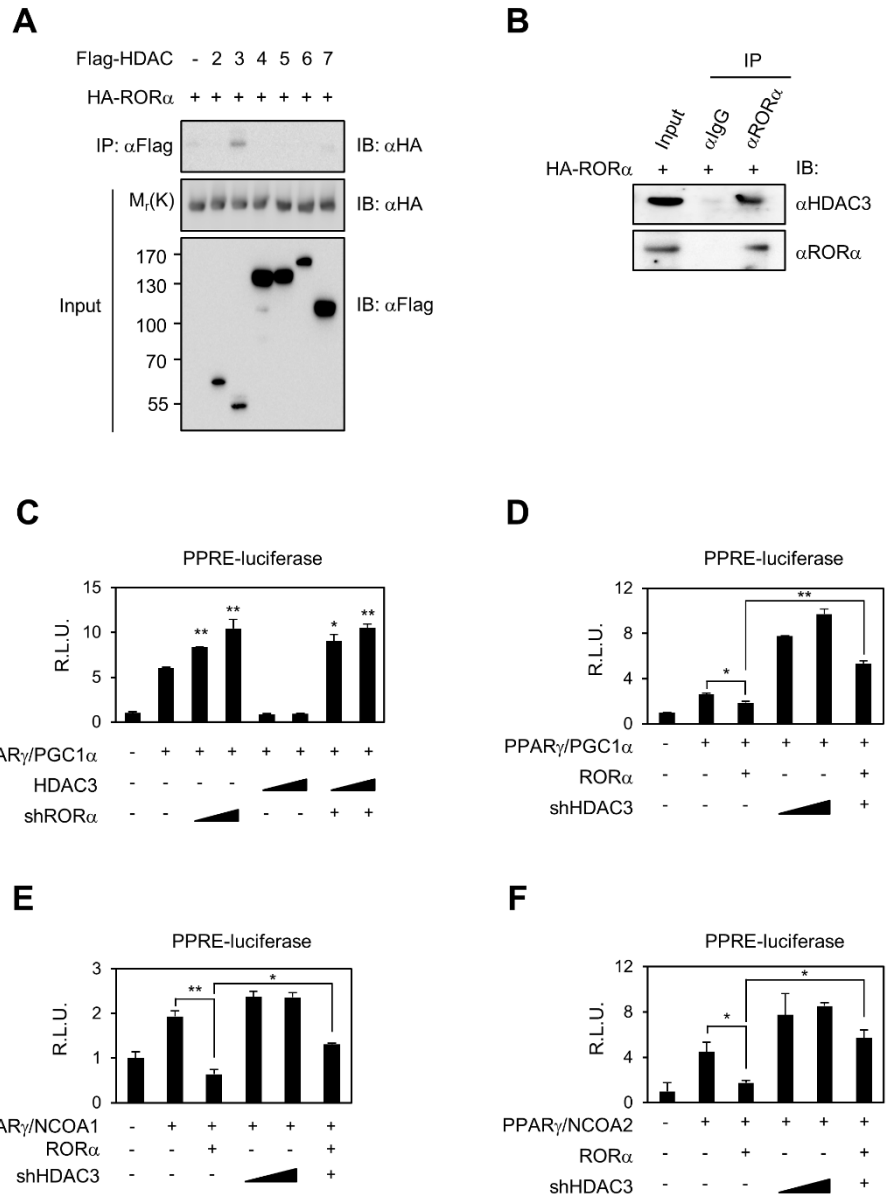
A
Flag-HDAC - 2 3 4 5 6 7
HA-RORα + + + + + + +
IP: αFlag
IB: αHA
Mr(K)
IB: αHA
Input
170
130
100
70
55
IB: αFlag
B
IP
Input
αIgG
αRORα
HA-RORα + + +
IB:
αHDAC3
αRORα
C
PPRE-luciferase
R.L.U.
15
10
5
0
PPARγ/PGC1α - + + + + + + +
HDAC3 - - - -
shRORα - -
D
PPRE-luciferase
R.L.U.
12
8
4
0
PPARγ/PGC1α - + + + + +
RORα - - + - - +
shHDAC3 - - -
E
PPRE-luciferase
R.L.U.
3
2
1
0
PPARγ/NCOA1 - + + + + +
RORα - - + - - +
shHDAC3 - - -
F
PPRE-luciferase
R.L.U.
12
8
4
0
PPARγ/NCOA2 - + + + + +
RORα - - + - - +
shHDAC3 - - -

Figure III-5. RORα interacts with HDAC3 to repress PPARγ transcriptional activity
(**A**) Co-immunoprecipitation assay was performed to detect the interaction between RORα and HDACs of HEK293T cells. (**B**) Co-immunoprecipitation assay was performed to detect the interaction between RORα and HDAC3 of HEK293T cells. (**C**) Effect of RORα on PPRE-luciferase reporter activity by HDAC3 overexpression. Data expressed as mean ± S.E.M. Statistical analysis was performed using one-way ANOVA followed by Tukey's post hoc analysis. *p<0.05, **p<0.01, compared to PPARγ/PGC1α group. (**D-F**) Effect of knockdown of HDAC3 with coactivator PGC1α (**D**) or NCOA1 (**E**) or NCOA2 (**F**) on PPRE-luciferase reporter activity. Data expressed as mean ± S.E.M. Statistical analysis was performed using one-way ANOVA followed by Tukey's post hoc analysis. *p<0.05, **p<0.01.

RORα recruits to the PPARγ target gene promoters with HDAC3 in liver of mice fed HFD without involvement of PPARα

PPRE consists of a Direct Repeat (DR) sequence of (A/G)GGTCA spaced by one nucleotide, whereas consensus RORα response element (RORE) consists of core motif (A/G)GGTCA preceded by a 6-bp A/T-rich sequence. Thus, given that RORE and PPRE share core motif, I hypothesized that RORα directly binds the PPRE of PPARγ target promoters for transcriptional repression. To examine whether RORα and HDAC3 are co-recruited to the PPARγ target promoters for the repression, I performed ChIP assay with anti-RORα, PPARγ, PPARα, RNA polymerase II (Pol II), acetylated H3 (H3Ac), and HDAC3 antibodies from the mouse liver extracts of CD or HFD-fed RORα$^{f/f}$ and RORα^{LKO} mice. ChIP assays revealed that RORα and HDAC3 were co-recruited to the *Cd36*, *Scd1* and *Plin2* promoters in the liver of HFD-fed RORα$^{f/f}$ mice (Fig. III-6), although no changes were observed with CD-fed RORα$^{f/f}$ mice (Fig. III-7). In the absence of RORα, PPARγ recruitment was markedly increased, whereas HDAC3 recruitment was largely diminished along with elevated acetylated H3 levels on the *Cd36*, *Scd1* and *Plin2* promoters in the liver of HFD-fed RORα^{LKO} mice (Fig. III-6). Unlike PPARγ, PPARα recruitment was barely detected from the PPARγ target promoters containing PPRE as assessed by ChIP assay (Fig. III-6-8).

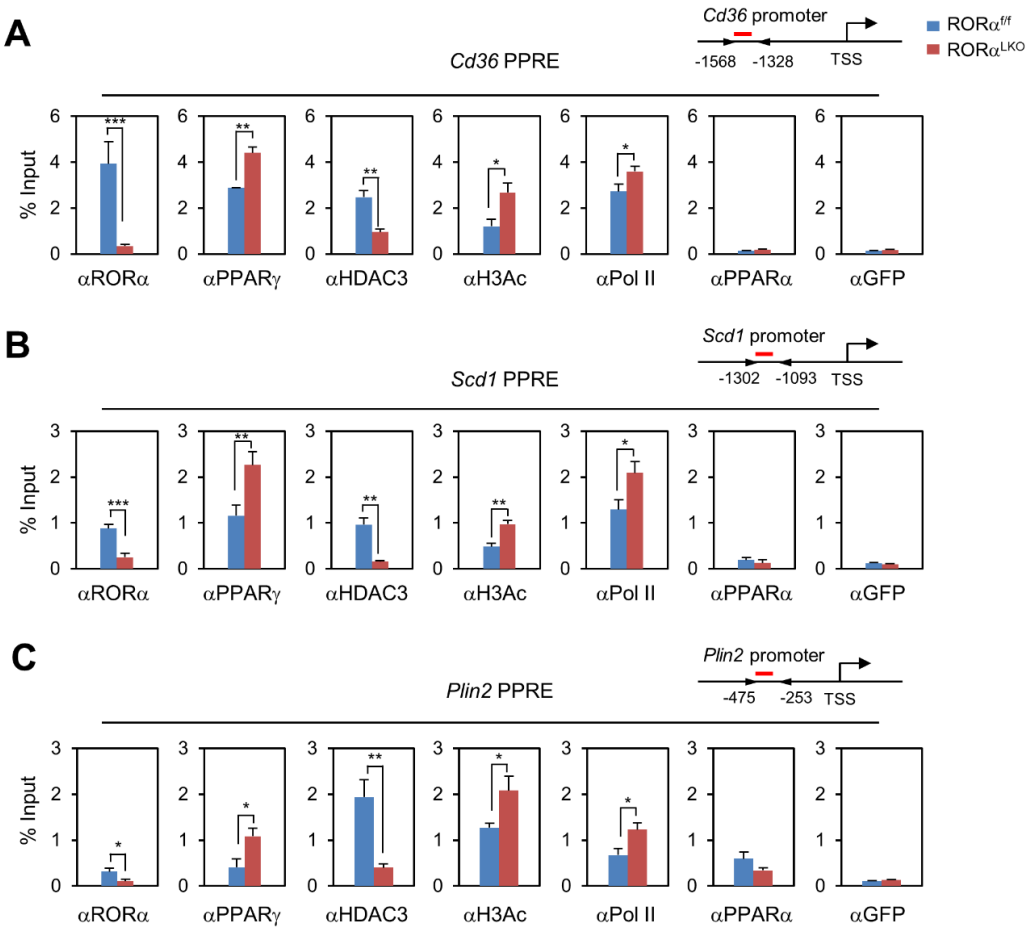

Figure III-6. RORα recruits to the PPARγ target gene promoters with HDAC3 in liver of mice fed HFD

(**A-C**) ChIP assays were performed on the *Cd36* (**A**), *Scd1* (**B**) and *Plin2* (**C**) promoters in liver extract form RORα$^{f/f}$ and RORα^{LKO} mice fed HFD for 10 weeks (n=3/group). Promoter occupancy by RORα, PPARγ, HDAC3, H3Ac, Pol II, PPARα and GFP was analyzed. Schematic of promoter region was represented with gene name. Red bar depicts locations of PPRE. Data expressed as mean ± S.E.M. Statistical analysis was performed using Student's unpaired t-test. *p<0.05, **p<0.01, ***p<0.001.

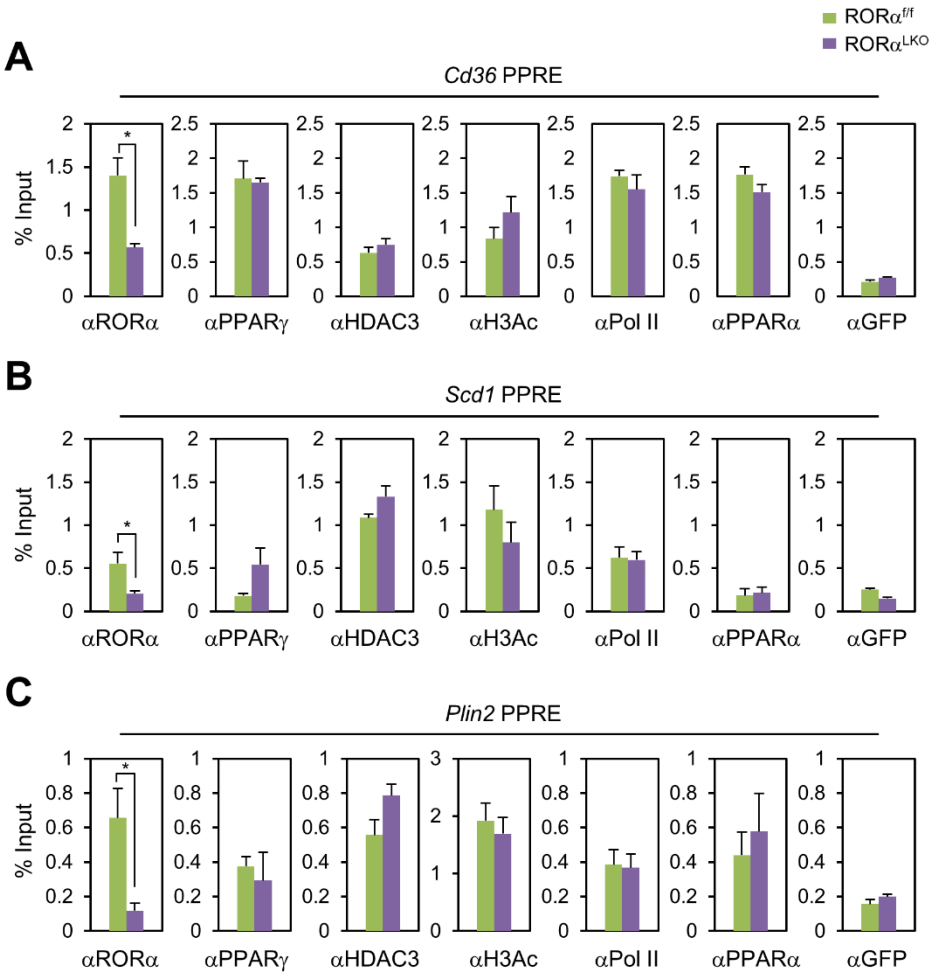

Figure III-7. The recruitment of PPARγ to the PPARγ target gene promoters is similar between RORα$^{f/f}$ and RORα^{LKO} mice fed CD unlike mice fed HFD

(**A-C**) ChIP assays were performed on the *Cd36* (**A**), *Scd1* (**B**) and *Plin2* (**C**) promoters in liver extract form RORα$^{f/f}$ and RORα^{LKO} mice fed CD for 10 weeks (n=3/group). Promoter occupancy by RORα, PPARγ, PGC1α, HDAC3, H3Ac, Pol II, PPARα and GFP was analyzed. Schematic of promoter region was represented in previous figure. Data expressed as mean ± S.E.M. Statistical analysis was performed using Student's unpaired t-test. *p<0.05, **p<0.01, ***p<0.001.

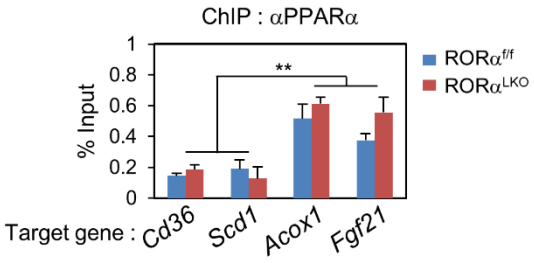

Figure III-8. PPARα recruitment is almost absent in the target gene promoter of PPARγ

ChIP assays were performed on the *Cd36, Scd1, Acox1 and Fgf21* promoters in liver extract form RORα$^{f/f}$ and RORα^{LKO} mice fed HFD for 10 weeks (n=3/group). Promoter occupancy by PPARα was analyzed. Data expressed as mean ± S.E.M. Statistical analysis was performed using two-way ANOVA followed by Tukey's post hoc analysis. **p<0.01.

PPARγ and RORα/HDAC3 dynamically regulate PPARγ target gene expression

Next, I determined if both RORα and HDAC3 are recruited to the PPRE in response to PPARγ agonist in Hep3B cells (Fig. III-9A). Treatment of rosiglitazone largely induced the expression of PPARγ target genes (Fig. III-9B). Interestingly, 8 hr washout after rosiglitazone treatment dramatically reduced PPARγ target gene expressions (Fig. III-9A, B). Consistent with gene expressions, treatment of rosiglitazone increased recruitment of PPARγ, PGC1α and Pol II with elevated histone H3 acetylation level on PPARγ target promoters as well as induction of PPARγ target genes (Fig. III-10). Strikingly, further increased recruitment of RORα to PPRE was observed along with enhanced HDAC3 recruitment in the setting of washout of rosiglitazone for 8 hours (Fig. III-10). Increased recruitment of RORα and HDAC3 substantially diminished PGC1α and Pol II recruitment on PPRE with decreased histone H3 acetylation level on PPRE (Fig. III-10).

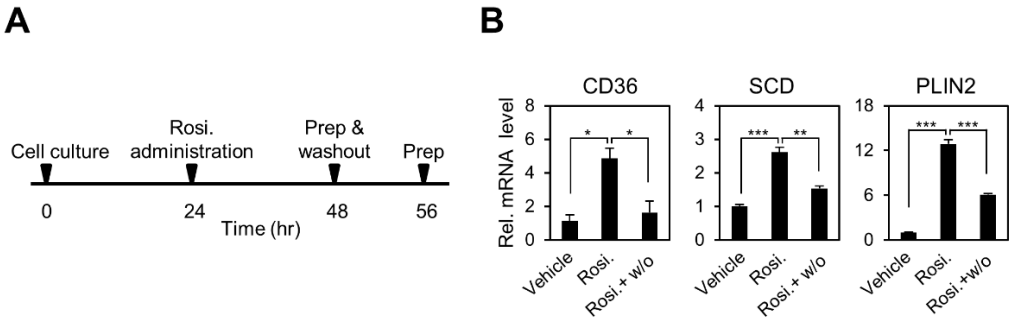

Figure III-9. Expression of PPARγ target genes changes in response to Rosi.+washout experimental conditions

(**A**) Schematic representation of experimental design. (**B**) Expression levels of PPARγ target genes in the absence or presence of RORα in Hep3B cells with or without Rosiglitazone (20 μM) treatment for 24 hr and washout 8 hr as determined by qRT-PCR. Expression was normalized to HPRT expression. Data expressed as mean ± S.E.M. Statistical analysis was performed using one-way ANOVA followed by Tukey's post hoc analysis. *p<0.05, **p<0.01, ***p<0.001.

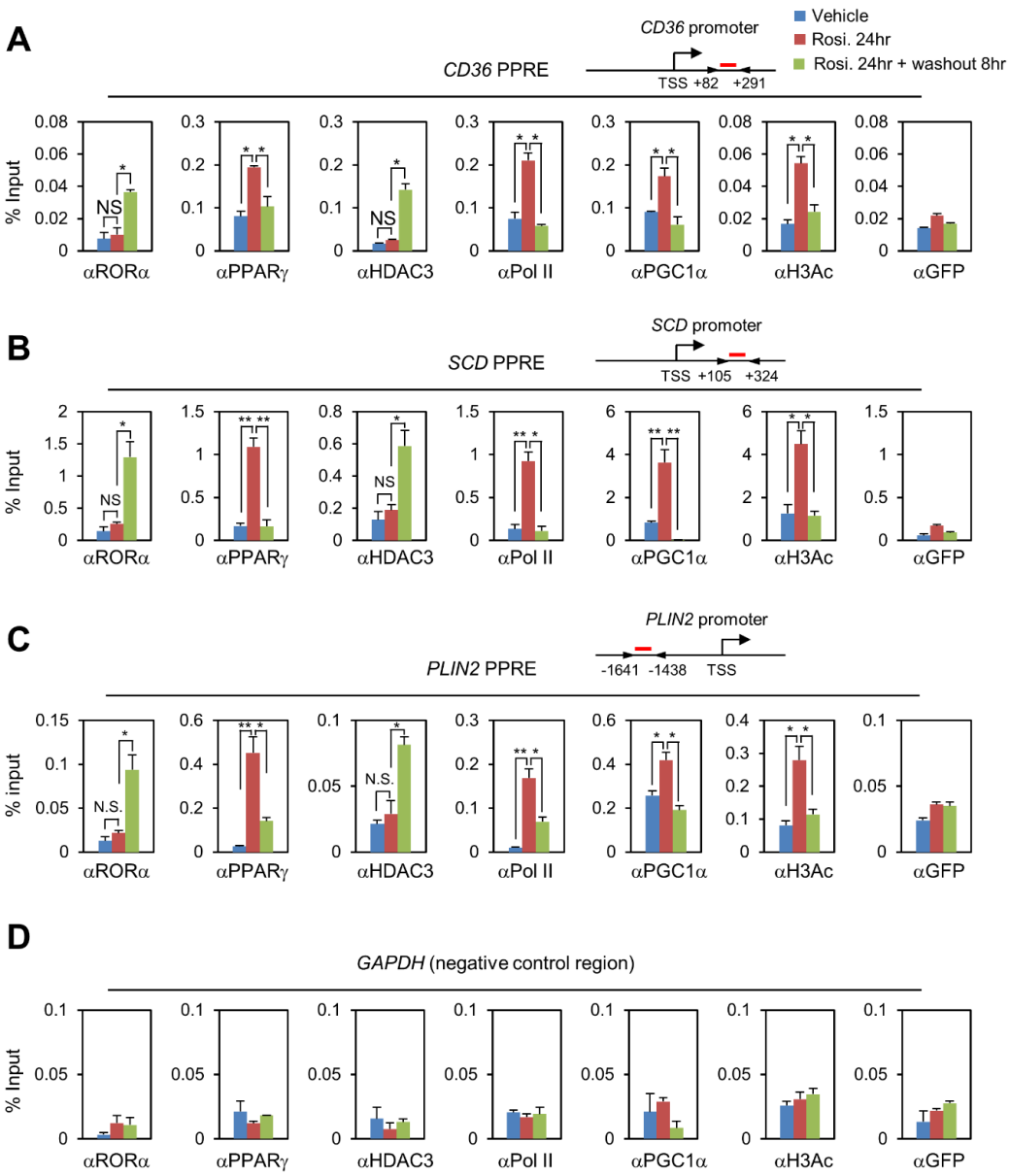
A
CD36 promoter
CD36 PPRE
TSS +82 +291
Vehicle
Rosi. 24hr
Rosi. 24hr + washout 8hr
% Input
NS
αRORα
αPPARγ
αHDAC3
αPol II
αPGC1α
αH3Ac
αGFP
B
SCD promoter
SCD PPRE
TSS +105 +324
C
PLIN2 promoter
PLIN2 PPRE
-1641 -1438 TSS
% input
N.S.
D
GAPDH (negative control region)

Figure III-10. ChIP assay in response to Rosi.+washout experimental conditions
(**A-D**) ChIP assays were performed on the *CD36* (**A**), *SCD* (**B**) and *PLIN2* (**C**) promoters and *GAPDH* negative region (**D**) in Hep3B cells with or without Rosiglitazone (20 μM) treatment for 24 hr and washout 8 hr. Promoter occupancy of RORα, PPARγ, HDAC3, Pol II, PGC1α, H3Ac and GFP was analyzed. Schematic of promoter region was represented with gene name. Red bar depicts locations of PPRE. Data expressed as mean ± S.E.M. Statistical analysis was performed using one-way ANOVA followed by Tukey's post hoc analysis. *$p<0.05$, **$p<0.01$.

The recruitment of RORα to PPARγ target genes promoter increases when PPARγ signal is reduced

Next, I further determined whether PPARγ antagonist GW9662 also resulted in the increased recruitment of RORα and HDAC3 to the PPARγ target promoters. Consistent with the results from 8 hr washout, GW9662 treatment significantly reduced the expression levels of PPARγ target genes (Fig. III-11A). ChIP assay revealed that recruitment of RORα and HDAC3 to the PPARγ target promoters were markedly increased, while PPARγ and Pol II recruitments were markedly reduced in response to GW9662 treatment (Fig. III-11B-D).

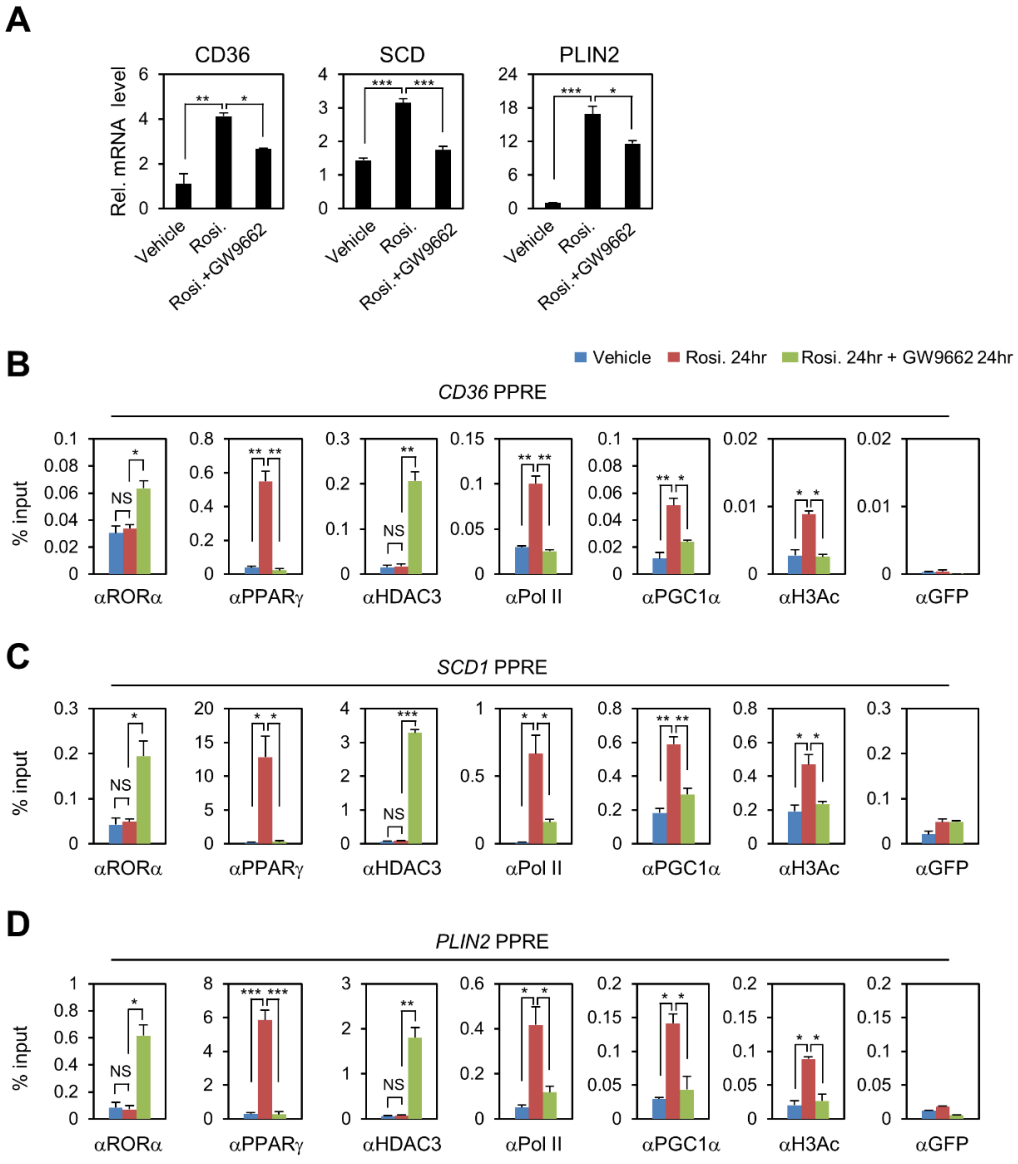
A
CD36
SCD
PLIN2
Rel. mRNA level
Vehicle
Rosi.
Rosi.+GW9662
B
Vehicle
Rosi. 24hr
Rosi. 24hr + GW9662 24hr
CD36 PPRE
% input
NS
αRORα
αPPARγ
αHDAC3
αPol II
αPGC1α
αH3Ac
αGFP
C
SCD1 PPRE
D
PLIN2 PPRE

Figure III-11. The recruitment of RORα to PPARγ target genes promoter increases when PPARγ signal is reduced and it is opposite to PPARγ recruitment

(**A**) Expression levels of PPARγ target genes in Hep3B cells with or without Rosiglitazone (20 μM) treatment for 24 hr and after treated GW9662 24 hr as determined by qRT-PCR. Expression was normalized to HPRT expression. Data expressed as mean ± S.E.M. (**B-D**) ChIP assays were performed on the *CD36* (**B**)*, SCD* (**C**) and *PLIN2* (**D**) promoters in Hep3B cells with or without Rosiglitazone (20 μM) treatment for 24 hr and after treated GW9662 24 hr. Promoter occupancy of RORα, PPARγ, HDAC3, Pol II, PGC1α, H3Ac and GFP was analyzed. Schematic of promoter region was represented in previous figure. Data expressed as mean ± SEM. Data expressed as mean ± S.E.M. Statistical analysis was performed using one-way ANOVA followed by Tukey's post hoc analysis. *p<0.05, **p<0.01, ***p<0.001.

RORα is required to recruit HDAC3 to PPARγ target genes promoter

To address HDAC3 recruitment to PPARγ target gene promoters requires RORα, I first examined the PPARγ target gene induction in the presence or absence of RORα. The induction of PPARγ target genes by rosiglitazone was further enhanced by RORα siRNA, indicating that RORα is a critical transcriptional repressor for PPARγ target gene expression (Fig. III-12A). RORα knockdown largely increased the recruitment of PPARγ for transcriptional activation with increased levels of H3 acetylation to the PPARγ target gene promoters (Fig. III-12B, C). While remarkably increased by rosiglitazone washout, the HDAC3 recruitment was substantially reduced by RORα knockdown even with setting of rosiglitazone washout (Fig. III-12B, C). Taken together, these data clearly indicate that RORα is required for recruitment of HDAC3 to PPARγ target gene promoters.

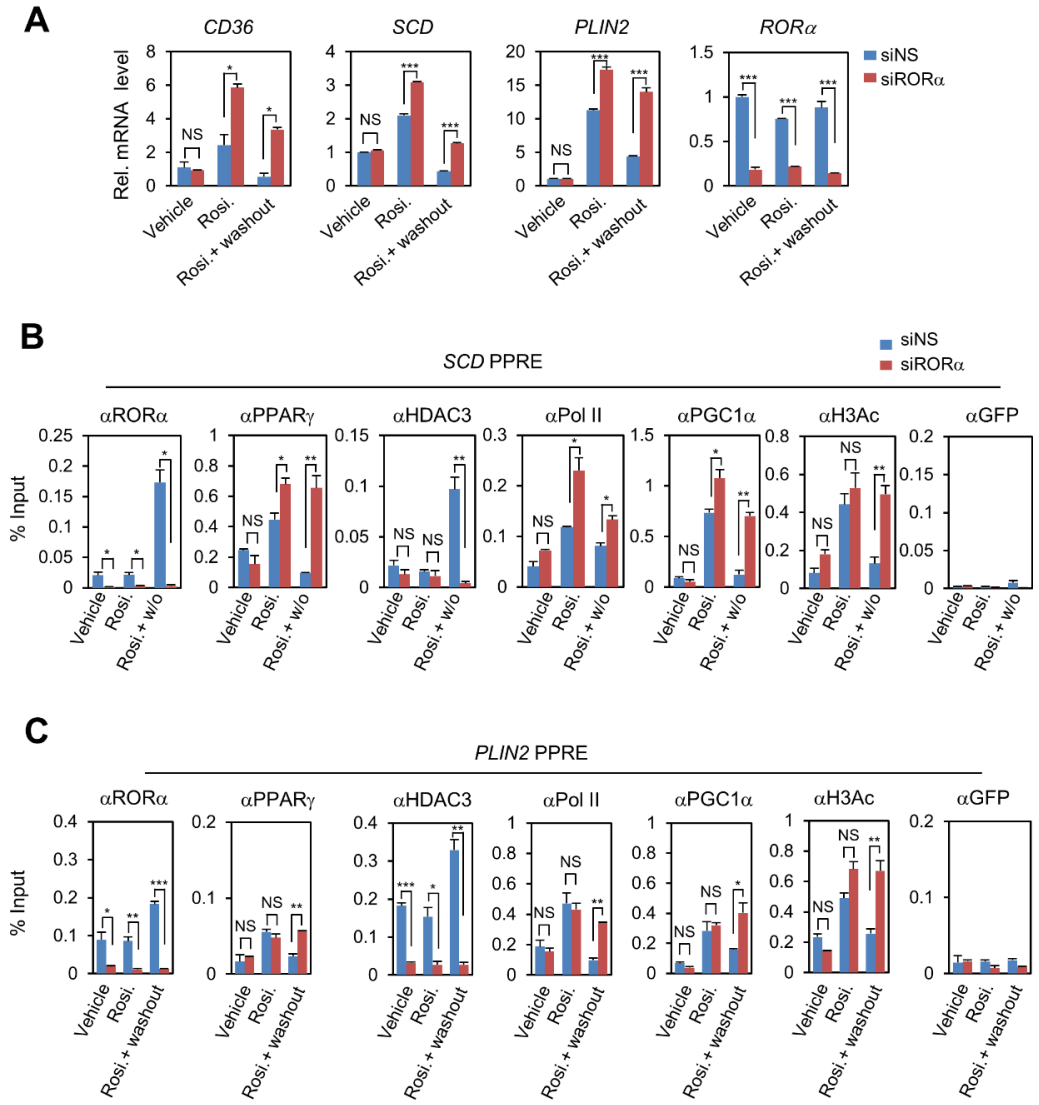
A
CD36
SCD
PLIN2
RORα
Rel. mRNA level
siNS
siRORα
NS
Vehicle
Rosi.
Rosi. + washout
B
SCD PPRE
αRORα
αPPARγ
αHDAC3
αPol II
αPGC1α
αH3Ac
αGFP
% Input
Rosi. + w/o
C
PLIN2 PPRE

Figure III-12. RORα is required to recruit HDAC3 to PPARγ target genes promoter
(**A**) Expression levels of PPARγ target genes and RORα in the absence or presence of RORα in Hep3B cells with or without Rosiglitazone (20 μM) treatment for 24 hr and washout 8 hr as determined by qRT-PCR. Expression was normalized to HPRT expression. Data expressed as mean ± S.E.M. Statistical analysis was performed using Student's unpaired t-test. *p<0.05, **p<0.01, ***p<0.001, NS=Non-Significant. (**B-C**) ChIP assays were performed in the absence or presence of RORα on *SCD* (**B**) or *PLIN2* (**C**) promoters in Hep3B cells with or without Rosiglitazone (20 μM) treatment for 24 hr and washout 8 hr. Promoter occupancy of RORα, PPARγ, HDAC3, Pol II, PGC1α, H3Ac and GFP was analyzed. Data expressed as mean ± S.E.M. Statistical analysis was performed using Student's unpaired t-test. *p<0.05, **p<0.01, ***p<0.001, NS=Non-Significant.

Recruitment of RORα and PPARγ to the PPARγ target gene promoters are mutually exclusive

To determine if RORα competes with PPARγ for the binding to the PPARγ target promoters, I transiently knocked down PPARγ in Hep3B cells. To mimic HFD feeding conditions *in vitro*, I treated cells with free fatty acid (FFA) and examined expression of PPARγ target genes. I observed that FFA treatment markedly increased PPARγ target gene expressions in both WT and *Pparα*-null mouse primary hepatocytes, indicating that PPARα failed to influence on PPARγ transcriptional network in the setting of HFD (Fig. III-13A). Next, I tested PPARγ target gene expressions in the presence of PPARγ siRNA or HDAC3 siRNA. While repressed by PPARγ siRNA, expression of PPARγ target genes was largely enhanced by HDAC3 siRNA in response to FFA treatment (Fig. III-13B). Consistent with gene expression, increased PPARγ recruitment by FFA was substantially diminished by PPARγ siRNA (Fig. III-14A, B). Interestingly, recruitment of RORα was dramatically increased to the PPARγ target gene promoters, and HDAC3 recruitment was accompanied by the RORα recruitment to PPARγ target promoters by knockdown of PPARγ (Fig. III-14A, B).

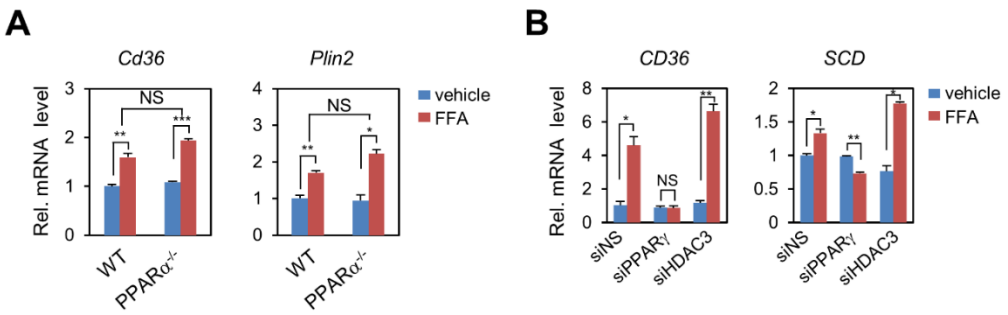

Figure III-13. PPARα fails to influence on PPARγ transcriptional network but HDAC3 affects PPARγ transcriptional network

(**A**) Expression levels of PPARγ target genes in primary hepatocyte from WT and PPARα$^{-/-}$ mice with or without free fatty acid (FFA: Oleic acid 200 μM and Palmitic acid 100 μM) treatment for 36 hr as determined by qRT-PCR. Expression was normalized to 36B4 expression. Data expressed as mean ± S.E.M. Statistical analysis was performed using two-way ANOVA. *p<0.05, **p<0.01, ***p<0.001, NS=Non-Significant. (**B**) Expression levels of PPARγ target genes in the absence or presence of PPARγ/HDAC3 in Hep3B cells with or without fatty acid (FFA: Oleic acid 200 μM and Palmitic acid 100 μM) treatment for 24 hr as determined by qRT-PCR. Expression was normalized to HPRT expression. Data expressed as mean ± S.E.M. Statistical analysis was performed using Student's unpaired t-test. *p<0.05, **p<0.01, NS=Non-Significant.

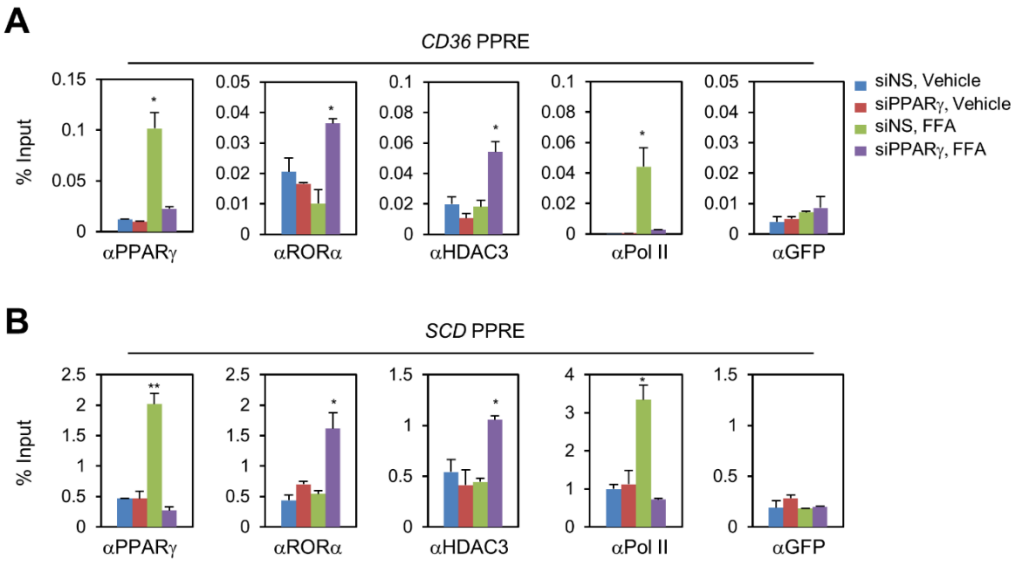

Figure III-14. Recruitment of RORα and PPARγ to the PPARγ target gene promoters are mutually exclusive

(**A-B**) ChIP assays were performed in the absence or presence of PPARγ on the *CD36* (**A**) and *SCD* (**B**) promoters in Hep3B cells with or without free fatty acid (FFA: Oleic acid 200 μM and Palmitic acid 100 μM) treatment for 24 hr. Promoter occupancy of PPARγ, RORα, HDAC3, Pol II and GFP was analyzed. Data expressed as mean ± S.E.M. S Statistical analysis was performed using one-way ANOVA. *p<0.05, **p<0.01, ***p<0.001.

RORα and HDAC3 compete with PPARγ for the binding to the PPARγ target gene promoter

Furthermore, Re-ChIP assay clearly indicated that PPARγ and RORα are able to bind to the same genomic region and their recruitments to promoter of target genes are mutually exclusive (Fig. III-15). These data strongly indicate that RORα and HDAC3 compete with PPARγ for the binding to the target gene promoters for regulation of gene expressions with opposite transcriptional outputs. Altogether, my data demonstrate that RORα functions as a corepressor along with HDAC3 and is co-recruited to the PPARγ target promoters for the repression of PPARγ-mediated transcriptional activity.

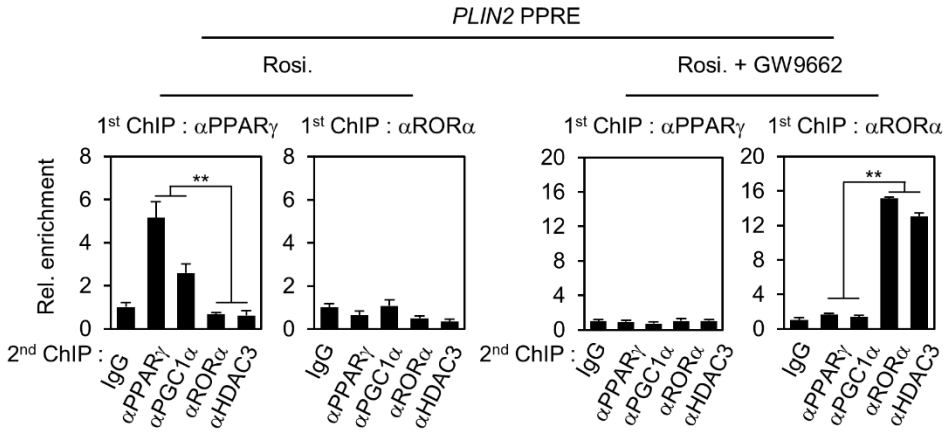

Figure III-15. RORα and HDAC3 compete with PPARγ for the binding to the target gene promoter

Re-ChIP assays were performed in the absence or presence of RORα on *PLIN2* promoters in Hep3B cells with or without Rosiglitazone (20 μM) treatment for 24 hr and after treated GW9662 24 hr to determine whether RORα and PPARγ are assembled on the same promoter. Data expressed as mean ± S.E.M. Statistical analysis was performed using one-way ANOVA followed by Tukey's post hoc analysis. *p<0.05, **p<0.01, ***p<0.001.

RORα is required to recruit HDAC3 and competes with PPARγ for the binding to the PPARγ target gene promoters

To determine whether RORα recruitment is accompanied by the presence of HDAC3, I examined recruitment of RORα to the PPARγ target gene promoters in the presence of HDAC3 siRNA. While little or no difference of the recruitment of RORα and PPARγ was observed, Pol II recruitment to the PPARγ target gene promoters was markedly increased by HDAC3 knockdown (Fig. III-16A, B), indicating that the presence of HDAC3 affected the recruitment of RNA polymerase II to the PPARγ target gene promoters. Taken together, these data indicate that both RORα and HDAC3 serve as transcriptional corepressors on the PPARγ target gene promoters for the repression of PPARγ target gene expressions.

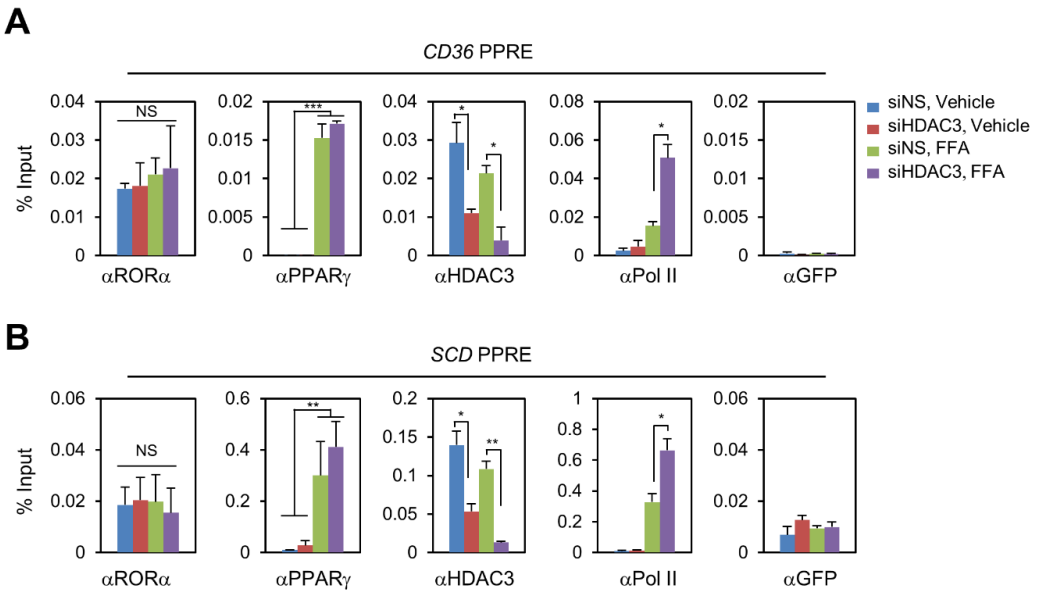

Figure III-16. The presence of HDAC3 affected the recruitment of RNA polymerase II to the PPARγ target gene promoters

(**A-B**) ChIP assays were performed in the absence or presence of HDAC3 on the *CD36* (**A**) and *SCD* (**B**) promoters in Hep3B cells with or without free fatty acid (FFA: Oleic acid 200 μM and Palmitic acid 100 μM) treatment for 24 hr. Promoter occupancy of PPARγ, RORα, HDAC3, Pol II and GFP was analyzed. Data expressed as mean ± S.E.M. S Statistical analysis was performed using one-way ANOVA. *p<0.05, **p<0.01, ***p<0.001.

PPARγ antagonism restores metabolic homeostasis in HFD-fed RORα^{LKO} mice

Since RORα turned out to play a key role to repress PPARγ transcriptional activity *in vitro* and *in vivo*, I next examined if inhibition of PPARγ transcriptional activities restores impaired metabolic homeostasis. For this, PPARγ antagonist GW9662 were treated to RORα$^{f/f}$ and RORα^{LKO} mice for 5 weeks with HFD. Intriguingly, the body weight gain of both RORα$^{f/f}$ and RORα^{LKO} mice were markedly reduced by GW9662 treatment compared with vehicle-treated control mice (Fig. III-17A). The reduction of body weight gain by GW9662 in RORα^{LKO} mice was much greater, leading to similar body weight to GW9662-treated RORα$^{f/f}$ mice, indicating that inhibition of PPARγ activity remarkably reduces body weight gain in RORα^{LKO} mice (Fig. III-17A). Similar to reduced body weight gain, tissue weights of the liver and eWAT were markedly reduced by GW9662 treatment in both RORα$^{f/f}$ and RORα^{LKO} mice (Fig. III-17B, C). Consistently, cross-sectional area of adipocytes was significantly reduced by GW9662 treatment (Fig. III-17D). In accordance with body weight reduction, PPARγ antagonism markedly reduced hepatic steatosis in both RORα$^{f/f}$ and RORα^{LKO} mice (Fig. III-17E). Consistently, gene expression profile analysis exhibited that target gene expression levels involved in hepatic gluconeogenesis and lipogenesis are largely reduced by GW9662 treatment (Fig. III-17F, G). Together, I demonstrate that enhanced PPARγ transcriptional activity by RORα deficiency is de-activated by PPARγ antagonism to restore metabolic homeostasis, including body weight gain, hepatic steatosis, and glucose and lipid metabolism.

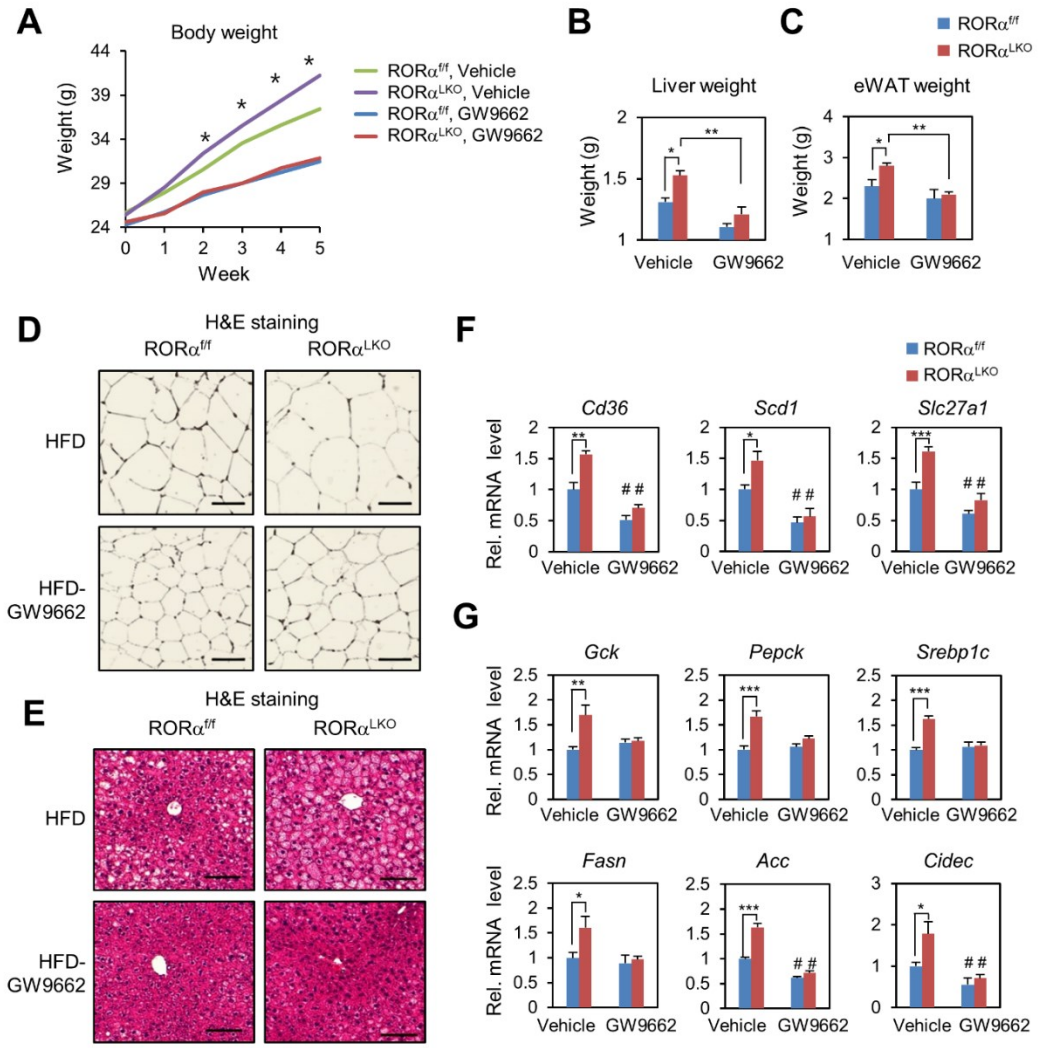
A
Body weight
Weight (g)
Week
RORα f/f, Vehicle
RORα LKO, Vehicle
RORα f/f, GW9662
RORα LKO, GW9662
B
Liver weight
Weight (g)
Vehicle
GW9662
C
eWAT weight
RORα f/f
RORα LKO
D
H&E staining
RORα f/f
RORα LKO
HFD
HFD-GW9662
E
H&E staining
F
Cd36
Scd1
Slc27a1
Rel. mRNA level
G
Gck
Pepck
Srebp1c
Fasn
Acc
Cidec

Figure III-17. PPARγ antagonism restores metabolic homeostasis in RORα^{LKO} mice
(**A-E**) RORα$^{f/f}$ and RORα^{LKO} mice were fed HFD with or without GW9662 for 5 weeks (n=4-5/group). (**A**) Body weight curves. Data expressed as mean ± SEM. Statistical analysis was performed using Student's unpaired t-test. *p<0.05, RORα$^{f/f}$ vs RORα^{LKO}, vehicle. (**B** and **C**) Liver (**B**) and eWAT (**C**) weight of RORα$^{f/f}$ and RORα^{LKO} mice were fed HFD with or without GW9662 for 5 weeks. Data expressed as mean ± S.E.M. Statistical analysis was performed using two-way ANOVA. *p<0.05, **p<0.01. (**D** and **E**) Representative histological section images from eWAT (**D**) and liver (**E**) of RORα$^{f/f}$ and RORα^{LKO} mice fed HFD with or without GW9662 for 5 weeks. Scale bar, 100 μm. (**F** and **G**) Expression levels of PPARγ target genes (**F**) or gluconeogenesis/lipogenesis/lipid sequestration genes (**G**) in liver from RORα$^{f/f}$ and RORα^{LKO} mice fed HFD with or without GW9662 for 5 weeks as determined by qRT-PCR. Expression was normalized to 36B4 expression. Data expressed as mean ± S.E.M. Statistical analysis was performed using Student's unpaired t-test. *p<0.05, **p<0.01, ***p<0.001, #p<0.05 compared to each vehicle group.

III-4. Discussion

Obesity is one of the most prominent metabolic disorders, and the danger of obesity has recently been emphasized. Obesity has been studied primarily as a result of living environmental factors such as overeating and the reduction of physical activities. However, recent studies have shown that obesity can also be caused by genetic factors. Therefore, identifying genetic phenomena that control obesity is emerging as a new way to treat various metabolic disorders including obesity (Heymsfield and Wadden, 2017).

PPARγ is known to play a role in regulating adipocyte differentiation and lipid storage as an important regulator of the adipogenesis genes in adipocytes (Tontonoz et al., 1994) However, the role of PPARγ in the liver, an important organ that regulates metabolism as well as adipocytes, has not yet been established. Recent studies have shown that PPARγ plays a role in promoting lipid accumulation in the liver. In ob/ob mice, deficiency of PPARγ resulted in the improvement of hepatic steatosis (Gavrilova et al., 2003; Matsusue et al., 2003), and liver-specific *Pparγ* deficient mice had decreased hepatic steatosis when fed HFD (Moran-Salvador et al., 2011). These results suggest that inhibition of PPARγ plays a role in inhibiting the progression of hepatic steatosis through inducing inhibition of lipid accumulation in the liver.

In this study, I found that liver-specific *Rorα* deficient mice fed HFD induced more severe obesity and promoted hepatic steatosis. To investigate what kind genetic changes caused the physiological consequences, I examined the expression pattern of total genes through total mRNA sequencing using the liver. As a result, it was confirmed that the PPARγ signal

was greatly increased by RORα deficiency. This means that RORα plays a role in suppressing the PPARγ signaling pathway in the liver. Since PPARγ plays a role in promoting lipid accumulation in the liver, RORα suppresses the lipid accumulation in the liver through inhibition of PPARγ signal.

PPRE has a DR1 motif, the DR1 motif consists of two repeats of the AGGTCA sequence (Kliewer et al., 1992). Since the AGGTCA sequence is identical to the sequence of the core motif of RORE, it can be expected that RORα can bind to PPRE. I confirmed RORα recruited to PPRE through ChIP assay. Moreover, RORα and PPARγ competed with each other on PPRE and that RORα suppressed the PPARγ transcriptional activity. At this point, I found that RORα bound with HDAC3 as a corepressor, then recruited HDAC3 to the PPRE and suppressed the PPARγ signaling pathway. HDAC3 is also known to inhibit lipid production and sequestration in the liver to inhibit hepatic steatosis. In this study, a role of HDAC3 in the liver is to suppress PPARγ signaling pathway via RORα.

Liver-specific *Rorα* deficient mice have severe obesity and hepatic steatosis because PPARγ signaling pathway is not suppressed by RORα deficiency. At this time, suppression of the PPARγ signaling may be expected to alleviate the metabolic disorder. Therefore, I examined whether the PPARγ antagonist, GW9662, was administered to liver-specific RORα deficient mice to reconstitute obese and hepatic steatosis phenotypes. Liver - specific *Rorα* deficient mice treated with GW9662 showed obesity and hepatic steatosis are ameliorated, and decreased expression of genes involved in lipogenesis and lipid sequestration. These results confirm that RORα is an important regulator of fine-tuning the

diet-induced obesity by inhibiting the PPARγ signaling pathway.

Taken together, my data shows that RORα binds HDAC3 and competes with PPARγ on PPRE to suppress PPARγ signaling in response to over-nutrient cue. These results clearly demonstrate the role of RORα in the liver, suggesting that modulation of RORα activity is a therapeutic target for metabolic disorders.

III-5. Materials and Methods

Analysis of mRNA-sequencing data

After removing adapter sequences (TrueSeq universal and index adapters), I used cutadapter software (Martin, 2011) to trim the reads that PHRED scores lower than 20. Remaining reads were aligned to the mouse reference genome (GRCm38) using TopHat aligner (Trapnell et al., 2009). After the alignment, I quantified the expression of genes as Fragments Per Kilobase of transcript per Million mapped reads (FPKM) for each gene using Cufflinks (Trapnell et al., 2010). To identify the DEGs, I first selected the 'expressed' genes as the ones with FPKM larger than 1 under at least one of the eight samples. For the expressed genes, $\log_2$(FPKM+1) values were normalized across eight samples using the quantile normalization method. To identify the DEGs, for each gene, I calculated a T-statistic and $\log_2$-fold-change in the comparisons of $ROR\alpha^{LKO}/ROR\alpha^{f/f}_{HFD}$ and $ROR\alpha^{LKO}/ROR\alpha^{f/f}_{CD}$. I then estimated empirical distributions of T-statistics and $\log_2$-fold-changes for the null hypothesis by random permutation of the eight samples (1000 permutations). Based on the distributions, for each gene, I computed adjusted P-values for the observed T-statistic and $\log_2$-fold-change and the combined these P-values with Stouffer's method (Hwang et al., 2005). Finally, I identified the DEGs as the ones that have the combined P-value ≤ 0.05 and absolute $\log_2$-fold-change ≥ 0.439, which is a cutoff value (the 95^{th} percentile of the empirical distribution for $\log_2$-fold-changes) for each comparison. I further identified RORα-dependent genes under HFD condition as the ones with

significant differences between the log_2-fold-change in the two comparisons above ($ROR\alpha^{LKO}/ROR\alpha^{f/f}_{HFD}$ and $ROR\alpha^{LKO}/ROR\alpha^{f/f}_{CD}$) larger than 0.439.

Functional enrichment analysis and TF enrichment analysis

For the genes in Groups 1-8, enrichment analysis of GOBPs and KEGG pathways were performed using a DAVID software (Huang da et al., 2009b). I selected the GOBPs and KEGG pathways with P-value<0.05 as the ones represented by the genes analyzed. For the genes in Group 1, TF enrichment analysis was performed using a ChEA2 software (Kou et al., 2013). Among the TF-target gene data, only mouse TF-target gene data were used for the enrichment analysis. I selected the TFs with P-value<0.01 as the ones significantly regulating the genes in Group 1.

Luciferase reporter assay

HEK293T cells and Hep3B cells were grown and transiently transfected by using Polyethylenimine (PEI) and turbofect (Thermo Scientific, R0531). For luciferase reporter assays, 1 x 10^5 cells were seeded in DMEM supplemented with 10 % FBS and 1 % antibiotics. Cells were transfected with PPRE-luciferase reporters and β-galactosidase expression constructs along with several expression constructs were indicated in each figure. Using a luciferase assay system (Promega), the luciferase activity was measured with a luminometer (Berthold Technologies) after 48 hr of transfection. Transfection efficiency was normalized by β-galactosidase expression. The results were obtained from at least three independent experiments.

Co-immunoprecipitation assay

HEK293T cells that transfected with Flag-HDACs and HA-RORα were cultured and lysed with lysis buffer (200 mM NaCl, 50 mM Tris-HCl, pH 8.0 and 0.5 % NP40). About 20 mg of cell extracts was immunoprecipitated with each 1 μg of anti-Flag antibody overnight and then incubated with 35 μl (50 % slurry) of protein A/G agarose beads for 1 h. The immunoprecipitated materials were washed with 500 μl of washing buffer (150 mM NaCl, 50 mM Tris-HCl, pH 8.0, and 0.5 % NP40) for four times and bound materials were eluted by boiling in 50 μl of sampling buffer (2 % β-mercaptoethanol, 5 % glycerol, 1 % SDS and 60 mM Tris-HCl, pH 6.8) and subjected to immunoblot analysis. Protein samples were resolved by sodium dodecyl sulphate-polyacrylamide gel electrophoresis (SDS-PAGE) Images of the immunoblots were visualized and recorded using the LAS 4000-mini system (Fujifilm).

Chromatin Immunoprecipitation (ChIP) and Re-ChIP assays

The ChIP assays were conducted as described. Cells were crosslinked with 1 % formaldehyde for 10 min at room temperature. Mouse livers were harvested and quickly washed with PBS and crosslinked with 1 % formaldehyde for 10 min at room temperature, followed by quenching with 0.125 M glycine solution for 5 min. Then, cells or harvested mouse livers were washed with ice-cold PBS two times. Chromatin fragmentation was performed by sonication in ChIP lysis buffer (50 mM Tris-HCl [pH 8.1], 1% SDS, 10 mM EDTA [pH 7.6], and protease inhibitor cocktail) with an average size of

approximately 500 bp. Proteins were immunoprecipitated in ChIP dilution buffer (1% Triton X-100, 2 mM EDTA, 150 mM NaCl, 20 mM Tris-HCl [pH 8.1], and protease inhibitor cocktail). Crosslinking was reversed overnight at 65 °C in elution buffer (1% SDS, 0.1 M NaHCO3), and DNA was purified with a QIAquick Gel Extraction Kit (QIAGEN). For the Re-ChIP assay, components were eluted from the first immunoprecipitation reaction by incubation with 10 mM DTT at 37°C for 30 min and diluted 1:50 with ChIP dilution buffer containing 20 mM Tris-HCl (pH 8.1), 150 mM NaCl, 2 mM EDTA, and 1% Triton X-100 followed by reimmunoprecipitation with the secondary antibody. Precipitated DNA was analyzed by quantitative PCR. For real-time quantitative PCR analysis, 2 μl from 60 μl DNA extractions was used. All reactions were performed in triplicates. Primers used for analysis are as follows;
mCd36 PPRE Fwd: 5′-GTGTGCCTTTTGCATCTTGA-3′ and Rev: 5′-GGGGCACTA-ACAGAAAACGA-3′; *mScd1* PPRE Fwd: 5′-CTTTGTGTAGCCCTGGCTGT-3′ and Rev: 5′-TGAGGTTACCTGTGGTCACG-3′; *mPlin2* PPRE Fwd: 5′-GCTGGGGATTA-CAGACCAGA-3′ and Rev: 5′-TCTTGGGGTTTTGGAAAATG-3′; *mAcox1* PPRE Fwd: 5′-CGGAAACCAGAAGGGAATG-3′ and Rev: 5′-TAGCCAACGACAATGAACC-3′; *mFgf21* PPRE Fwd: 5′-TTTCTCCTGTGTTGAATCCC-3′ and Rev: 5′-GTTCCTGCCA-AGTGTGTC-3′; *CD36* PPRE Fwd: 5′-AGGGGGTGTGGTTGCATATT-3′ and Rev: 5′-TCTGGGTGATGGGAAAAATC-3′; *SCD* PPRE Fwd: 5′-GTGGTGTGGTGTCGGTG-TC-3′ and Rev: 5′-AGCCGGGAATTTAAAGGCTA-3′; *GAPDH* negative region Fwd: 5′-CACCGTCAAGGCTGAGAAC-3′ and Rev: 5′-GCCACACCATCCTAGTTGC-3′

GW9662 treated mice

HFD-fed RORα$^{f/f}$ and RORα^{LKO} male mice at 8 weeks of age were subjected to GW9662 at a dose of 0.35 mg/kg body weight/day in their drinking water for 5 weeks or to an equivalence volume of vehicle. The sample sizes for this study was announced in figure legend.

Quantitative real-time RT-PCR

Total RNAs were extracted using Trizol (Invitrogen) and reverse transcription was performed from 2.5 μg of total RNAs using the M-MLV cDNA Synthesis kit (Enzynomics). The abundance of mRNA was detected by a CFX384 Touch^{TM} Real-Time PCR Detection System (Bio-Rad) with SYBR Green (Enzynomics). The quantity of mRNA was calculated using ΔΔCt method and normalized by using primers indicated in each figure legend. All reactions were performed as triplicates. Primers used for analysis are as follows:

CD36 Fwd: 5′-AAGCCAGGTATTGCAGTTCTTT-3′ and Rev: 5′-GCATTTGCTGATG-TCTAGCACA-3′; *SCD* Fwd: 5′-GCCCCTCTACTTGGAAGACGA-3′ and Rev: 5′-AA-GTGATCCCATACAGGGCTC-3′; *PLIN2* Fwd: 5′-ATGGCATCCGTTGCAGTTGAT-3′ and Rev: 5′-GGACATGAGGTCATACGTGGAG-3′; *RORα* Fwd: 5′-CGGTGCGCAG-ACAGAGCTAT-3′ and Rev: 5′-CCACAGATCTTGCATGGAATAATT-3′; *HPRT* Fwd: 5′-TGACACTGGCAAAACAATGCA-3′ and Rev: 5′-GGTCCTTTTCACCAGCAAG-CT-3′

Antibodies

Commercially available antibodies were used: anti-RORα (sc-28612; 1:1,000 dilution for IB analysis, 5 μg for ChIP assay), anti-PPARα (sc-9000x, 1 μg for ChIP assay) and anti-GFP (sc-9996 , 1 μg for ChIP assay) from Santa Cruz Biotechnology; anti-β-actin (A5441; 1:5,000 dilution for IB analysis) and anti-FLAG (F3165, Sigma, 1:5,000 dilution for IB analysis, 1 μg for IP assay) from Sigma; anti-HA (MMS-101R; 1:5,000 dilution for IB analysis, 1 μg for IP assay) from Covance; anti-H3Ac (#06-599, 1 μg for ChIP assay) from Millipore; anti-PPARγ (ab41928, 1 μg for ChIP assay), anti-PGC1α (ab54481, 1 μg for ChIP assay) and anti-HDAC3 (ab7030, 1 μg for ChIP assay) from Abcam; anti-RNA polymerase II (MMS-126R, 1 μg for ChIP assay) from Berkeley antibody company; anti-V5 (R96025; 1:5,000 dilution for IB analysis) from Invitrogen.

Statistical analysis

The statistical analysis of different groups is realized using the Student's unpaired t-test or one-way ANOVA followed by Tukey post hoc test or two-way ANOVA. SPSS software (IBM) was used for all analyses.

Accession Number

The accession number for the mRNA sequencing data reported in this paper is GEO: GSE83338.

CHAPTER IV
Conclusion

Hepatic nuclear receptors play critical roles in the regulation of lipid and glucose metabolism in response to environmental stress, including nutrient and hormonal cues (Wagner et al., 2011). Dysfunction of hepatic nuclear receptors is largely linked to metabolic diseases including obesity and type II diabetes. I found that PPARγ signaling is a critical pathway affected by hepatic deletion of RORα. Dysregulated PPARγ signaling in RORα^{LKO} mice results in uncontrolled lipogenesis, contributing to the development of hepatic steatosis and diet-induced obesity on a HFD. Furthermore, treatment of PPARγ antagonist GW9662 decreased the susceptibility to obesity (Ma et al., 2015; Nakano et al., 2006). Consistent with previous reports, I also observed that elevated PPARγ transcriptional activity in RORα^{LKO} mice are down-regulated after treatment of GW9662, resulting in decrease of diet-induced hepatic steatosis and obesity. My data confirm that RORα is a key factor for the repression of PPARγ signaling to protect against diet-induced hepatic steatosis and obesity *in vivo.*

It has been widely accepted that PPARα is a major nutrient-sensing PPAR isoform to modulate hepatic gene expressions (Lee et al., 2014). As no substantial activation of PPARα has been observed in the fasted or HFD-fed RORα^{LKO} mice, I believe that RORα mainly controls PPARγ transcriptional network to maintain hepatic homeostasis in response to HFD. PPARγ signaling turns out to be significantly activated in HFD-fed RORα^{LKO} mice while increased RORα reduces PPARγ transcriptional activity, providing a direct molecular link between RORα and PPARγ. Furthermore, my data indicate that RORα regulates PPARγ signaling through RORα-mediated HDAC3 recruitment to the PPARγ target

promoters. Thus, RORα plays a crucial role in maintaining homeostasis of lipid metabolism in liver by negatively regulating PPARγ signaling via HDAC3 recruitment to the PPARγ target promoters for transcriptional repression (Fig. IV-1).

While PPARγ is a key regulator of adipogenesis and activates target genes that are involved in lipid storage mechanism in adipocyte to improve glucose homeostasis (Tontonoz and Spiegelman, 2008), the molecular mechanism of how PPARγ induces hepatic steatosis still remains unclear. Though PPARγ activation has shown to reduce blood glucose level and hepatic gluconeogenesis, and improve glucose tolerance (Saltiel and Olefsky, 1996; Way et al., 2001), several reports have shown that PPARγ activation leads to hepatic steatosis (Mayerson et al., 2002; Musso et al., 2012). In general, the expression of PPARγ is very low in human and mouse liver. Interestingly, the expression level of hepatic PPARγ is significantly upregulated in obese rodent model (Vidal-Puig et al., 1996) and high level of PPARγ in mouse liver is sufficient for the induction of adipogenic transformation of hepatocytes with adipose tissue-specific gene expression and lipid accumulation (Yu et al., 2003). These data indicate that PPARγ plays a key role in development of hepatic steatosis. Accordingly, inhibition of PPARγ signaling and hepatic deficiency of PPARγ in ob/ob mice have shown to ameliorate fatty liver (Gavrilova et al., 2003; Matsusue et al., 2003). Intriguingly, liver-specific PPARγ deficient mice exhibit resistance to HFD-induced hepatic steatosis (Moran-Salvador et al., 2011). Expression of numerous genes involved in lipid uptake and lipid transport was remarkably decreased in the liver-specific PPARγ-deficient mice, resulting in reduction of hepatic steatosis (Moran-

Salvador et al., 2011). Therefore, these results strongly indicate that the PPARγ signaling pathway is involved in diet-induced hepatic steatosis, and hepatic lipid accumulation is prevented by suppression of PPARγ transcriptional network in the liver.

It has been reported that RORα may compete with PPARγ for the binding to PPRE (Ohoka et al., 2009). It is well established that PPRE contains a DR1 motif consisting of two core direct repeats of AGGTCA separated by a single nucleotide (Kliewer et al., 1992). Among nucleotides of DR1 motif, the four nucleotides immediately 5' of DR1 motif are highly conserved and exhibit a consensus of A(A/T)CT. Previous study has reported that the binding of the DBD of PPARs to the single core binding site requires the AT-rich 5'-extended binding site which is quite similar to the binding site for the monomer of RORα (Palmer et al., 1995). Thus, the similarity in the binding sequences for PPARγ and RORα appears to allow RORα to modulate PPAR signaling by competing with PPARγ for binding to PPREs (Harding and Lazar, 1995).

The physiological role of HDAC3 has been reported to repress hepatic steatosis. In liver-specific *Hdac3* deficient mice, little or no body weight change was observed. As HDAC3 regulates the expression of lipogenic genes in an enzymatic activity-independent manner (Sun et al., 2013), fasting phase markedly promotes hepatic steatosis in liver-specific *Hdac3* deficient mice (Sun et al., 2012). An intriguing observation in this study is that RORα is crucial to recruit HDAC3 to repress hepatic PPARγ-mediated lipogenic genes and protect against diet-induced hepatic steatosis and obesity. Furthermore, repressive role of RORα-mediated HDAC3 on lipid metabolism is coupled with elevated hepatic gluconeogenesis.

Though hepatic HDAC3 has been shown to promote gluconeogenesis by repressing lipid synthesis and sequestration (Sun et al., 2012), I observed notable increase of gene expression involved in hepatic gluconeogenesis in HFD-fed RORα^{LKO} mice. Intriguingly, HDAC3 ablation upregulated hepatic expression of perilipin gene which contributes to lipid sequestration to ameliorate glucose tolerance (Sun et al., 2012). I also noticed that perilipin 2, hepatic isoform of perilipin was substantially elevated in HFD-fed RORα^{LKO} mice. Unlike hepatic HDAC3 ablation, impaired RORα-mediated HDAC3 transcriptional repression led to interfere hepatic homeostasis of PPARγ signaling. Therefore, disturbed regulatory mechanism of PPARγ signaling in HFD-fed RORα^{LKO} mice would be the main cause of the insulin resistance and glucose intolerance. Consistent with elevated fasting glucose level in HFD-fed RORα^{LKO} mice, mRNA level of the rate-limiting enzyme, phosphoenol pyruvate carboxykinase (PEPCK), in the hepatic gluconeogenesis pathway, was largely elevated in HFD-fed RORα^{LKO} mice. Together, my data strongly indicate that physiological role of HDAC3 in the liver is to suppress PPARγ transcriptional activity via RORα to control hepatic lipid and glucose metabolism.

Previously, it has been reported that bile acid signaling pathway is critical to modulate energy expenditure in brown adipose tissue. Bile acids activates mitogen-activated protein kinase pathways and serve as ligands for the G protein coupled receptor (GPCR) TGR5 (Watanabe et al., 2006). Thus, hepatic bile acid synthesis and bile acid pool size in the serum is critical to control metabolic rate. Bile acids induces cyclic-AMP-dependent thyroid hormone activating enzyme type 2 iodothyronine deiodinase (Dio2) (Watanabe et al., 2006).

Thus, bile acid-TGR5-cAMP-Dio2 signaling pathway in the brown adipose tissue has been known as a crucial mechanism to modulate energy expenditure (Watanabe et al., 2006). I observed that several key genes involved in bile acid synthesis were largely downregulated as well as serum bile acid pool size in HFD-fed RORα^{LKO} mice. Though I still do not know the direct mechanism of how hepatic bile acid signaling was impaired in RORα^{LKO} mice, I speculate that impaired hepatic bile acid synthesis would impair TGR5 activation in brown adipose tissue to reduce energy expenditure.

Several of the observed metabolic alterations in the RORα^{LKO} mice are indeed different from those observed in *Staggerer* mice. For example, RORα^{LKO} mice gain significantly more weight than WT mice and develop hepatic steatosis when fed with HFD. However, *Staggerer* mice are protected from HFD-induced obesity and fatty liver and display improved insulin sensitivity (Lau et al., 2011; Lau et al., 2008). A strong difference between these two mouse models is their overall growth condition. RORα^{LKO} mice have no obvious phenotypic abnormalities under normal dietary conditions, whereas *Staggerer* mice suffer from severe growth retardation that would likely be attributed to a number of developmental defects. In addition, defective RORα function in other tissues including brain is likely to systemically affect energy intake and expenditure in the *Staggerer* mice, making it difficult to specifically dissect hepatic function of RORα. Therefore, it would be helpful to utilize these two mice and compare their phenotypes in certain conditions together for understanding of RORα function *in vivo*. Collectively, my data indicate that liver-specific RORα deficient mice were successfully developed and the utilization of the mice allowed

us to be able to study *in vivo* functions of RORα in liver more precisely by excluding the potential secondary effect of *Staggerer* mice.

In conclusion, my data indicate that RORα requires HDAC3 to regulate PPARγ signaling to maintain lipid homeostasis in response to over-nutrient cue. I demonstrate that major target of RORα in the liver is the PPARγ signaling and lipid/glucose metabolism. My findings provide a direct link between RORα and hepatic fatty acid and glucose metabolism. Thus, therapeutic strategies designed to modulate RORα activity may be beneficial for the treatment of hepatic disease as well as obesity-associated metabolic diseases.

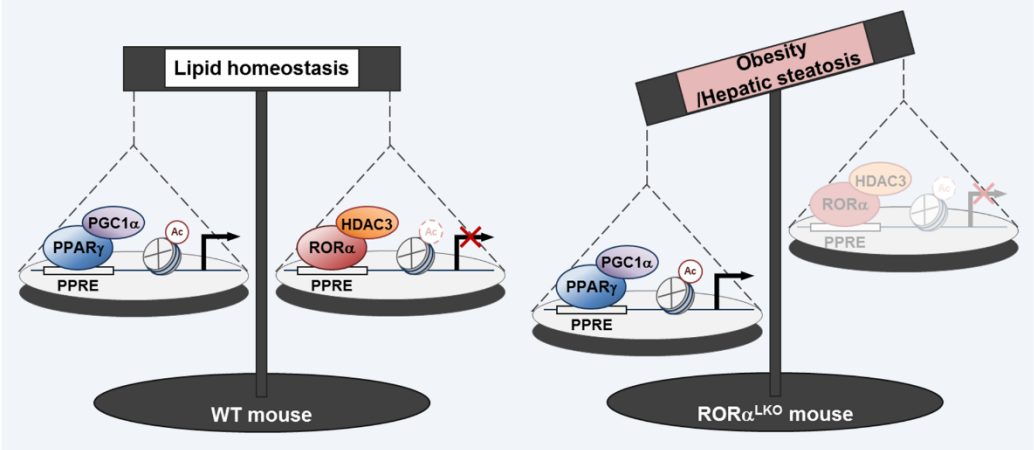

Figure IV-1. Graphical summary of the newly identified role of RORα that negatively regulated PPARγ signaling via HDAC3 recruitment to the PPARγ target promoters
Proposed model for the role of RORα in hepatocyte. RORα regulates PPARγ signaling via HDAC3 recruitment to the PPARγ target promoters for transcriptional repression.

REFERENCES

Agarwal, A.K., and Garg, A. (2002). A novel heterozygous mutation in peroxisome proliferator-activated receptor-γ gene in a patient with familial partial lipodystrophy. J Clin Endocrinol Metab *87*, 408-411.

Aranda, A., and Pascual, A. (2001). Nuclear hormone receptors and gene expression. Physiol Rev *81*, 1269-1304.

Atkins, G.B., Hu, X., Guenther, M.G., Rachez, C., Freedman, L.P., and Lazar, M.A. (1999). Coactivators for the orphan nuclear receptor RORα. Mol Endocrinol *13*, 1550-1557.

Bain, D.L., Heneghan, A.F., Connaghan-Jones, K.D., and Miura, M.T. (2007). Nuclear receptor structure: implications for function. Annu Rev Physiol *69*, 201-220.

Barak, Y., Nelson, M.C., Ong, E.S., Jones, Y.Z., Ruiz-Lozano, P., Chien, K.R., Koder, A., and Evans, R.M. (1999). PPARγ is required for placental, cardiac, and adipose tissue development. Mol Cell *4*, 585-595.

Barish, G.D., Narkar, V.A., and Evans, R.M. (2006). PPARδ: a dagger in the heart of the metabolic syndrome. J Clin Invest *116*, 590-597.

Becker-Andre, M., Andre, E., and DeLamarter, J.F. (1993). Identification of nuclear receptor mRNAs by RT-PCR amplification of conserved zinc-finger motif sequences. Biochem Biophys Res Commun *194*, 1371-1379.

Bedoucha, M., Atzpodien, E., and Boelsterli, U.A. (2001). Diabetic KKA y mice exhibit increased hepatic PPARγ1 gene expression and develop hepatic steatosis upon chronic treatment with antidiabetic thiazolidinediones. Journal of hepatology *35*, 17-23.

Bookout, A.L., Jeong, Y., Downes, M., Yu, R.T., Evans, R.M., and Mangelsdorf, D.J. (2006). Anatomical profiling of nuclear receptor expression reveals a hierarchical transcriptional network. Cell *126*, 789-799.

Browning, J.D., and Horton, J.D. (2004). Molecular mediators of hepatic steatosis and liver injury. J Clin Invest *114*, 147-152.

Brunt, E.M., and Tiniakos, D.G. (2010). Histopathology of nonalcoholic fatty liver disease. World J Gastroenterol *16*, 5286-5296.

Butler, R., and Bates, G.P. (2006). Histone deacetylase inhibitors as therapeutics for polyglutamine disorders. Nat Rev Neurosci *7*, 784-796.

Carlberg, C., Hooft van Huijsduijnen, R., Staple, J.K., DeLamarter, J.F., and Becker-Andre, M. (1994). RZRs, a new family of retinoid-related orphan receptors that function as both

monomers and homodimers. Mol Endocrinol *8*, 757-770.
Chawla, A., Boisvert, W.A., Lee, C.H., Laffitte, B.A., Barak, Y., Joseph, S.B., Liao, D., Nagy, L., Edwards, P.A., Curtiss, L.K.*, et al.* (2001a). A PPARγ-LXR-ABCA1 pathway in macrophages is involved in cholesterol efflux and atherogenesis. Mol Cell *7*, 161-171.
Chawla, A., Repa, J.J., Evans, R.M., and Mangelsdorf, D.J. (2001b). Nuclear receptors and lipid physiology: opening the X-files. Science *294*, 1866-1870.
Choi, J.H., Banks, A.S., Kamenecka, T.M., Busby, S.A., Chalmers, M.J., Kumar, N., Kuruvilla, D.S., Shin, Y., He, Y., Bruning, J.B.*, et al.* (2011). Antidiabetic actions of a non-agonist PPARγ ligand blocking Cdk5-mediated phosphorylation. Nature *477*, 477-481.
Chopra, A.R., Louet, J.F., Saha, P., An, J., Demayo, F., Xu, J., York, B., Karpen, S., Finegold, M., Moore, D.*, et al.* (2008). Absence of the SRC-2 coactivator results in a glycogenopathy resembling Von Gierke's disease. Science *322*, 1395-1399.
Cohen, J.C., Horton, J.D., and Hobbs, H.H. (2011). Human fatty liver disease: old questions and new insights. Science *332*, 1519-1523.
Despres, J.P., and Lemieux, I. (2006). Abdominal obesity and metabolic syndrome. Nature *444*, 881-887.
Doulazmi, M., Frederic, F., Lemaigre-Dubreuil, Y., Hadj-Sahraoui, N., Delhaye-Bouchaud, N., and Mariani, J. (1999). Cerebellar Purkinje cell loss during life span of the heterozygous staggerer mouse (Rora(+)/Rora(sg)) is gender-related. J Comp Neurol *411*, 267-273.
Dreyer, C., Krey, G., Keller, H., Givel, F., Helftenbein, G., and Wahli, W. (1992). Control of the peroxisomal beta-oxidation pathway by a novel family of nuclear hormone receptors. Cell *68*, 879-887.
Dubbink, H.J., Hersmus, R., Pike, A.C., Molier, M., Brinkmann, A.O., Jenster, G., and Trapman, J. (2006). Androgen receptor ligand-binding domain interaction and nuclear receptor specificity of FXXLF and LXXLL motifs as determined by L/F swapping. Mol Endocrinol *20*, 1742-1755.
Dutchak, P.A., Katafuchi, T., Bookout, A.L., Choi, J.H., Yu, R.T., Mangelsdorf, D.J., and Kliewer, S.A. (2012). Fibroblast growth factor-21 regulates PPARγ activity and the antidiabetic actions of thiazolidinediones. Cell *148*, 556-567.
Evans, R.M., Barish, G.D., and Wang, Y.X. (2004). PPARs and the complex journey to obesity. Nat Med *10*, 355-361.
Fischer, D.D., Cai, R., Bhatia, U., Asselbergs, F.A., Song, C., Terry, R., Trogani, N., Widmer, R., Atadja, P., and Cohen, D. (2002). Isolation and characterization of a novel class II histone deacetylase, HDAC10. J Biol Chem *277*, 6656-6666.

Forman, B.M., Chen, J., and Evans, R.M. (1996). The peroxisome proliferator-activated receptors: ligands and activators. Ann N Y Acad Sci *804*, 266-275.
Gao, L., Cueto, M.A., Asselbergs, F., and Atadja, P. (2002). Cloning and functional characterization of HDAC11, a novel member of the human histone deacetylase family. J Biol Chem *277*, 25748-25755.
Gavrilova, O., Haluzik, M., Matsusue, K., Cutson, J.J., Johnson, L., Dietz, K.R., Nicol, C.J., Vinson, C., Gonzalez, F.J., and Reitman, M.L. (2003). Liver peroxisome proliferator-activated receptor γ contributes to hepatic steatosis, triglyceride clearance, and regulation of body fat mass. J Biol Chem *278*, 34268-34276.
Giguere, V. (1999). Orphan nuclear receptors: from gene to function. Endocr Rev *20*, 689-725.
Giguere, V., McBroom, L.D., and Flock, G. (1995). Determinants of target gene specificity for RORα 1: monomeric DNA binding by an orphan nuclear receptor. Mol Cell Biol *15*, 2517-2526.
Giguere, V., Tini, M., Flock, G., Ong, E., Evans, R.M., and Otulakowski, G. (1994). Isoform-specific amino-terminal domains dictate DNA-binding properties of RORα, a novel family of orphan hormone nuclear receptors. Genes Dev *8*, 538-553.
Gold, D.A., Baek, S.H., Schork, N.J., Rose, D.W., Larsen, D.D., Sachs, B.D., Rosenfeld, M.G., and Hamilton, B.A. (2003). RORα coordinates reciprocal signaling in cerebellar development through sonic hedgehog and calcium-dependent pathways. Neuron *40*, 1119-1131.
Gregoretti, I.V., Lee, Y.M., and Goodson, H.V. (2004). Molecular evolution of the histone deacetylase family: functional implications of phylogenetic analysis. J Mol Biol *338*, 17-31.
Guenther, M.G., Barak, O., and Lazar, M.A. (2001). The SMRT and N-CoR corepressors are activating cofactors for histone deacetylase 3. Mol Cell Biol *21*, 6091-6101.
Guillaumond, F., Dardente, H., Giguere, V., and Cermakian, N. (2005). Differential control of Bmal1 circadian transcription by REV-ERB and ROR nuclear receptors. J Biol Rhythms *20*, 391-403.
Hamilton, B.A., Frankel, W.N., Kerrebrock, A.W., Hawkins, T.L., FitzHugh, W., Kusumi, K., Russell, L.B., Mueller, K.L., van Berkel, V., Birren, B.W.*, et al.* (1996). Disruption of the nuclear hormone receptor RORα in staggerer mice. Nature *379*, 736-739.
Harding, H.P., and Lazar, M.A. (1995). The monomer-binding orphan receptor Rev-Erb represses transcription as a dimer on a novel direct repeat. Mol Cell Biol *15*, 4791-4802.

Harms, M., and Seale, P. (2013). Brown and beige fat: development, function and therapeutic potential. Nat Med *19*, 1252-1263.
Harris, J.M., Lau, P., Chen, S.L., and Muscat, G.E. (2002). Characterization of the retinoid orphan-related receptor-α coactivator binding interface: a structural basis for ligand-independent transcription. Mol Endocrinol *16*, 998-1012.
Herrup, K., and Mullen, R.J. (1979). Staggerer chimeras: intrinsic nature of Purkinje cell defects and implications for normal cerebellar development. Brain Res *178*, 443-457.
Heymsfield, S.B., and Wadden, T.A. (2017). Mechanisms, Pathophysiology, and Management of Obesity. N Engl J Med *376*, 254-266.
Higa, M., Zhou, Y.T., Ravazzola, M., Baetens, D., Orci, L., and Unger, R.H. (1999). Troglitazone prevents mitochondrial alterations, β cell destruction, and diabetes in obese prediabetic rats. Proc Natl Acad Sci U S A *96*, 11513-11518.
Hong, H., Kohli, K., Trivedi, A., Johnson, D.L., and Stallcup, M.R. (1996). GRIP1, a novel mouse protein that serves as a transcriptional coactivator in yeast for the hormone binding domains of steroid receptors. Proc Natl Acad Sci U S A *93*, 4948-4952.
Huang da, W., Sherman, B.T., and Lempicki, R.A. (2009a). Bioinformatics enrichment tools: paths toward the comprehensive functional analysis of large gene lists. Nucleic Acids Res *37*, 1-13.
Huang da, W., Sherman, B.T., and Lempicki, R.A. (2009b). Systematic and integrative analysis of large gene lists using DAVID bioinformatics resources. Nat Protoc *4*, 44-57.
Hwang, D., Rust, A.G., Ramsey, S., Smith, J.J., Leslie, D.M., Weston, A.D., de Atauri, P., Aitchison, J.D., Hood, L., Siegel, A.F*., et al.* (2005). A data integration methodology for systems biology. Proc Natl Acad Sci U S A *102*, 17296-17301.
Imai, T., Takakuwa, R., Marchand, S., Dentz, E., Bornert, J.-M., Messaddeq, N., Wendling, O., Mark, M., Desvergne, B., and Wahli, W. (2004). Peroxisome proliferator-activated receptor γ is required in mature white and brown adipocytes for their survival in the mouse. Proceedings of the National Academy of Sciences of the United States of America *101*, 4543-4547.
Jetten, A.M. (2009). Retinoid-related orphan receptors (RORs): critical roles in development, immunity, circadian rhythm, and cellular metabolism. Nucl Recept Signal *7*, e003.
Jetten, A.M., and Joo, J.H. (2006). Retinoid-related Orphan Receptors (RORs): Roles in Cellular Differentiation and Development. Adv Dev Biol *16*, 313-355.
Kahn, B.B., and Flier, J.S. (2000). Obesity and insulin resistance. J Clin Invest *106*, 473-

481.
Kang, H.S., Cho, H.C., Lee, J.H., Oh, G.T., Koo, S.H., Park, B.H., Lee, I.K., Choi, H.S., Song, D.K., and Im, S.S. (2016). Metformin stimulates IGFBP-2 gene expression through PPARα in diabetic states. Sci Rep *6*, 23665.
Kang, H.S., Okamoto, K., Takeda, Y., Beak, J.Y., Gerrish, K., Bortner, C.D., DeGraff, L.M., Wada, T., Xie, W., and Jetten, A.M. (2011). Transcriptional profiling reveals a role for RORα in regulating gene expression in obesity-associated inflammation and hepatic steatosis. Physiol Genomics *43*, 818-828.
Katz, A., Udata, C., Ott, E., Hickey, L., Burczynski, M.E., Burghart, P., Vesterqvist, O., and Meng, X. (2009). Safety, pharmacokinetics, and pharmacodynamics of single doses of LXR-623, a novel liver X-receptor agonist, in healthy participants. J Clin Pharmacol *49*, 643-649.
Kazantsev, A.G., and Thompson, L.M. (2008). Therapeutic application of histone deacetylase inhibitors for central nervous system disorders. Nat Rev Drug Discov *7*, 854-868.
Kersten, S., Seydoux, J., Peters, J.M., Gonzalez, F.J., Desvergne, B., and Wahli, W. (1999). Peroxisome proliferator-activated receptor α mediates the adaptive response to fasting. J Clin Invest *103*, 1489-1498.
Kim, E.J., Yoon, Y.S., Hong, S., Son, H.Y., Na, T.Y., Lee, M.H., Kang, H.J., Park, J., Cho, W.J., Kim, S.G.*, et al.* (2012). Retinoic acid receptor-related orphan receptor α-induced activation of adenosine monophosphate-activated protein kinase results in attenuation of hepatic steatosis. Hepatology *55*, 1379-1388.
Kim, H., Lee, J.M., Lee, G., Bhin, J., Oh, S.K., Kim, K., Pyo, K.E., Lee, J.S., Yim, H.Y., Kim, K.I.*, et al.* (2011). DNA damage-induced RORα is crucial for p53 stabilization and increased apoptosis. Mol Cell *44*, 797-810.
Kim, H.I., Cha, J.Y., Kim, S.Y., Kim, J.W., Roh, K.J., Seong, J.K., Lee, N.T., Choi, K.Y., Kim, K.S., and Ahn, Y.H. (2002). Peroxisomal proliferator-activated receptor-γ upregulates glucokinase gene expression in β-cells. Diabetes *51*, 676-685.
Kliewer, S.A., Umesono, K., Noonan, D.J., Heyman, R.A., and Evans, R.M. (1992). Convergence of 9-cis retinoic acid and peroxisome proliferator signalling pathways through heterodimer formation of their receptors. Nature *358*, 771-774.
Knutson, S.K., Chyla, B.J., Amann, J.M., Bhaskara, S., Huppert, S.S., and Hiebert, S.W. (2008). Liver-specific deletion of histone deacetylase 3 disrupts metabolic transcriptional networks. EMBO J *27*, 1017-1028.

Kojetin, D.J., and Burris, T.P. (2014). REV-ERB and ROR nuclear receptors as drug targets. Nat Rev Drug Discov *13*, 197-216.
Kou, Y., Chen, E.Y., Clark, N.R., Duan, Q., Tan, C.M., and Ma'ayan, A. (2013). ChEA2: gene-set libraries from ChIP-X experiments to decode the transcription regulome. Paper presented at: International Conference on Availability, Reliability, and Security (Springer).
Kruhlak, M.J., Hendzel, M.J., Fischle, W., Bertos, N.R., Hameed, S., Yang, X.J., Verdin, E., and Bazett-Jones, D.P. (2001). Regulation of global acetylation in mitosis through loss of histone acetyltransferases and deacetylases from chromatin. J Biol Chem *276*, 38307-38319.
Lau, P., Fitzsimmons, R.L., Pearen, M.A., Watt, M.J., and Muscat, G.E. (2011). Homozygous staggerer (sg/sg) mice display improved insulin sensitivity and enhanced glucose uptake in skeletal muscle. Diabetologia *54*, 1169-1180.
Lau, P., Fitzsimmons, R.L., Raichur, S., Wang, S.C., Lechtken, A., and Muscat, G.E. (2008). The orphan nuclear receptor, RORα, regulates gene expression that controls lipid metabolism: staggerer (SG/SG) mice are resistant to diet-induced obesity. J Biol Chem *283*, 18411-18421.
Lee, J.M., Kim, I.S., Kim, H., Lee, J.S., Kim, K., Yim, H.Y., Jeong, J., Kim, J.H., Kim, J.Y., Lee, H.*, et al.* (2010). RORα attenuates Wnt/β-catenin signaling by PKCα-dependent phosphorylation in colon cancer. Mol Cell *37*, 183-195.
Lee, J.M., Lee, J.S., Kim, H., Kim, K., Park, H., Kim, J.Y., Lee, S.H., Kim, I.S., Kim, J., Lee, M.*, et al.* (2012). EZH2 generates a methyl degron that is recognized by the DCAF1/DDB1/CUL4 E3 ubiquitin ligase complex. Mol Cell *48*, 572-586.
Lee, J.M., Wagner, M., Xiao, R., Kim, K.H., Feng, D., Lazar, M.A., and Moore, D.D. (2014). Nutrient-sensing nuclear receptors coordinate autophagy. Nature *516*, 112-115.
Lehmann, J.M., Moore, L.B., Smith-Oliver, T.A., Wilkison, W.O., Willson, T.M., and Kliewer, S.A. (1995). An antidiabetic thiazolidinedione is a high affinity ligand for peroxisome proliferator-activated receptor γ (PPARγ). Journal of Biological Chemistry *270*, 12953-12956.
Li, L., Xie, X., Qin, J., Jeha, G.S., Saha, P.K., Yan, J., Haueter, C.M., Chan, L., Tsai, S.Y., and Tsai, M.J. (2009). The nuclear orphan receptor COUP-TFII plays an essential role in adipogenesis, glucose homeostasis, and energy metabolism. Cell Metab *9*, 77-87.
Ma, S., Jing, F., Xu, C., Zhou, L., Song, Y., Yu, C., Jiang, D., Gao, L., Li, Y., Guan, Q.*, et al.* (2015). Thyrotropin and obesity: increased adipose triglyceride content through glycerol-3-phosphate acyltransferase 3. Sci Rep *5*, 7633.
Mamontova, A., Seguret-Mace, S., Esposito, B., Chaniale, C., Bouly, M., Delhaye-

Bouchaud, N., Luc, G., Staels, B., Duverger, N., Mariani, J., *et al.* (1998). Severe atherosclerosis and hypoalphalipoproteinemia in the staggerer mouse, a mutant of the nuclear receptor RORα. Circulation *98*, 2738-2743.
Martin, M. (2011). Cutadapt removes adapter sequences from high-throughput sequencing reads. EMBnet journal *17*, pp. 10-12.
Martin, M., Kettmann, R., and Dequiedt, F. (2007). Class IIa histone deacetylases: regulating the regulators. Oncogene *26*, 5450-5467.
Matsusue, K., Haluzik, M., Lambert, G., Yim, S.H., Gavrilova, O., Ward, J.M., Brewer, B., Jr., Reitman, M.L., and Gonzalez, F.J. (2003). Liver-specific disruption of PPARγ in leptin-deficient mice improves fatty liver but aggravates diabetic phenotypes. J Clin Invest *111*, 737-747.
Mayerson, A.B., Hundal, R.S., Dufour, S., Lebon, V., Befroy, D., Cline, G.W., Enocksson, S., Inzucchi, S.E., Shulman, G.I., and Petersen, K.F. (2002). The effects of rosiglitazone on insulin sensitivity, lipolysis, and hepatic and skeletal muscle triglyceride content in patients with type 2 diabetes. Diabetes *51*, 797-802.
McKinsey, T.A., Zhang, C.L., Lu, J., and Olson, E.N. (2000). Signal-dependent nuclear export of a histone deacetylase regulates muscle differentiation. Nature *408*, 106-111.
Medina-Gomez, G., Gray, S.L., Yetukuri, L., Shimomura, K., Virtue, S., Campbell, M., Curtis, R.K., Jimenez-Linan, M., Blount, M., Yeo, G.S., *et al.* (2007). PPAR gamma 2 prevents lipotoxicity by controlling adipose tissue expandability and peripheral lipid metabolism. PLoS Genet *3*, e64.
Memon, R.A., Tecott, L.H., Nonogaki, K., Beigneux, A., Moser, A.H., Grunfeld, C., and Feingold, K.R. (2000). Up-regulation of peroxisome proliferator-activated receptors (PPAR-α) and PPAR-γ messenger ribonucleic acid expression in the liver in murine obesity: troglitazone induces expression of PPAR-γ-responsive adipose tissue-specific genes in the liver of obese diabetic mice. Endocrinology *141*, 4021-4031.
Moller, D.E., and Kaufman, K.D. (2005). Metabolic syndrome: a clinical and molecular perspective. Annu Rev Med *56*, 45-62.
Moran-Salvador, E., Lopez-Parra, M., Garcia-Alonso, V., Titos, E., Martinez-Clemente, M., Gonzalez-Periz, A., Lopez-Vicario, C., Barak, Y., Arroyo, V., and Claria, J. (2011). Role for PPARγ in obesity-induced hepatic steatosis as determined by hepatocyte- and macrophage-specific conditional knockouts. FASEB J *25*, 2538-2550.
Moras, D., and Gronemeyer, H. (1998). The nuclear receptor ligand-binding domain: structure and function. Curr Opin Cell Biol *10*, 384-391.

Musso, G., Cassader, M., Rosina, F., and Gambino, R. (2012). Impact of current treatments on liver disease, glucose metabolism and cardiovascular risk in non-alcoholic fatty liver disease (NAFLD): a systematic review and meta-analysis of randomised trials. Diabetologia *55*, 885-904.

Nakano, R., Kurosaki, E., Yoshida, S., Yokono, M., Shimaya, A., Maruyama, T., and Shibasaki, M. (2006). Antagonism of peroxisome proliferator-activated receptor γ prevents high-fat diet-induced obesity in vivo. Biochem Pharmacol *72*, 42-52.

Nissen, S.E., and Wolski, K. (2007). Effect of rosiglitazone on the risk of myocardial infarction and death from cardiovascular causes. N Engl J Med *356*, 2457-2471.

Ohoka, N., Kato, S., Takahashi, Y., Hayashi, H., and Sato, R. (2009). The orphan nuclear receptor RORα restrains adipocyte differentiation through a reduction of C/EBPβ activity and perilipin gene expression. Mol Endocrinol *23*, 759-771.

Palmer, C.N., Hsu, M.H., Griffin, H.J., and Johnson, E.F. (1995). Novel sequence determinants in peroxisome proliferator signaling. J Biol Chem *270*, 16114-16121.

Pearen, M.A., and Muscat, G.E. (2012). Orphan nuclear receptors and the regulation of nutrient metabolism: understanding obesity. Physiology (Bethesda) *27*, 156-166.

Perissi, V., Jepsen, K., Glass, C.K., and Rosenfeld, M.G. (2010). Deconstructing repression: evolving models of co-repressor action. Nat Rev Genet *11*, 109-123.

Poulsen, L., Siersbaek, M., and Mandrup, S. (2012). PPARs: fatty acid sensors controlling metabolism. Semin Cell Dev Biol *23*, 631-639.

Puigserver, P., and Spiegelman, B.M. (2003). Peroxisome proliferator-activated receptor-γ coactivator 1 α (PGC-1 α): transcriptional coactivator and metabolic regulator. Endocr Rev *24*, 78-90.

Ratziu, V., Giral, P., Jacqueminet, S., Charlotte, F., Hartemann-Heurtier, A., Serfaty, L., Podevin, P., Lacorte, J.M., Bernhardt, C., Bruckert, E.*, et al.* (2008). Rosiglitazone for nonalcoholic steatohepatitis: one-year results of the randomized placebo-controlled Fatty Liver Improvement with Rosiglitazone Therapy (FLIRT) Trial. Gastroenterology *135*, 100-110.

Ribeiro, R.C., Kushner, P.J., and Baxter, J.D. (1995). The nuclear hormone receptor gene superfamily. Annu Rev Med *46*, 443-453.

Rosen, E.D., Kulkarni, R.N., Sarraf, P., Ozcan, U., Okada, T., Hsu, C.-H., Eisenman, D., Magnuson, M.A., Gonzalez, F.J., and Kahn, C.R. (2003). Targeted elimination of peroxisome proliferator-activated receptor γ in β cells leads to abnormalities in islet mass without compromising glucose homeostasis. Molecular and Cellular Biology *23*, 7222-

7229.
Rutkowski, J.M., Stern, J.H., and Scherer, P.E. (2015). The cell biology of fat expansion. J Cell Biol *208*, 501-512.
Saltiel, A.R., and Olefsky, J.M. (1996). Thiazolidinediones in the treatment of insulin resistance and type II diabetes. Diabetes *45*, 1661-1669.
Samad, F., Pandey, M., and Loskutoff, D.J. (1998). Tissue factor gene expression in the adipose tissues of obese mice. Proc Natl Acad Sci U S A *95*, 7591-7596.
Sato, T.K., Panda, S., Miraglia, L.J., Reyes, T.M., Rudic, R.D., McNamara, P., Naik, K.A., FitzGerald, G.A., Kay, S.A., and Hogenesch, J.B. (2004). A functional genomics strategy reveals Rora as a component of the mammalian circadian clock. Neuron *43*, 527-537.
Savage, D.B., Tan, G.D., Acerini, C.L., Jebb, S.A., Agostini, M., Gurnell, M., Williams, R.L., Umpleby, A.M., Thomas, E.L., Bell, J.D.*, et al.* (2003). Human metabolic syndrome resulting from dominant-negative mutations in the nuclear receptor peroxisome proliferator-activated receptor-γ. Diabetes *52*, 910-917.
Seeley, R.J., and Woods, S.C. (2003). Monitoring of stored and available fuel by the CNS: implications for obesity. Nat Rev Neurosci *4*, 901-909.
Shao, D., and Lazar, M.A. (1999). Modulating nuclear receptor function: may the phos be with you. J Clin Invest *103*, 1617-1618.
Sidman, R.L., Lane, P.W., and Dickie, M.M. (1962). Staggerer, a new mutation in the mouse affecting the cerebellum. Science *137*, 610-612.
Strahl, B.D., and Allis, C.D. (2000). The language of covalent histone modifications. Nature *403*, 41-45.
Sun, J.M., Spencer, V.A., Chen, H.Y., Li, L., and Davie, J.R. (2003). Measurement of histone acetyltransferase and histone deacetylase activities and kinetics of histone acetylation. Methods *31*, 12-23.
Sun, Z., Feng, D., Fang, B., Mullican, S.E., You, S.H., Lim, H.W., Everett, L.J., Nabel, C.S., Li, Y., Selvakumaran, V.*, et al.* (2013). Deacetylase-independent function of HDAC3 in transcription and metabolism requires nuclear receptor corepressor. Mol Cell *52*, 769-782.
Sun, Z., Miller, R.A., Patel, R.T., Chen, J., Dhir, R., Wang, H., Zhang, D., Graham, M.J., Unterman, T.G., Shulman, G.I.*, et al.* (2012). Hepatic Hdac3 promotes gluconeogenesis by repressing lipid synthesis and sequestration. Nat Med *18*, 934-942.
Thiagalingam, S., Cheng, K.H., Lee, H.J., Mineva, N., Thiagalingam, A., and Ponte, J.F. (2003). Histone deacetylases: unique players in shaping the epigenetic histone code. Ann N Y Acad Sci *983*, 84-100.

Tomaru, T., Steger, D.J., Lefterova, M.I., Schupp, M., and Lazar, M.A. (2009). Adipocyte-specific expression of murine resistin is mediated by synergism between peroxisome proliferator-activated receptor γ and CCAAT/enhancer-binding proteins. J Biol Chem *284*, 6116-6125.

Tontonoz, P., Hu, E., and Spiegelman, B.M. (1994). Stimulation of adipogenesis in fibroblasts by PPARγ2, a lipid-activated transcription factor. Cell *79*, 1147-1156.

Tontonoz, P., and Spiegelman, B.M. (2008). Fat and beyond: the diverse biology of PPARγ. Annu Rev Biochem *77*, 289-312.

Trapnell, C., Pachter, L., and Salzberg, S.L. (2009). TopHat: discovering splice junctions with RNA-Seq. Bioinformatics *25*, 1105-1111.

Trapnell, C., Williams, B.A., Pertea, G., Mortazavi, A., Kwan, G., van Baren, M.J., Salzberg, S.L., Wold, B.J., and Pachter, L. (2010). Transcript assembly and quantification by RNA-Seq reveals unannotated transcripts and isoform switching during cell differentiation. Nat Biotechnol *28*, 511-515.

Trivedi, C.M., Lu, M.M., Wang, Q., and Epstein, J.A. (2008). Transgenic overexpression of Hdac3 in the heart produces increased postnatal cardiac myocyte proliferation but does not induce hypertrophy. J Biol Chem *283*, 26484-26489.

Uno, K., Katagiri, H., Yamada, T., Ishigaki, Y., Ogihara, T., Imai, J., Hasegawa, Y., Gao, J., Kaneko, K., Iwasaki, H.*, et al.* (2006). Neuronal pathway from the liver modulates energy expenditure and systemic insulin sensitivity. Science *312*, 1656-1659.

van den Berghe, G. (1991). The role of the liver in metabolic homeostasis: implications for inborn errors of metabolism. J Inherit Metab Dis *14*, 407-420.

Vidal-Puig, A., Jimenez-Linan, M., Lowell, B.B., Hamann, A., Hu, E., Spiegelman, B., Flier, J.S., and Moller, D.E. (1996). Regulation of PPARγ gene expression by nutrition and obesity in rodents. J Clin Invest *97*, 2553-2561.

Vogel, M.W., Sinclair, M., Qiu, D., and Fan, H. (2000). Purkinje cell fate in staggerer mutants: agenesis versus cell death. J Neurobiol *42*, 323-337.

Vu-Dac, N., Gervois, P., Grotzinger, T., De Vos, P., Schoonjans, K., Fruchart, J.C., Auwerx, J., Mariani, J., Tedgui, A., and Staels, B. (1997). Transcriptional regulation of apolipoprotein A-I gene expression by the nuclear receptor RORα. J Biol Chem *272*, 22401-22404.

Wagner, M., Zollner, G., and Trauner, M. (2011). Nuclear receptors in liver disease. Hepatology *53*, 1023-1034.

Wang, G., and Sadar, M.D. (2006). Amino-terminus domain of the androgen receptor as a

molecular target to prevent the hormonal progression of prostate cancer. J Cell Biochem *98*, 36-53.
Watanabe, M., Houten, S.M., Mataki, C., Christoffolete, M.A., Kim, B.W., Sato, H., Messaddeq, N., Harney, J.W., Ezaki, O., Kodama, T.*, et al.* (2006). Bile acids induce energy expenditure by promoting intracellular thyroid hormone activation. Nature *439*, 484-489.
Watson, P.J., Fairall, L., Santos, G.M., and Schwabe, J.W. (2012). Structure of HDAC3 bound to co-repressor and inositol tetraphosphate. Nature *481*, 335-340.
Way, J.M., Harrington, W.W., Brown, K.K., Gottschalk, W.K., Sundseth, S.S., Mansfield, T.A., Ramachandran, R.K., Willson, T.M., and Kliewer, S.A. (2001). Comprehensive Messenger Ribonucleic Acid Profiling Reveals That Peroxisome Proliferator-Activated Receptor γ Activation Has Coordinate Effects on Gene Expression in Multiple Insulin-Sensitive Tissues. Endocrinology *142*, 1269-1277.
Weatherman, R.V., Fletterick, R.J., and Scanlan, T.S. (1999). Nuclear-receptor ligands and ligand-binding domains. Annu Rev Biochem *68*, 559-581.
Wen, Y.D., Perissi, V., Staszewski, L.M., Yang, W.M., Krones, A., Glass, C.K., Rosenfeld, M.G., and Seto, E. (2000). The histone deacetylase-3 complex contains nuclear receptor corepressors. Proc Natl Acad Sci U S A *97*, 7202-7207.
Wilcox, R., Kupfer, S., Erdmann, E., and investigators, P.R.S. (2008). Effects of pioglitazone on major adverse cardiovascular events in high-risk patients with type 2 diabetes: results from PROspective pioglitAzone Clinical Trial In macro Vascular Events (PROactive 10). Am Heart J *155*, 712-717.
Yang, W.M., Tsai, S.C., Wen, Y.D., Fejer, G., and Seto, E. (2002). Functional domains of histone deacetylase-3. J Biol Chem *277*, 9447-9454.
Yang, X.J., and Seto, E. (2003). Collaborative spirit of histone deacetylases in regulating chromatin structure and gene expression. Curr Opin Genet Dev *13*, 143-153.
Yang, X.J., and Seto, E. (2008). The Rpd3/Hda1 family of lysine deacetylases: from bacteria and yeast to mice and men. Nat Rev Mol Cell Biol *9*, 206-218.
You, S.H., Lim, H.W., Sun, Z., Broache, M., Won, K.J., and Lazar, M.A. (2013). Nuclear receptor co-repressors are required for the histone-deacetylase activity of HDAC3 in vivo. Nat Struct Mol Biol *20*, 182-187.
Yu, S., Matsusue, K., Kashireddy, P., Cao, W.Q., Yeldandi, V., Yeldandi, A.V., Rao, M.S., Gonzalez, F.J., and Reddy, J.K. (2003). Adipocyte-specific gene expression and adipogenic steatosis in the mouse liver due to peroxisome proliferator-activated receptor γ1 (PPARγ1) overexpression. J Biol Chem *278*, 498-505.

Zhang, Y., Kwon, S., Yamaguchi, T., Cubizolles, F., Rousseaux, S., Kneissel, M., Cao, C., Li, N., Cheng, H.L., Chua, K.*, et al.* (2008). Mice lacking histone deacetylase 6 have hyperacetylated tubulin but are viable and develop normally. Mol Cell Biol *28*, 1688-1701.
Zhang, Y., Proenca, R., Maffei, M., Barone, M., Leopold, L., and Friedman, J.M. (1994). Positional cloning of the mouse obese gene and its human homologue. Nature *372*, 425-432.
Zhang, Y.L., Hernandez-Ono, A., Siri, P., Weisberg, S., Conlon, D., Graham, M.J., Crooke, R.M., Huang, L.S., and Ginsberg, H.N. (2006). Aberrant hepatic expression of PPARγ2 stimulates hepatic lipogenesis in a mouse model of obesity, insulin resistance, dyslipidemia, and hepatic steatosis. J Biol Chem *281*, 37603-37615.
Zhu, Y., McAvoy, S., Kuhn, R., and Smith, D.I. (2006). RORA, a large common fragile site gene, is involved in cellular stress response. Oncogene *25*, 2901-2908.
Zilliacus, J., Wright, A.P., Carlstedt-Duke, J., Nilsson, L., and Gustafsson, J.A. (1995). Modulation of DNA-binding specificity within the nuclear receptor family by substitutions at a single amino acid position. Proteins *21*, 57-67.

국문 초록 / ABSTRACT IN KOREAN

간 내 대사작용 조절에 이상이 생기면 지방간, 인슐린 저항성 및 비만을 유도하는 것으로 알려져 있다. Retinoic acid receptor-related orphan receptor α (RORα) 는 소뇌 발달, 일주기 리듬 및 암을 비롯한 다양한 생물학적 과정의 중요한 조절 자로 알려져 있다. 자연적인 *Rorα* 돌연변이 생쥐인 *Staggerer* 생쥐가 옛날부터 RORα의 생체 내 연구에 유용하게 이용되고 있다. *Staggerer* 생쥐에서 고지방식을 제공하였을 때 정상 유전자형 생쥐에 비해 체중이 적게 증대되며 지방대사를 조절하는 유전자가 간에서 발현이 감소되어 있음이 보고되었다. 그러나 또 다른 연구에서는 RORα를 생쥐의 간에서 과발현 시켰을 경우 오히려 반대로 지방간이 덜 진행되는 것으로 알려져 있다. 이러한 이유는 *Staggerer* 생쥐가 소뇌발달이 제대로 이루어지지 않음으로써 소뇌 위축증이 유발되어 이에 따라 운동 실조증이 일어나 정상적인 식이가 불가능함으로써 생겨나는 부수적인 현상으로 생각된다. 즉, 아직까지는 RORα의 대작작용에서의 역할, 특히 간에서의 역할은 정확히 밝혀지지 않았다. 이를 해결하기 위해서는 간 특이적인 RORα의 결핍 생쥐가 필요하다.

본 연구에서는 간 특이적인 RORα의 결핍 생쥐를 이용해서 간 내 지질 대사를 매개하는 핵 수용체인 peroxisome proliferators-activated receptor γ (PPARγ)의 전사 활성을 RORα가 저해하여 RORα가 간 내 지질의 항상성을 조절한다는 것을 발견했다. 간 특이적 *Rorα* 결핍 생쥐는 고지방식 (HFD)을 제공하였을 때 정상 유전자형 생쥐에 비해 지방간, 비만 및 인

슐린 저항성이 더 빠르고 심하게 유발됨을 확인하였다. 간 내 전체 전사체 분석을 통해 RORα의 간 특이적인 결핍은 PPARγ 신호 전달 체계의 조절에 이상이 생겨 간 내의 포도당 대사와 지질 대사의 이상을 유발한다. RORα는 PPARγ 전사 조절 기능을 억제 하기 위해 HDAC3과 결합한 뒤 PPARγ의 표적 유전자 프로모터에 위치한다. 마지막으로, PPARγ의 억제제를 이용하여 PPARγ의 기능을 저해하는 경우 고지방식을 제공한 간 특이적 *Rorα* 결핍 생쥐에서 간 내 대사 항상성이 현저히 회복되는 것을 관찰하였다. 이번 연구를 통해 RORα는 PPARγ 신호 전달 체계를 조절하여 간 내 지방의 항상성 조절에 중추적인 역할을 한다는 것을 알 수 있다. 결과적으로 RORα의 활성을 조절하는 것이 지방간 및 비만과 같은 대사 장애의 치료를 위한 새로운 치료전략임을 본 연구를 통해 제시하였다.

주요어:
RORα, 간 특이적 *Rorα* 결핍 생쥐, 고지방식, 비만, 간, 간 내 대사 작용, PPARγ, HDAC3, GW9662

학번: 2011-30106